

ACKNOWLEDGEMENTS AND DEDICATIONS

Work on this project would have been impossible without the help and support of **Dr. Ronald Doll**, my parents, **Eva Said** and **Raafat Barsoom**, and my brother, **Shady Barsoom**. I also thank **God** for the opportunity to participate in such amazing work, for placing many wonderful people around me that have given me support and motivation, and for the strength and patience needed to continue work on this project. **It is to Dr. Doll, my family, and God that I dedicate my work and thesis.**

Additionally, I wish to thank **Drew University**, specifically the **Biology, Chemistry, Neuroscience, Physics, and Research Institute for Science Emeriti (RISE) departments**, with special mentions to the rest of the **Dr. Doll lab, Dr. Bimal DasMahapatra and his lab, Dr. Adam Cassano, Dr. Christina McKittrick, Dr. Jason Bishop, and Dr. C. Anderson Evans.**

For the financial support needed for all of the materials and equipment, I would like to thank **Drew Summer Science Institute (DSSI), Henry Dreyfus Foundation, and the Paolo Cucchi research grant.**

**Drew University
College of Liberal Arts**

**Drug Discovery Efforts Targeting Mutant p53
for the Treatment of Glioblastoma**

**A Thesis in Neuroscience
By: Randa R Barsoom**

**Submitted in partial fulfillment
Of the Requirements
For the degree of
Bachelor in Arts
With Specialized Honors in Neuroscience**

May 2014

ABSTRACT

Targeted approaches to treating cancers including glioblastoma multiforme (GBM) are limited and partially effective, at best. By attacking specific oncogenic drivers for a tumor, an on-target and effective drug might be possible. The transcription factor p53 is a cell control tumor suppressor protein responsible for maintaining the integrity of a cell's genome and eliminating cells with DNA mutations. Mutant p53 is found, and believed to be causative, in 50% of all human cancers. The oncogenic driver for a high percentage of GBM is thought to be mutant p53. In this thesis, a drug discovery effort that targets mutant p53 in GBM cells is described. The goal is to identify compounds that reactivate mutant p53 and allow normal biological function of p53 in the GBM cells. The process of identification of lead structures and efforts in developing new analogues that optimize potency, selectivity, metabolic stability and other drug-like properties, including the ability of the compounds to cross the blood brain barrier, BBB, are explained. Crossing the BBB is a critical step for drugs used in central nervous system (CNS) diseases. Here, seven synthesized compounds in two classes, quinoline and benzimidazoles, are discussed. Six of these compounds reactivate mutant p53 in the GBM cells and allow for production of proteins downstream of p53. Of these six active compounds, three cross the blood brain barrier. A structure activity relationship, SAR, regarding in-cell potency, selectivity, metabolic stability and the ability to cross the BBB is then developed. This SAR and drug discovery effort can be further expanded to develop compounds with an optimized biological profile that would lead to potential drug candidates for the treatment of glioblastoma multiforme.

TABLE OF CONTENTS

<u>ABBREVIATIONS</u>	1
<u>INTRODUCTION</u>	
CANCER	2
CELL REPLICATION AND P53 ACTIVATION	4
MUTANT P53	8
GLIOBLASTOMA MULTIFORME	9
BLOOD BRAIN BARRIER	11
PROJECT GOAL	12
DRUG DISCOVERY PROCESS	14
<u>MATERIALS AND METHODS</u>	
SYNTHESIS OF ANALOGOUS STRUCTURES	16
RD 1	17
RD 4	18
RD 13	19
RD 14	20
RD 27	21
RD 29	22
RD 39	23
DEVELOPMENT OF <i>IN VITRO</i> HUMAN CELL ASSAY	24
ASSESSMENT OF THERAPEUTIC INDEX	28
DEVELOPMENT OF BBBTR ASSAY	30
ASSESSMENT OF METABOLIC RATE	34
<u>RESULTS AND DISCUSSION</u>	
1. IDENTIFYING SUITABLE LEAD STRUCTURES	34
2. SYNTHESIS OF ANALOGOUS STRUCTURES	36
3. DEVELOPING <i>IN VITRO</i> HUMAN CELL ASSAYS	43
4. DEVELOPING <i>IN VITRO</i> BBBTR ASSAYS	46
5. DEVELOPING <i>IN VITRO</i> HUMAN METABOLISM ASSAY	52
6. OPTIMIZING STRUCTURES BASED ON OBTAINED DATA	55
CONCLUSION	58
FUTURE DIRECTIONS	59
<u>APPENDIX A</u>	61
<u>APPENDIX B</u>	79
<u>BIBLIOGRAPHY</u>	85

TABLE OF FIGURES

FIGURE.....	PAGE
FIGURE 1:SOME MECHANISMS OF ACTIVATION OF P53	4
FIGURE 2:BLOOD BRAIN BARRIER MODEL	11
FIGURE 3:RD 1 SYNTHETIC ROUTE.....	17
FIGURE 4:RD 4 SYNTHETIC ROUTE.....	18
FIGURE 5:RD 13 SYNTHETIC ROUTE.....	19
FIGURE 6:RD 14 SYNTHETIC ROUTE.....	20
FIGURE 7:RD 27 SYNTHETIC ROUTE.....	21
FIGURE 8:RD 29 SYNTHETIC ROUTE.....	22
FIGURE 9:RD 39 SYNTHETIC ROUTE.....	23
FIGURE 10:SF295 GLIOBLASTOMA CELLS	24
FIGURE 11:ATTEMPT AT CREATING BBBTR APPARATUS 1	30
FIGURE 12:ATTEMPT AT CREATING BBBTR APPARATUS 2	31
FIGURE 13: BBBTR APPARATUS	32
FIGURE 14: BBBTR APPARATUS PLATE SET UP.....	33
FIGURE 15:LEAD STRUCTURES	35
FIGURE 16:POSSIBLE MODIFICATION TO QUINOLINE STRUCTURE.....	36
FIGURE 17:GENERAL SYNTHETIC ROUTES	37
FIGURE 18:RD 1 LC/MS CHROMATOGRAM.....	41
FIGURE 19:RD 1 MS AREA UNDER PEAK	42
FIGURE 20:RD 1 NMR SPECTRUM	43
FIGURE 21:SAMPLE WESTERN BLOT.....	44
FIGURE 22:REACTIVATION OF MUTANT P53	45
FIGURE 23: BBBTR APPARATUS.....	47
FIGURE 24:CONTROLS USED IN BBBTR ASSAY	48
FIGURE 25:OVERALL BBBTR DATA	49
FIGURE 26:PROGESTERONE BBBTR CHROMATOGRAM.....	50
FIGURE 27:HYDROCORTISONE BBBTR CHROMATOGRAM	51
FIGURE 28:RD 1 METABOLISM STUDY	54
FIGURE 29:RD 39 METABOLISM STUDY	55
FIGURE 30:STRUCTURE ACTIVITY RELATIONSHIP	56-57
FIGURES 31-48:CHARACTERIZATIONS OF RD 4, 13, 14, 27, 29 AND 39.....	61-78
FIGURES 49-54:BBBTR CHROMATORGRAMS OF RD 1, 4, 14, 27, 29 AND 39.....	79-84

ABBREVIATIONS

Å: Angstrom	Reagent
ADME: Absorption Distribution Metabolism Excretion	MS: Mass spectrogram
ACN: Acetonitrile	MTT: 3-(4,5-dimethylthiazol-2-yl)-2,5-diphenyltetrazolium bromide
Akt: Protein kinase B	MW: Molecular weight
ATM: ataxia telangiectasia mutated	NBT-BCIP: Nitro-Blue Tetrazolium and 5-bromo-4-chloro-3'-indolyphosphate
ATR: ataxia telangiectasia and Rad3-related protein	NMR: Nuclear Magnetic Resonance
BAII: Brain-specific angiogenesis inhibitor 1	NOXA: Phorbol-12-myristate-13-acetate-induced protein 1
BAX: BCL2-associated X protein	P14ARF: p14 alternate reading frame
CDK: Cyclin-dependent kinase	P53AIP1: Tumor protein p53 regulated apoptosis inducing protein 1
CHK1: checkpoint kinase 1	P+2: Parent compound (in LC/MS= M+1) plus 2
CHK2: checkpoint kinase 2	PAMPA: Parallel Artificial Membrane Partition Assay
CLogP: Calculated LogP	PBS: Phosphate Buffered Saline
CNS: Central Nervous System	PERP: p53 apoptosis effector related to PMP-22
DMSO: Dimethyl Sulfoxide solvent	PIDD: p53-induced death domain protein
DTT: Dithiothreitol	PVDF: polyvinylidene difluoride
EGFR: Epidermal growth factor receptor	Ras: rat sarcoma
ET₃N: Triethylamine	RD #: Sequential number of compound synthesized in Dr. Doll's lab (RISE)
GADD45: growth arrest and DNA damage	RPMI: Roswell Park Memorial Institute
GAP-DH: Glyceraldehyde 3-phosphate dehydrogenase	SAR: Structure Activity Relationship
GBM: Glioblastoma Multiforme	SDS: Sodium dodecyl sulfate
GD-AIF: glioma-derived angiogenesis inhibitory factor	TBS: TRIS-buffered Saline
HPV: human papillomavirus	TGS: Tris-Glycine
kDa: Kilodaltons	TI: Therapeutic Index
KILLER/DR5: death receptor 5	TLC: Thin Layer Chromatography
LC/MS: Liquid Chromatography Mass Spectroscopy	tPSA: Topological Polar Surface Area
M+1: Molecular weight plus 1 (addition of H atom)	TMZ: Temozolomide
Maspin: mammary serine protease inhibitor	TRIS: tris(hydroxymethyl) aminomethane
MDM2: mouse double minute 2 homolog	Trypsin-EDTA: Trypsin-Ethylenediaminetetraacetic acid
MGMT: O-6-methylguanine-DNA methyltransferase	TSP1: Thrombospondin 1
MPER: Mammalian Protein Extraction	XRCC4: X-ray repair cross-complementing protein 4

Drug Discovery Efforts Targeting Mutant p53 for the Treatment of Glioblastoma

Randa R. Barsoom and Dr. Ronald J. Doll

INTRODUCTION

Cancer

The devastating effects of cancer are universally known and felt. In a census published annually by the American Cancer Society, it was estimated that in 2013, there were over 1.6 million new cases of cancer, with over half a million deaths due to cancer in the United States, alone (2013, American Cancer Society, Inc., Surveillance Research). Cancer has been cited as the leading cause of death in people ages 40-79, and the second leading cause of death, nationally (Siegel et al. 2013). The causes of cancer can vary greatly and can include environmental factors, such as exposure to pesticides, asbestos, tobacco, etc. (Christiani, 2011), viral infections (Mesri et al. 2014), genetics, and spontaneous mutations (Gordon, et al, 2012). Any single one of these factors can lead to any one of over 200 types of cancer (Jemal et al. 2011).

Treatment of cancer largely depends on the type of cancer. With every kind of cancer, strategies and the aggressiveness widely vary (Edwards et al. 2005). In many cases, treatment of cancer involves several surgeries and/or various rounds of chemotherapy and radiation therapy, depending on how advanced the cancer is, precise locations of tumors, and other factors, including aggressiveness of the specific cancer. With any surgery, many risks are involved, including chances of infection and long recovery times. The alternatives, chemo and radiation therapies have detrimental effects

on the whole body. Instead of focusing only on the tumor, the therapies are nonspecific, causing many unpleasant side effects including gastrointestinal problems, hair loss, immunodeficiency, cognitive effects, etc. (Tager et al. 2010).

There are several types of chemotherapy, some administered alone, others in combination to maximize effects. Chemotherapy drugs, unfortunately, target aspects of the cell that are not exclusive to just tumors; thus, causing harm to normal cells throughout the body, as well. For example, commonly used chemotherapy drugs include topoisomerase inhibitors (Zhao et al. 2012), which work on the topoisomerase I and topoisomerase II enzymes that aid in the unwinding of DNA during cell replication. Other examples include antimetabolite drugs (Liekens et al. 2009), alkylating agents (Minotti et al. 2004), and anti-microtubule drugs (Yue et al. 2010). Because DNA replication is a necessary process for most cells, interfering with metabolites, microtubules, DNA, etc. incurs more damage, even to the healthy cells.

While not every cancer diagnosis leads to a fatality, treatment is often aggressive and degenerative to many parts of the body (Coates et al. 1983). Thus, a drug that is both effective and specific to the tumor would be highly advantageous and favorable to any cancer patient. However, to develop such a drug, specific aspects of the overarching category of cancer must first be understood and assessed.

The hallmark of cancer is uncontrolled cell growth and tissue invasion as a result of accumulations of mutations in a cell (Anand et al. 2008); thus, cancer has generally been believed to be a disease of the genome (Hanahan et al. 2011). These mutations result in oncogenic alteration of proteins, such as growth factor receptors, signal

transduction proteins, transcription factors, DNA repair enzymes, cell-cycle control proteins such as cyclins, and apoptosis regulating proteins such as p53 (Dingli et al. 2006; Greenblatt et al. 1994).

Cell Replication and p53 Activation

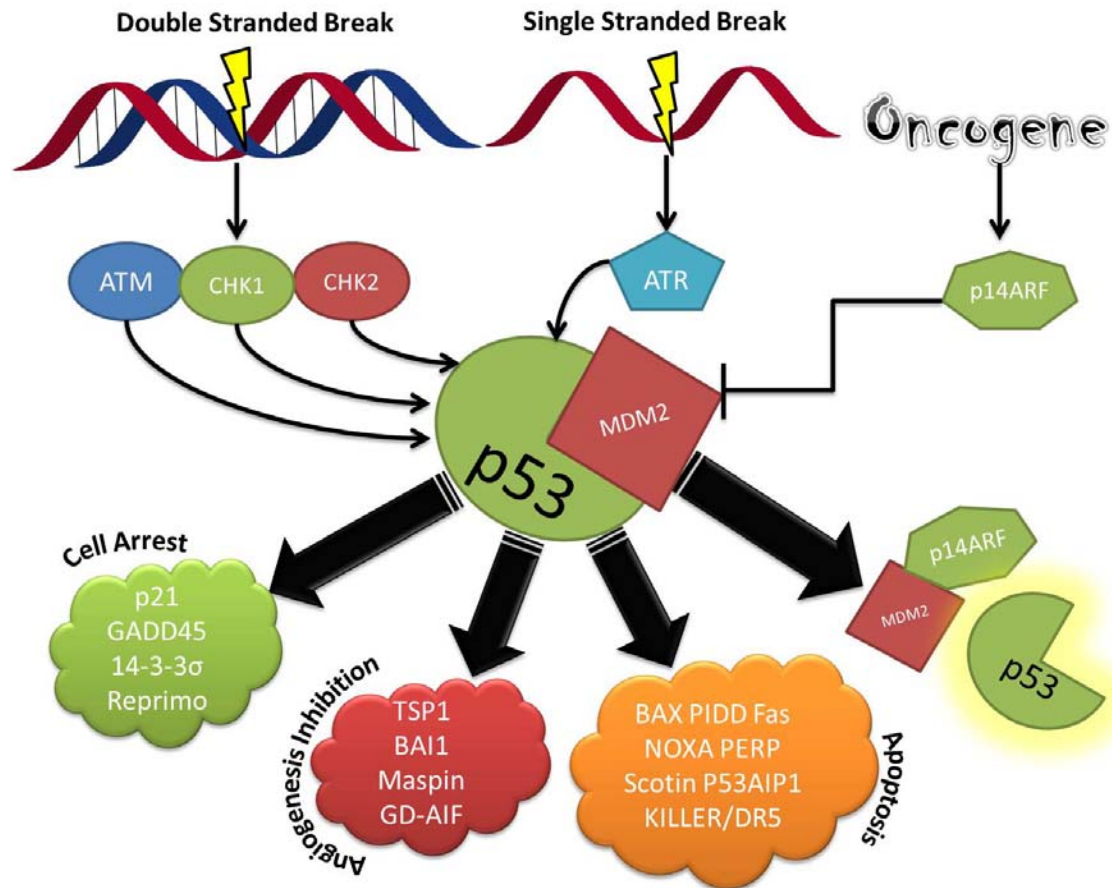


Figure 1: Some mechanisms by which p53 can be reactivated in the presence of a double stranded DNA break, single stranded DNA break, and oncogene expression. Activation of p53 can lead to cell arrest, angiogenesis inhibition, and/or apoptosis. Additionally, when p14ARF inhibits MDM2, p53 dissociates from MDM2 and becomes active.

Dividing cells pass through the process of cell division continuously throughout their lives. This cycle is divided into phases (G_1 , S, G_2 , and M). Regulation of this cycle

is conducted through combinations of cyclins and cyclin-dependent kinases (CDK) (Nigg 1995). CDK is activated by binding to cyclin; thus, allowing CDK to phosphorylate downstream proteins. The combination of CDK-cyclin determines which proteins are phosphorylated (Truman et al. 2012). Phosphorylation of a protein can work to either activate or inhibit the protein, depending on its properties. This system of phosphorylation drives the cell into the phases of cell division, but can also work to arrest the cell in the case of a DNA mutation.

Along the process of cell division, there are certain checkpoints that the cell must pass before completing necessary steps (Elledge 1996; Pietsenpol et al 2002). These checkpoints exist mainly at the junctions between G₁/S and G₂/M and act like “border-patrol”, working to detect DNA damage using sensor mechanisms (Li et al. 2004), some of which are associated with DNA replicase. Multiple stimuli stemming from DNA damage can activate the checkpoints allowing them to signal proteins that can attenuate cell division, to allow time for repair, or target the cell for apoptosis.

DNA damage is communicated throughout the cell through signaling that activates kinases. A double stranded break in the DNA can activate ataxia telangiectasia mutated (ATM) (Abraham 2001), checkpoint kinase 1 (CHK1) (Ma et al. 2011), checkpoint kinase 2 (CHK2) (Smith et al. 2010), while single stranded damage leads to ataxia telangiectasia and Rad3-related protein (ATR) activation (Sorensen et al. 2012). These kinases can then cause the phosphorylation of proteins that activate the proper checkpoint, leading to cell arrest. The targets of ATM, CHK1, CHK2, and ATR commonly include tumor suppressors, such as p53 (Vogelstein et al. 2000). When p53 is

activated (some activating mechanisms of p53 are summarized in Figure 1), the expression of p21, growth arrest and DNA damage (GADD45), 14-3-3 σ , and Reprimo are stimulated. These proteins then arrest the cell cycle by various mechanisms. For example, p21 works to arrest the cell cycle by inhibiting CDKs that would normally promote the transition of the cell into the next phase of the cell cycle. Additionally, 14-3-3 σ inhibits the binding of cyclin B1 and CDK1 outside the nucleus to block the cell from leaving G₂ and entering into mitosis. GADD45 also arrests the cell in G₂ by a similar mechanism. During the cell arrest, DNA repair proteins, such as X-ray repair cross-complementing protein 4 (XRCC4) are activated and/or recruited (Yurchenko et al. 2006).

Because phosphorylation and acylation of p53 (that cause activation) can occur on multiple sites by multiple kinases, the expressions of proteins downstream of p53 can vary depending on the stimuli, and are not limited to proteins responsible for cell cycle arrest (Vousden et al. 2002; Slee et al. 2004). Consequently, the varying stimuli on p53 can also induce the expression of proteins that target the cell for apoptosis and proteins that inhibit angiogenesis (Vogelstein et al. 2000). These proteins include BCL2-associated X protein (BAX) (Morris et al. 2001), Scotin (Bourdon et al. 2002), p53 apoptosis effector related to PMP-22 (PERP) (Attardi et al. 2000), Phorbol-12-myristate-13-acetate-induced protein 1 (NOXA) (Oda et al. 2000), death receptor 5(KILLER/DR5) (Wu et al 2002), Tumor protein p53 regulated apoptosis inducing protein 1 (P53AIP1) (Oda et al. 2000), Fas (Bennett et al. 1998), and p53-induced death domain protein (PIDD) (Berube et al. 2005). BAX, NOXA, and P53AIP1 are located in the mitochondria

(Vogelstein et al. 2000), allowing for the production of excess of toxic reactive oxygen species that kill the cell. The other proteins mimic the “death signal”, which stimulates the proteins that target the cell for apoptosis. In addition to cell arrest and promoting apoptosis, activated p53 can also stimulate the expression of proteins that inhibit angiogenesis (new blood vessel formation) (Vogelstein et al 2000). These proteins include: Thrombospondin 1 (TSP1), Brain-specific angiogenesis inhibitor 1 (BAI1), mammary serine protease inhibitor (Maspin), and glioma-derived angiogenesis inhibitory factor (GD-AIF).

While p53 can be activated by kinases that are signaled in the event of DNA damage, it can also become active when mouse double minute 2 homolog (MDM2) is inhibited. MDM2 works to repress p53 activity by binding to it. This is the common status of MDM2/p53 in the normal cell. However, the complex between MDM2 and p53 may be broken by phosphorylation of MDM2 using proteins such as p14 alternate reading frame (p14ARF), which are stimulated when oncogenes are expressed (Vogelstein et al. 2000). An oncogene is defined as a gene that has been mutated and has the potential to cause cancer (McCormick 1999). One of the most common oncogenes is rat sarcoma (Ras) (Goodsell 1999). When expressed, Ras activates proteins that promote cell growth and survival—ultimately, producing a cancerous cell. Thus, as the oncogene is expressed, p14ARF continues to inhibit MDM2, leading to the disassociation of MDM2 and p53, which stimulates p53 activity, leading to the expression of proteins that cause cell cycle arrest, apoptosis, and angiogenic inhibition.

Activation of p53 is only stimulated in the presence of a DNA mutation or

damage. Without the damage, p53 is available in the cell, but is bound to MDM2 and its activity is repressed (Vogelstein et al 2000). Additionally, proteins downstream of p53 are not all produced simultaneously, but depend on the stimulus activating p53 (Slee et al. 2004).

Mutant p53

While p53 was only first discovered in 1979, a lot of work has gone into understanding its functions and mutations (Vogelstein 2010). The functions of p53 are crucial for eluding the accumulation of cancer-causing mutations (Liu, et al 2013). However, like any protein, p53 can suffer genomic alterations, due to toxins, viral infections, genetics, etc., leading to mutations that alter the conformation of p53 (Levine et al. 1991). Studies have indicated that viral infections, such as human papillomavirus (HPV) may cause p53 mutations (Jakate et al. 1993).

When p53 is mutated, cells containing oncogenic mutations continue to proliferate, resulting in cancer (Chen et al. 1990). The mutations on p53 commonly occur in six positions – Arg-248, Arg-273, Arg-175, Gly-245, Arg-249, Arg-282 (Joerger, et al 2006). These point mutations are located in the DNA binding domain, causing a conformational shift in p53, leading to the inability of p53 to bind to DNA (a necessary step for p53 to activate the expression of proteins downstream).

Glioblastoma Multiforme

Mutant p53 is found in nearly 50% of all human cancers (Shaheen, et al 2011). One significant type of cancer in which mutant p53 is found is glioblastoma multiforme (GBM), the most common and most aggressive brain cancer (Raoofian et al. 2013). Prognosis for GBM typically varies between five months to less than four years, with a median of around a year (Johnson et al. 2012). Risk factors for developing GBM include age (typically above 50), exposure to previous radiotherapy, having multiple CT scans at an early age, and carrying traits for genetic disorders such as neurofibromatosis, tuberous sclerosis, Von Hippel-Lindau disease, Li-Fraumeni syndrome, and Turcot's syndrome (Ohgaki et al. 2005). There are two types of GBM: primary (or de novo) and secondary. The first is an occurrence of a tumor that was not preceded by another type of brain tumor (Clarke et al. 2013). It is believed to be the more aggressive of the two types with prognosis being around 8 months. Secondary GBM grow more slowly than primary, but occur subsequent to other lower-grade tumors, such as astrocytoma (Ohgaki et al. 2007).

Studies have indicated the significance of p53 in GMB. In one study, mutant p53 was reported in 28% of primary GBM cases and 65% of secondary GBM cases (Nagpal et al. 2006). While other oncogenes, such as Ras, protein kinase B (Akt), and epidermal growth factor receptor (EGFR), can be expressed in GMB (Mischel et al 2003; Rajasekhar et al. 2003), by reactivating the mutant p53, the cancer cell with the oncogenes will die.

Similar to most cancers, GBM is generally treated with surgical resection of the tumor, followed by about six weeks of radiation therapy (five times a week) in addition to

chemotherapy, such as daily oral Temozolomide (TMZ) treatment (Clarke et al. 2013). TMZ is a drug that methylates DNA, causing damage to the DNA and, eventually, cell death. TMZ has been quite effective in many cancers, except those that express O-6-methylguanine-DNA methyltransferase (MGMT), which demethylates the methylated DNA (Stupp et al. 2009). Tumor cells that express MGMT require chemotherapy drugs that work by different mechanisms. Even a tumor that may initially respond to TMZ, may stop responding due to resistance. Both radiation and TMZ treatments are non-specific to the tumor, damaging non-tumor cells in the body. They rely heavily on the rapid multiplication of the tumor cells to inflict the most damage to them rather than the healthy cells in the body (Shaheen et al. 2011). Even with the various treatment methods, prognosis for GBM patients remains only in months. Thus treatments rarely provide a permanent means of eliminating the cancer. In fact, the five-year survival rate of patients is 1.9% (Johnson et al. 2012). However, with the use of TMZ, this percentage has increased to 9.8% five-year survival rate.

In addition to general treatments, targeted approaches are also in development. For example, studies have indicated that there are common mutations in the sodium ion channels of the GMB tumor cells that may be a novel target for anti-cancer therapies (Joshi et al. 2011). This study indicated that targeting GBM cells with cardiac glycosides such as digoxin and ouabain induces more tumor cell death than death of normal cells. While this treatment seems promising, it was only tested *in vitro*; so, it is still unclear if the drugs will have other off target effects throughout the body.

Treatment of GBM is further complicated because the tumor is in the brain. The brain is protected from toxins and drugs in the systemic plasma by the blood brain barrier (BBB), making development of CNS drugs especially difficult (Siti, 2010).

Blood Brain Barrier (BBB)

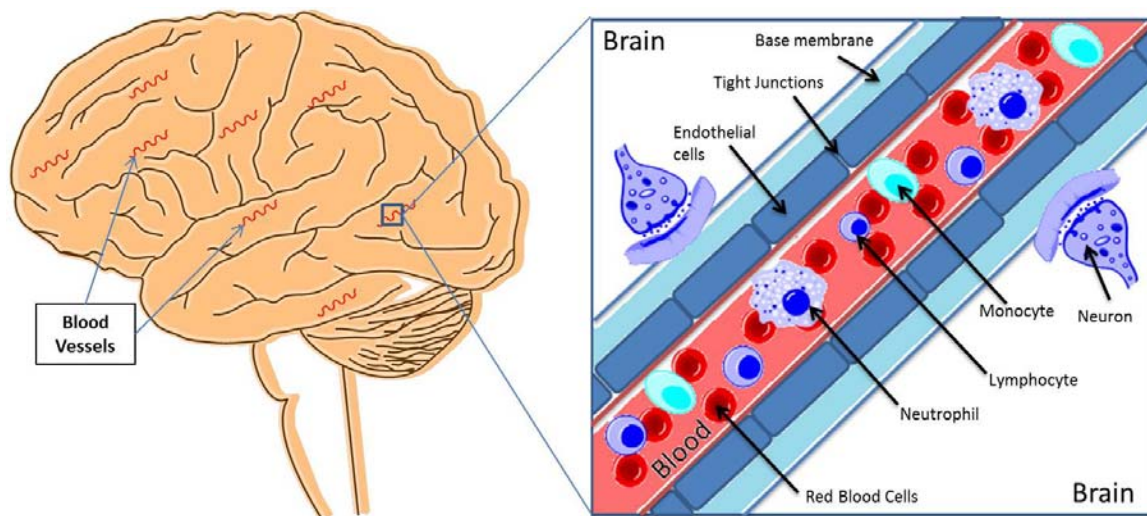


Figure 2: cellular model of the blood brain barrier. A close up of a blood vessel in the brain reveals tightly packed endothelial cells and a membrane lining the blood vessel. Thus, all transport in and out of the blood vessel is very selective. Figure was created using ChemBio Draw ®.

As a CNS drug, the compound must transport or cross the blood brain barrier (BBB) (Figure 2). The BBB is a group of tightly packed brain endothelial cells separating the brain from the rest of the body (Di et al. 2003). It functions as a selectively permeable gate, allowing for and inhibiting transport of drugs, proteins, bacteria, etc. The membrane relies heavily on the tight junctions between the cells (Armulik et al. 2010), but also features transport channels and active transporters that line the membrane and are very selective for certain substrates (Gabathuler, 2010). This provides extra difficulty in the

drug discovery process as the most effective drug may be impossible to enter into the CNS. In fact, more than 90% of drugs on the market today do not cross the BBB.

Literature indicates that molecular properties such as size, lipophilicity, topological polar surface area (tPSA)¹, LogP or calculated log (CLogP)², etc. can be used to predict which compounds may cross the BBB (Liu, 2004). Common compounds and molecules that cross the BBB include glucose, oxygen, carbon dioxide, and many lipophilic structures (Rubin 1999). Literature also states that compounds with tPSA>80 Å do not cross the BBB (Muehlbacher et al. 2011). Additionally, those with CLogP>6.1 may have difficulty crossing the BBB (Jeffrey et al. 2010). (Both the CLogP and tPSA are calculated via a commercial software) These predictions are accurate for many of the leading CNS drugs available today.

Project Goal

The common approaches to treating cancers have generally included surgery and combinations of radiation and chemotherapies. However, each of these treatments led to off-target effects such as hair loss, immunosuppression, gastrointestinal issues, infections, etc. To avoid these complications, a more targeted approach to treating the cancer that is less harmful to healthy tissue is necessary. One approach would be to identify compounds that would reactivate mutant p53, thus restoring its normal biological activity. The effects on normal cells would be minimized with these compounds because normal cells

¹ Sum over polar atoms—OH, NH, etc.; measured in angstroms (Å).

² Partition coefficient of a compound between octanol and water; usually expressed as LogP or CLogP (calculated LogP).

do not possess activate p53. Thus, the compounds should only work on the tumor cells. Of course, such compounds must possess effective drug-like properties that would allow them to be suitable for brain cancer therapy.

Recent literature reports disclose small organic compounds that reactivate mutant p53 in human tumor cells. One such example is Prima-1, a development compound reported to reactivate mutant p53 (Wiman, 2010), but that was later shown to be working by other mechanisms (Cui et al. 2014), including forming covalent bonds with mutant p53 as well as causing apoptosis in p53 null cells (cells without p53) (Lambert et al. 2009). This means that Prima-1 could cause general toxicity to the cells, making Prima-1 a poor drug for the treatment of cancers with mutant p53.

Another compound, CP-31398 provided very promising results in its ability to induce apoptosis in cancer cells with mutant p53 (Takimoto et al. 2002). However, the compound was highly toxic to healthy cells due to its binding to DNA, as well (Wang et al. 2003). In a review published in 2003, it was suggested that small organic compounds that reactivate mutant p53 would be very advantageous and effective if they possessed properties of selectivity to tumor cells, limiting their toxicity to healthy cells (Bykov et al. 2003).

Thus, this project has aimed to develop small organic molecules that will bind to and reactivate mutant p53. This would allow for the targeted apoptosis of tumor cells, with decreased toxicity to healthy cells. This is because in normal cells, p53 is not activated. Thus, the compounds should not affect p53 in normal cells. The steps in the drug discovery process followed are detailed below.

The Drug Discovery Process

The drug discovery process followed in the pharmaceutical industry can be summarized as follows:

1. Identify and validate biological targets responsible for the disease state
(Mutant p53 is the accepted biological target for this project)
2. Identify potential lead structures and test their activity in the assays
3. Optimize the lead structures for potency, selectivity, and drug like properties
4. Perform *in vivo* efficacy studies on promising compounds

Productivity in all of the drug discovery steps, except *in vivo* efficacy studies, will be demonstrated. Drew does not have the necessary facilities to perform *in vivo* anti-tumor studies with human tumors in immune compromised mice. A large part of the discussion involves the synthesis and characterization of the compounds and the development assays and evaluation of drug like properties of these compounds. Good drug like properties, as pertaining to this project, include a suitable human metabolic rate and the ability of these compounds to cross the blood brain barrier (BBB), in addition to the compound's potency and selectivity for mutant p53 in tumor cell lines. Thus, the drug discovery approach guiding this project followed these steps:

1. Identify suitable lead structures that work on the biological target, mutant p53
2. Synthesize analogous structures to optimize potency, selectivity, and drug-like

properties

3. Evaluate the potency and selectivity of compounds in human tumor cell assays
4. Develop an assay to determine transport across the BBB membrane
5. Develop an assay that measures the relative human metabolic rate for compounds
6. Optimize the lead structures to improve the total profile of the compounds

In the design of the compound targets, Lipinski's Rule of Five (Lipinski et al. 2012) served as a guide. This is an empirical rule based on 73 marketed drugs that states that a compound should have good oral drug like properties if a compound:

1. Has a molecular weight less than 500 Daltons
2. Has no more than 5 hydrogen bond donors
3. Has no more than 10 hydrogen bond acceptors
4. Has a LogP, or CLogP no greater than 5

All of the synthesized compounds discussed here are within the guidelines of Lipinski's rules.

MATERIALS AND METHODS

Synthesis of Analogous Structures

All starting materials were available commercially from Sigma-Aldrich or Acros Organics. All reactions were run under nitrogen or dry air using a drying tube and final products were purified to at least 95% purity, as specified by the American Chemical Society. Compounds were then characterized using nuclear magnetic resonance (NMR) and liquid chromatography mass spectroscopy (LC/MS).

NMR spectra were recorded on a 400 MHz, Bruker instrument. Chemical shifts were expressed in ppm (δ) relative to Tetramethylsilane (TMS), the accepted standard for calibrating chemical shift in NMRs. LC/MS were recorded on a Waters TOF, Micromass-MS coupled to an Agilent 1100 HPLC. The HPLC column was an Analytical, Echelon 100 x 4.6 mm C18 column with an acetonitrile (ACN)-water mobile phase flow rate of 1.5 mL/min and the following gradient: 0 min 30% ACN, 8 min 70% ACN, 9 min 70% ACN, 11 min 80% ACN, 12 min 85% ACN, 13 min 30% ACN, 15 min 30% ACN. Purified and characterized compounds were designated with “RD numbers”, sequential numbers given to compounds from the Ronald Doll lab, and stored in glass containers at room temperature.

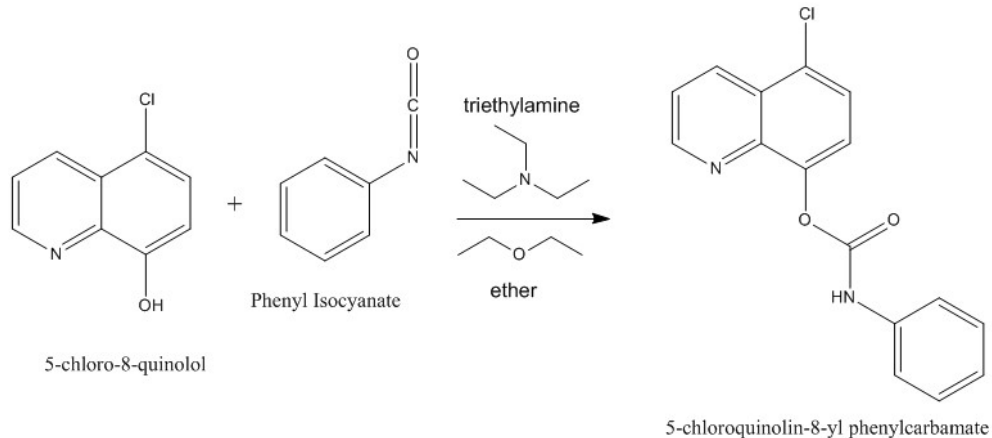
RD 1 Synthesis

Figure 3: Reaction mechanism of RD 1 depicts the reaction between 5-chloro-8-quinolol and phenyl isocyanate in ether and Et₃N to produce 5-chloroquinolin-8-yl phenylcarbamate, RD 1

Synthesis of RD 1 was performed using a 100-ml round bottom flask charged with 20 ml of ether, 0.5 g (2.784 mmol) of 5-chloro-8-quinolol, 0.3 ml (2.784 mmol) of phenyl isocyanate, and 3 drops of triethyl amine (Et₃N) (Figure 3). The reaction was allowed to take place overnight at room temperature while stirring magnetically. The supernatant was then extracted and solid product was washed three times with ether. The precipitate was then filtered and solid product was washed three times with ether. Total yield was 0.76 g (91.57%). To confirm purity, the compound was characterized using LC/MS (Figures 18 and 19) and NMR (Figure 20) analyses.

MS Electrospray-TOF, $m/z = 299$, M+H

NMR H (400 MHz, DMSO) 10.5 (H, s, NH), 10.2 (H, s, NH), 9.1 (1H, d, 2-quinoline aromatic), 8.6 (1H, d 4-quinoline aromatic), 7.9 (1H, d, 6-quinoline aromatic), 7.8 (1H, m, 3-quinoline aromatic), 7.6 (2H, d, ortho-phenyl), 7.6 (2H, t, meta-phenyl), 7.1 (1H, m, para-phenyl)

RD 4 Synthesis

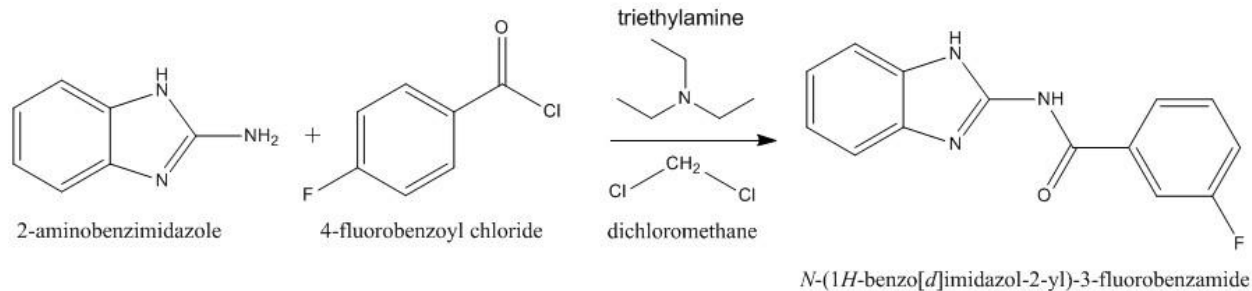


Figure 4: Reaction mechanism of RD 4 depicts the reaction 2-aminobenzimidazole and 4-fluorobenzoyl chloride in dichloromethane and Et₃N to produce N-(1 H-benzo[d]imidazole-2-yl)-3-fluorobenzamide, RD 4

The synthesis and characterization of RD 4 was conducted by colleague, Megan McAleavy. A 3-neck round bottom flask was charged with 25 ml of anhydrous dichloromethane, 0.5 g (3.76 mmol) of 2-aminobenzimidazole, and 0.524 ml (3.76 mmol) of triethylamine. 4-fluorobenzoyl chloride (0.45 ml; 3.76 mmol) was then added in, dropwise (Figure 4). The reaction was allowed to take place overnight at room temperature while stirring magnetically. The mixture was then washed with 20 ml NaHCO₃, followed by 20 ml of brine, dried over magnesium sulfate and concentrated under vacuum. The crude product was recrystallized in about 60 ml ethyl acetate and 10 ml hexane and cooled in freezer. Total yield was 0.9 g (93.75%). To confirm purity, compound was characterized using LC/MS (Figure 31 and 32) and NMR (Figure 33) analyses.

MS Electrospray-TOF, m/z = 256 (M+H)

¹H NMR (400 MHz, DMSO) 12.3(1H, s, NH), 8.3(2H, m, 4,7-benzimidazole aromatic), 7.5(2H, m, 5,6-benzimidazole aromatic), 7.4 (2H, m meta-phenyl), 7.1(2H, ortho-phenyl)

RD 13 Synthesis

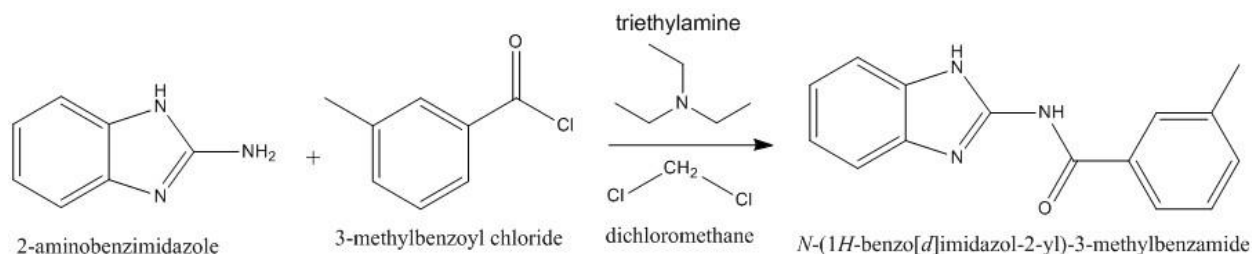


Figure 5: Reaction mechanism of RD 13 depicts the reaction 2-aminobenzimidazole and 3-methylbenzoyl chloride in dichloromethane and Et₃N to produce N-(1 H-benzo[d]imidazole-2-yl)-3-methylbenzamide, RD 13

This synthesis and characterization of RD 13 was conducted by colleague, Megan McAleavy. A 100 ml round bottom flask was charged with 25 ml of anhydrous dichloromethane, 0.5 g (3.76 mmol) of 2-aminobenzimidazole, 0.5241 ml (3.76 mmol) of triethyl amine (Et₃N). 4-fluorobenzoyl chloride (0.43 ml 3.76 mmol) was then drop-wise over 15 minutes (Figure 5). The reaction was allowed to take place overnight at room temperature while stirring magnetically. The mixture was then washed with 20 ml NaHCO₃, followed by ethyl acetate and methylene chloride. The solution was dried over magnesium sulfate and concentrated under vacuum. The crude product was recrystallized in ethanol yielding 0.4 g (42.55%). To confirm purity, compound was characterized using LC/MS (Figure 34 and 35) and NMR (Figure 36) analyses.

MS Electrospray-TOF, $m/z = 252$ (M+H)

¹H NMR (400 MHz, DMSO) 12.4(2H, s, NH), 7.9(2H, m, ortho-phenyl), 7.4(4H, m, 4,5,6,7-benzimidazole aromatic), 7.1 (2H, m meta and para-phenyl), 3.4 (3H, s, methyl)

RD 14 Synthesis

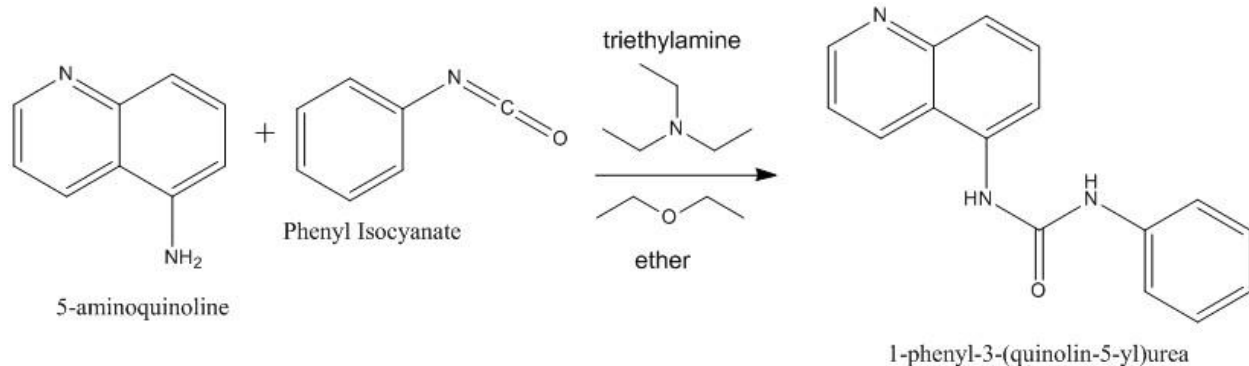


Figure 6: Reaction mechanism of RD 14 depicts the reaction between 5-aminoquinoline and phenyl isocyanate in ether and Et₃N to produce 1-phenyl-3-(quinolin-5-yl) urea, RD 14

The synthesis of RD 14 was performed using a 100-ml round bottom flask charged with 5 ml of ether, 0.1 g (0.6935 mol) of 5-aminoquinoline, 0.075 ml (0.6935 mol) of phenyl isocyanate, and 3 drops of -Et₃N were added (Figure 6). The reaction was allowed to take place overnight at room temperature while stirring magnetically. The precipitate was filtered and solid product was washed three times with ether. The compound was then recrystallized in 3 ml of ACN. After cooling on ice, mother liquor was decanted and a TLC of the solid indicated purity. Total yield was 0.16 g (90.41%). To confirm purity, compound was characterized using LC/MS (Figure 37 and 38) and NMR (Figure 39) analyses.

MS Electrospray-TOF, $m/z = 264.09$ (M+H)

¹H NMR (400 MHz, DMSO) 9.1(1H, s, NH), 8.86(1H, d, 2-quinoline aromatic), 8.82 (1H, s, NH), 8.46(1H,d, 4-quinoline aromatic), 8.03 (1H,dd 6- quinoline aromatic), 7.67 (2H, m, 7,8-quinoline aromatic), 7.61 (1H, dd, 3-quinoline aromatic), 7.43 (2H, d, ortho-phenyl), 7.23 (2H, t, meta-phenyl), 7.0 (1H, t, para-phenyl)

RD 27 Synthesis

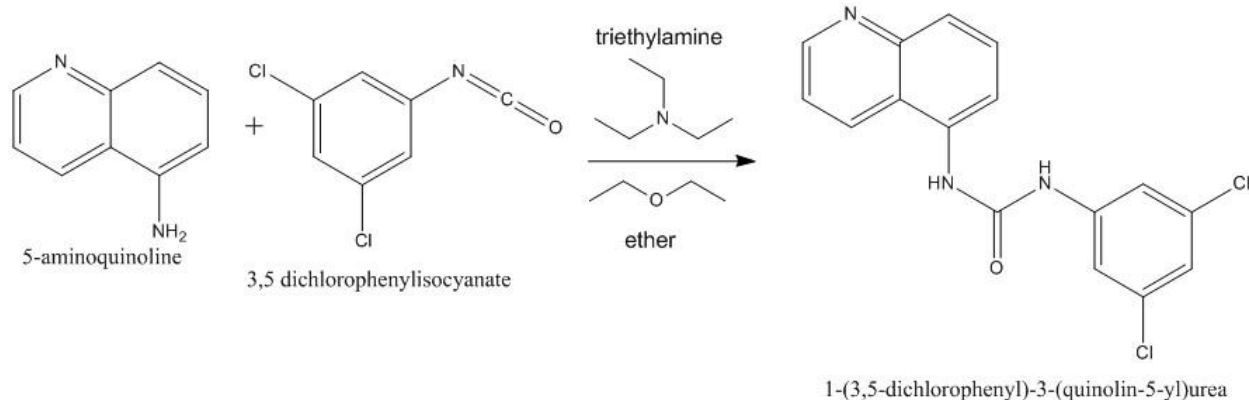


Figure 7: Reaction mechanism of RD 27 depicts the reaction between 5-aminoquinoline and 3,5 dichlorophenylisocyanate in ether and Et₃N to produce 1-(3,5-dichlorophenyl)-3-(quinolin-5-yl) urea, RD 27

The synthesis of RD 27 was performed using a 100-ml round bottom flask charged with a nitrogen inlet tube and a magnetic stir bar. To the flask, 10 ml of ether, 0.1 g (0.6935 mol) of 5-aminoquinoline, 0.1304 g (0.6935 mol) of 3,5-dichlorophenylisocyanate, and 3 drops of -Et₃N were added (Figure 7). The reaction was allowed to take place overnight at room temperature while stirring magnetically. The reaction was allowed to take place overnight at room temperature while stirring magnetically. The precipitate was filtered and solid product was washed three times with ether. To confirm purity, compound was characterized using LC/MS (Figure 40 and 41) and NMR (Figure 42) analyses.

MS Electrospray-TOF, $m/z = 332$ (M+H)

¹H NMR (400 MHz, DMSO) 9.4(1H, s, NH), 9.1 (1H, s, NH), 9.2(1H, d, 2-quinoline), 8.0(1H, d, 4-quinoline), 7.8(2H, m, 3 and 6-quinoline), 7.65(1H, m, 7-quinoline), 7.60(2H, s, 2 and 6-phenyl), 7.2(1H, s, 4-phenyl)

RD 29 Synthesis

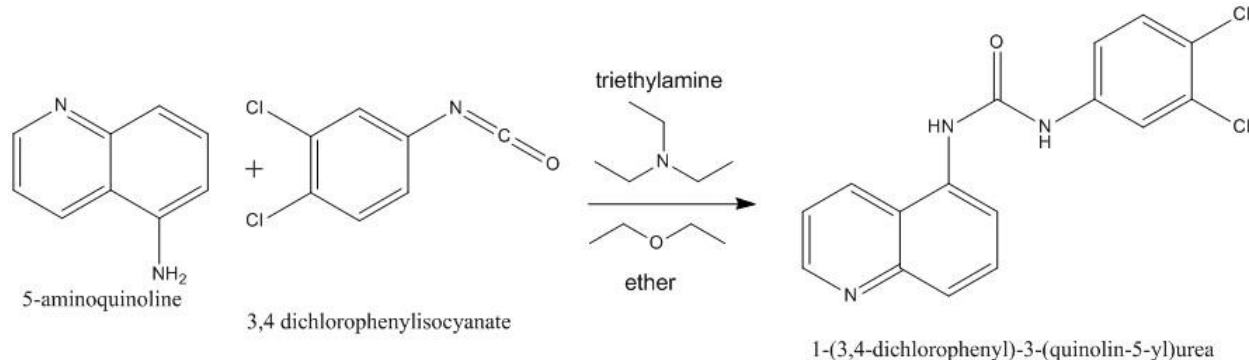


Figure 8: Reaction mechanism of RD 29 depicts the reaction between 5-aminoquinoline and 3,4 dichlorophenylisocyanate in ether and Et₃N to produce 1-(3,4-dichlorophenyl)-3-(quinolin-5-yl) urea, RD 29

The synthesis of RD 29 was performed using a 100-ml round bottom flask charged with a nitrogen inlet tube and a magnetic stir bar. To the flask, 5 ml of ether, 0.1 g (0.6935 mol) of 5-aminoquinoline, 0.1304 g (0.6935 mol) of 3,4-dichlorophenylisocyanate, and 3 drops of -Et₃N were added (Figure 8). The reaction was allowed to take place overnight at room temperature while stirring magnetically. The precipitate was filtered and solid product was washed three times with ether. A recrystallization in ACN/water was then performed. To confirm, the compound was characterized using LC/MS (Figure 43 and 44) and NMR (Figure 45) analyses.

MS Electrospray-TOF, m/z = 332 (M+H)

¹H MNR (400 MHz, DMSO) 9.3(1H, s, NH), 9.0 (1H, s, NH), 8.9(1H, d, 2-quinoline), 8.5(1H, d, 4-quinoline), 8.0(2H, m, 6 and 8-quinoline), 7.8(2H, m, 3 and 7-quinoline), 7.7(1H, m, 5-phenyl), 7.6(1H, d, 2-phenyl), 7.4(1H, d, 5-phenyl).

RD 39 Synthesis

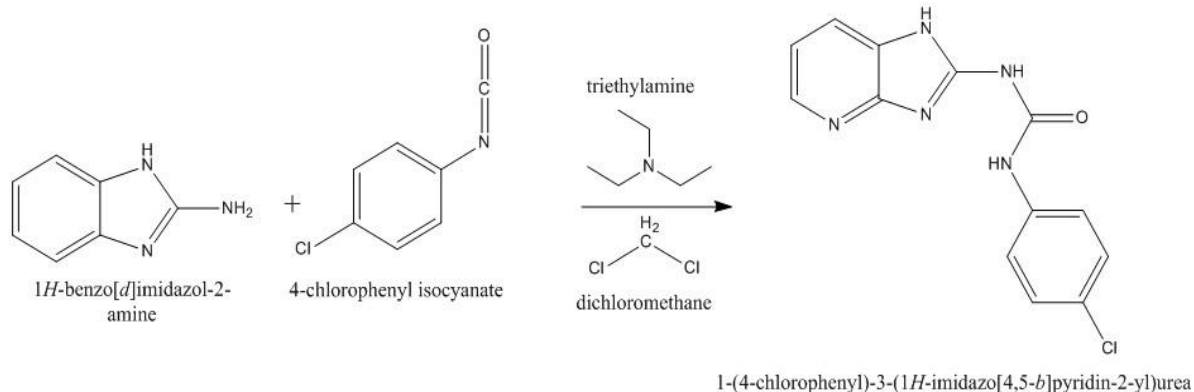


Figure 9: Reaction mechanism of RD 39 depicts the reaction between 1H-benzo[d]imidazol-2-amine and 4-chlorophenyl isocyanate in dichloromethane and Et₃N to produce 1-(4-chlorophenyl)-3-(1H-imidazo[4,5-b]pyridine-2-yl)urea, RD 39

The synthesis and characterization of RD 39 was conducted by colleague, Taras Varshavsky. A 100 ml round bottom flask was charged with 25 ml of anhydrous dichloromethane, 0.2 g (1.5 mmol) of 1H-benzo[d]imidazol-2-amine, 0.23 g (1.5 mmol) of 4-chlorophenyl isocyanate, and 3 drops of triethyl amine (Et₃N) (Figure 9). The reaction was allowed to take place overnight at room temperature while stirring magnetically. The mixture was washed then with 20 ml of water, dried over magnesium sulfate, and concentrated under vacuo. The crude material was recrystallized in 250 ml acetonitrile giving the product as a white solid, To confirm purity, the compound was characterized using LC/MS (Figure 46 and 47) and NMR (Figure 48) analyses.

MS Electrospray-TOF, $m/z = 287$ (M+H)

¹H NMR (400 MHz, DMSO) 11.4(1H, s, NH), 9.6(1H, s, NH), 7.64(2H, d, 4,7-quinoline), 7.36 (3H, m, 5,6-benzimidazole, ortho-[phenyl]), 7.10 (2H,m, meta-phenyl)

Developing the necessary human tumor cell assays to identify active compounds

The activity of a compound to reactivate mutant p53 was measured by assessing presence of p21, a protein produced downstream of active p53. The production of p21 was followed using western blot analysis. This procedure was largely conducted by members of the Dr. DasMahapatra lab.

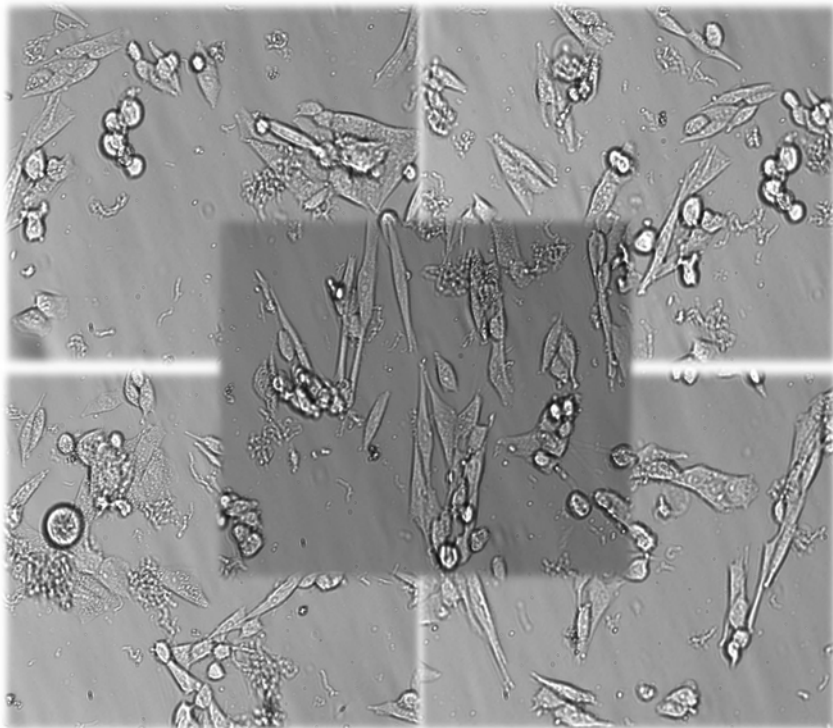


Figure 10: image of SF295 GBM cells under 100x magnification

Glioblastoma SF295 cells (with mutant p53) (Figure 10) were grown in an incubator (5% CO₂ at 37°C) and plated at 200,000 cells/well in RPMI media (enriched with 10% Fetal Bovine Serum and 10% Penicillin Streptomycin) in a 6-well dish (max 2 mL media per well). Purified and analyzed RD compounds were diluted from 100% DMSO to less than 1% DMSO (40 mL compound + 360 mL RPMI). The cells were treated with 150 mL of diluted compounds, making the final drug concentration 15

$\mu\text{g/mL}$. The dishes were then incubated (5% CO_2 at 37°C) for 16-18 hours.

After incubation, the media was removed from dishes and the wells were washed with 1X PBS (5 mL 10X PBS + 45 mL deionized water). After an addition of 0.8 mL Trypsin-EDTA to each well, the plates were placed in the incubator (5% CO_2 at 37°C) for 5-7 minutes, or until cells were dislodged. After removal of the plates from the incubator, 1 mL RPMI was added to each well and entirety of liquid was collected and placed in 2 mL microcentrifuge tubes. The tubes were then spun down in centrifuge (5000 rpm for 5 minutes at 5°C). The supernatant was removed and the cell pellet was re-suspended in 200 μL PBS. The suspensions were then transferred to Eppendorf tubes and spun down again (5000 rpm for 5 minutes at 5°C). The supernatant was removed and the cell pellet was re-suspended in 70 μL MPER lysis buffer (enriched with 1% EDTA, 1% protease inhibitor and 1% DTT). The suspension was spun down again (3000 rpm for 5-8 minutes). The tubes were then incubated on ice for 30 minutes. Following incubation the tubes were spun down in centrifuge again (13,000 rpm for 15-20 minutes at 5°C). Finally, the supernatant was transferred into labeled Eppendorf tubes and placed in 20°C freezer.

The lysate was thawed when preparation for western blot procedure was complete. In Eppendorf tubes, 30 μL lysate was mixed with 3 μL loading buffer (2.5 mL Tris- HCl [at pH 6.8] + 1g SDS + 5 mL glycerol + 0.5 mL 6-mercaptoethanol + 1.25 mL EDTA + 10 mg bromophenol blue). The tubes were heated in 96°C water bath for 5 minutes. The center part of tank in assembled western blot apparatus was filled with 1X running buffer. The combs were removed from the two 10-20% Tris-Glycine gels and the gels were rinsed with the buffer.

The first well was loaded with 7 μ L of Novex Pre-Stained Molecular Marker. The remaining wells received 27 μ L of each sample. The assembly was powered on and allowed to run at 200 V for the first 5 minutes, then at 125 V for 1.75 hours (or until blue dye ran completely off gel). The transfer buffer (750 mL distilled water + 50 mL 20X TGS-SDS + 200 mL methanol) was prepared and 2 transfer cassettes, 2 spatulas, 4 foam pads, 4 disposable filter papers, and 2 nitrocellulose membranes labeled p53 on top and p21 on bottom were soaked in it.

After blue dye ran off the gel, the gels were removed and placed in transfer buffer. The “transfer sandwich” was assembled in the following order: black half of cassette on bottom, sponge, disposable filter paper, gel, nitrocellulose membrane (markings facing down), disposable filter paper, sponge. The cassettes were closed, sealed, and placed in transfer apparatus with black half of the cassette touching the black part of the tank. A bio-ice cooling unit was placed in the back of the transfer apparatus, and the tank was filled with transfer buffer. The apparatus was attached to power supply and allowed to run at 100 V for 1 hour.

After transfer, the membranes were removed and placed into dishes containing 10 mL blocking buffer (5g powdered milk + 100 mL TBS-Tween). The dishes were placed on shaker for 1-3 hours at room temperature and then left overnight in a -5°C refrigerator.

The following day, the membranes were removed from blocking solution and washed with 10-15 mL TBS-T for 10 minutes 3-4 times. The gels were cut in half horizontally to allow for separate treatment of the p53 and p21.

1° antibodies were prepared and placed on ice:

p53- (10 μ L Santa Cruz Mouse monoclonal anti-p53 + 10 mL blocking buffer) 1:1000 dilution

p21- (50 μ L BD Pharmingen Purified Mouse anti-p21 + 7 mL blocking buffer) 1:150 dilution

The membranes were treated with respective 1° antibodies and placed on shaker at room temperature for 1-3 hours, then in blocking buffer overnight in -5°C freezer. The next day, the membranes were removed from blocking buffer and washed in 10-15 mL TBS-T 4-5 times. Membranes were treated with 1° GAP-DH antibody (5 μ L anti- GAP-DH + 10 mL blocking buffer) 1:2000 dilution.

After 1 hour, the membranes were removed from 1° GAP-DH antibody and washed 3-4 times with TBS-T. The membranes were then treated with the 2° antibody (7 μ L alkaline phosphatase 2° antibody + 10 mL blocking buffer) 1:1500 dilution and stored overnight in -5°C freezer.

The next day, the membranes were washed 3-4 times with TBS-T. The NBT-BCIP substrate (tablet substrate dissolved in 10 mL distilled water) was used to visualize results. The p53 membrane was kept in dark drawer for roughly 15 minutes, then removed and washed with distilled water, so as not to over-develop. The p21 membrane stayed in substrate in a dark drawer for roughly 1 hour. The substrate was removed and the p21 membrane was washed with distilled water to stop development.

Therapeutic Index To Assess Selectivity of Compounds

Compounds that reactivate the mutant p53 in the tumor cells should induce apoptosis in those cells. To assess whether the reactivation of p53 or general toxicity is causing the tumor cells to die, an MTT assay that aimed to determine selectivity of the compound was performed. This colorimetric assay involves the addition of the dye 3-(4,5-dimethylthiazol-2-yl)-2,5-diphenyltetrazolium bromide (MTT) to wells containing the cells and a varying concentration of the compounds. MTT is reduced by cellular oxidoreductase enzymes, present in the mitochondria of cells, into formazan crystals (Meerlo et al. 2011). The crystals are purple in color, thus causing the living cells (which would have mitochondrial activity) to appear purple. Thus, this assay provides a correlation between the absorbance at 490 nm (wavelength at which purple has a maximum absorbance) to amount of living cells.

The assay was used in this study to assess the viability of p53 null cells (cells without p53) and tumor cells in the presence of varying concentrations of a compound. The procedure was performed by members of the Dr. DasMahapatra lab. A growth curve of each cell line, using formazan as an indicator, was first measured. This curve compares the number of cells to the intensity of color caused by formazan. An absorbance of 1.5 was chosen because it was a point at which enough cells would be used to incur reliable colorimetric data, but not too much as to saturate the detector. Cells in the stock solution of 5.0×10^4 cells/mL were counted using a hemocytometer. Working stock was then diluted to 2.5×10^3 cells/50 μ L. Cells, compound, and media were aliquotted into a 96 well plate. Each well received 50 μ L of cells and 20 μ L of Celltiter 96 AQueousOne Solution.

One column of the plate served as the no cells control. Another column served as a no compound control. The rest of the columns received one of eight concentrations of the compounds, including 0, 0.15, 0.30, 0.63, 1.25, 2.50, 5.00, and 10.00 $\mu\text{g/mL}$. The plate was incubated (5% CO_2 at 37°C) for 3 hours and read using Microplate Manager 5.2.1. The color developing agent added to each well, Celltiter 96 AQueousOne, causes living cells to absorb formazan. Because these cells then appear purple, absorption at a wavelength of 490 nm can be obtained. Thus, the quantity of formazan absorbed is directly proportional to the amount of living cells. This means that the higher the absorption is at 490 nm, the more formazan absorbed, the greater amount of living cells are present in the well.

The results were attained by using the average absorbance reading of the wells within a specific compound concentration. The average absorbance in the control columns was then subtracted from the concentration absorbance average, resulting in a quantification of the viability of the cells at that concentration of compound. This helped identify an EC_{50} number, which was the concentration of compound at which 50% of cells died.

The assay was performed for the tumor cells as well as the H1299 cell line (p53 null cells). The EC_{50} of the H1299 cells was compared to the EC_{50} of the tumor cells. By dividing the EC_{50} of the H1299 cells by the EC_{50} of the tumor cells, a therapeutic index (TI) can be attained, using the equation:

$$TI = \frac{\text{Apoptosis EC}_{50} \text{ H1299 Cells}}{\text{Apoptosis EC}_{50} \text{ Tumor Cells}}$$

The greater this number is, the more selective the compound is at inducing

apoptosis by reactivating mutant p53. A TI of one indicates that the cells are dying due to general toxicity rather than selectivity of reactivation of mutant p53.

Develop an assay to determine transport across the BBB membrane

To test active compounds for BBB permeability, a double chamber apparatus was assembled (Figure 15). Literature suggested an *in vitro* model that mimics the BBB. However, the recommended apparatus was unobtainable due to financial constraints. Thus, an attempt to create an apparatus, in-lab, was initiated. Trials included fabricating a new 96 well sandwich plate using Plexiglass (Figure 11). Another attempt consisted on creating a Boyden chamber out of 1 ml glass vials with a hole in the cap containing the membrane. This involved creating rubber gaskets to seal 1 ml glass vials and creating disks of a membrane to test individual compounds (Figure 12).



Figure 11: Attempt at creating improvised BBB mimicking apparatus. Here, holes are being drilled into the bottom of a 96 well plate to form a top plate onto which an artificial membrane can be placed. This apparatus failed due to the instability of the membrane on top of the hole in the plate.



Figure 12: Another attempt at creating an improvised version of the BBB mimicking apparatus. This involved the replacement of rubber in the caps of 1 ml vials with the artificial membrane. The membrane was supposed to be held in place by a rubber gasket created out of bored rubber that was originally the cap of the vial. This apparatus failed due to leaks.

When all improvised chambers failed, either by leaking or not functioning, authors from a recent *in vitro* BBB transport paper were contacted. They advised using the commercially available material described below. A new apparatus was recommended along with the procedure. A PAMPA (Parallel Artificial Membrane Partition Assay) Boyden chamber (Pion #110243 PAMPA Sandwich Plates) featuring PVDF (polyvinylidene difluoride) membrane with 0.45 μM pore size was recommended, purchased, and used as an *in vitro* model for BBB transport (Figure 13). Protocol for blood brain barrier transport assay was adapted from Li Di et al. 2003, but modified slightly. For

example, concentration of compound and lipids was doubled and wells were washed with ACN to pick up compounds stuck to walls of wells. These modifications led to duplication of experimental results as indicated in publication.

Stock solutions of compounds were made (10 mg/ml in DMSO). A portion of the each solution (10 μ l) was aliquotted and diluted (200x) in 0.05 M TRIS buffer. Porcine polar brain lipids were diluted in dodecane (40 mg/ml). According to literature (Di et al 2003), progesterone serves as a positive control while hydrocortisone serves as a negative control for the blood brain barrier transport.

The bottom plate served as receiver: each well received 200 μ L of 0.05M TRIS buffer. The filters of the top well were coated with the lipid/dodecane solution. The top plate was placed on the bottom plate so that the top wells fit into the bottom wells. The top plate, serving as the donor, received 200 μ L of the compound (5 μ L/ml) in duplicates (Figure 14). The plate cover was then placed on top of the donor plate. The plate sandwich was wrapped in Parafilm® and stored in plastic container lined with damp paper towels (to decrease evaporation) for 18 hours at room temperature.

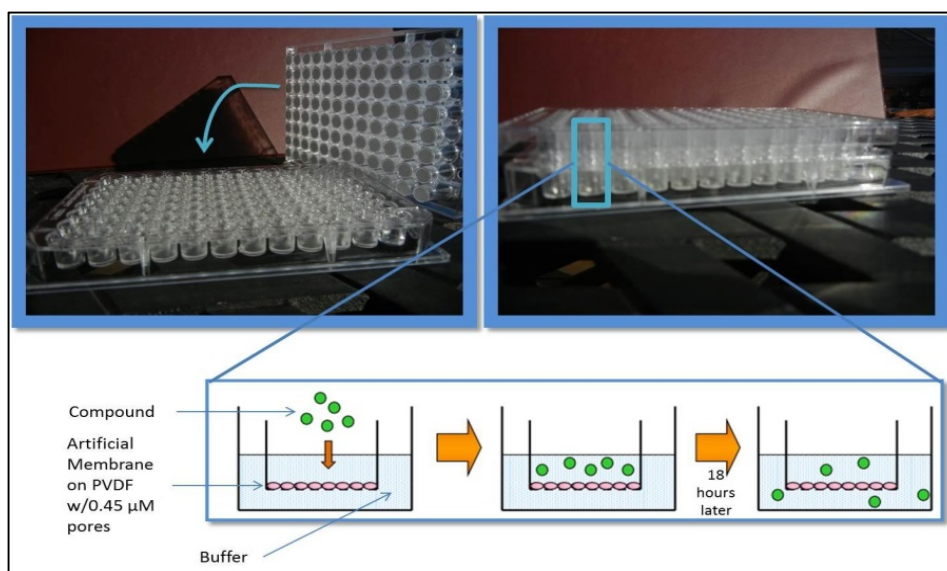


Figure 13: BBB permeability apparatus Close-up of wells displaying two individual plates: top plate with PVDF membrane and bottom plate with wells. Close up reveals process by which compound will cross the membrane in the 18-hour period.

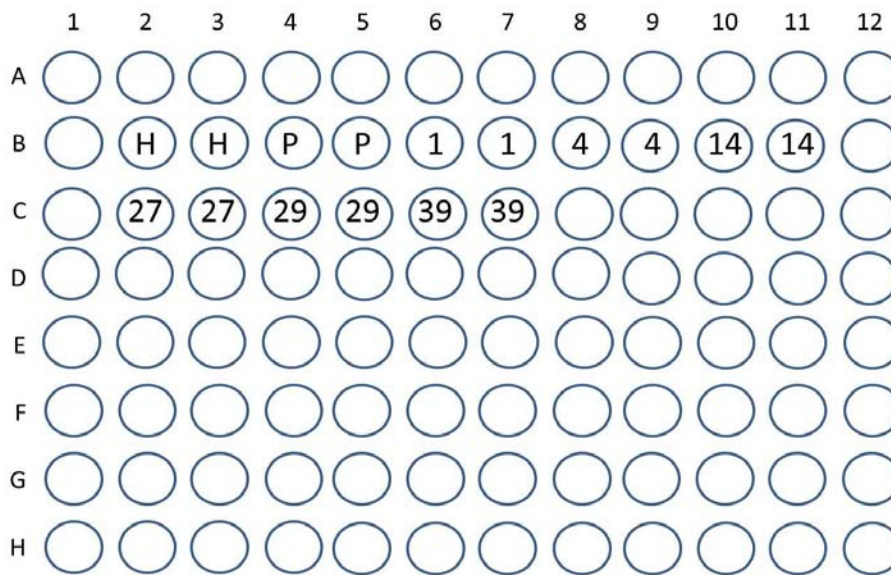


Figure 14: Blood Brain Barrier Assay top plate set up: Edge wells were not used to standardize evaporation, each compound was tested in duplicates, H=hydrocortisone, P=progesterone, numbers=RD compounds

After 18 hours, 50 μ L of acetonitrile was pipetted into each donor well, mixed well with pipet and aliquotted into glass LC/MS vials. The same process was repeated for the receiver wells. Following an LC/MS run similar to that obtained in the synthesis stage, the molecular weight of the compound peak was selected. An integration of the chromatographic peaks was used to quantify the amount of compound in the donor and receiver wells. The blood brain barrier transport rate (BBBTR) was determined with the following equation: **BBBTR = [compound]_{receiver}/[compound]_{donor}**. A BBBTR = 1.0 indicates equilibrium between donor and receiver. The assay was run for such a time (18 hr. at 25° C) so that equilibrium was not reached.

Developing an assay that measures the relative human metabolic rate for compounds

In a 16 x 100 mm glass culture tube, 865 μ l of 100 mM TRIS pH 7.4 and 3 mM $MgCl_2$, 50 μ l 1.0 mg/ml microsomal protein and 10 μ l of 50 μ M compound (in DMSO) were combined. The mixture was vortexed and pre-incubated for 5 minutes in shaking water bath at 37° C. The reaction was then initiated with the addition of 75 μ l of 1 mM NADPH. Control reactions were also set up without the addition of NADPH. Reactions were allowed to continue for various time periods in a 37° C water bath and halted using addition of 1 ml of acetonitrile. After cooling on ice, the mixtures were transferred to microcentrifuge tubes and centrifuged for 3 minutes at max RPM. Supernatant was transferred into an LC/MS vial and used directly for LC/MS analysis. The LC/MS analysis was searched for the presence of the parent compound and metabolites of the compound, which are the parent compound + 16, 32, etc. (compound-OH, compound with 2 OH, etc.). The presence of only parent compound at certain time periods indicates the lack of clearance of the compound at that time period. The extent of metabolism of the compounds for the incubation time, gives a relative metabolic stability of the compounds.

RESULTS and DISCUSSION***1. Identify suitable lead structures that work on the biological target, mutant p53***

To identify suitable lead structures, a search through scientific literature identified two sources of potential lead structures. A recent patent (Wang et al. 2013) disclosed a benzimidazole compound that bound to p53 in a biochemical binding assay (Figure 15a).

However, there was no data to indicate reactivation of mutant p53. Data from previous work in the lab showed that compounds in this benzimidazole class do indeed reactivate mutant p53 in human tumor cells. A second lead structural type in the quinoline class of compounds was identified. Recent studies have shown that Nitroxoline (Shim et al. 2010) and a class of 8-quinolyl carbamates, represented by Figure 15b, c respectively (Liu et al. 2009 WO 2010/042163 A2) inhibit angiogenesis, the development of new blood vessels, by inhibiting the protease MetAB2, an enzyme involved in promoting the angiogenesis cascade.

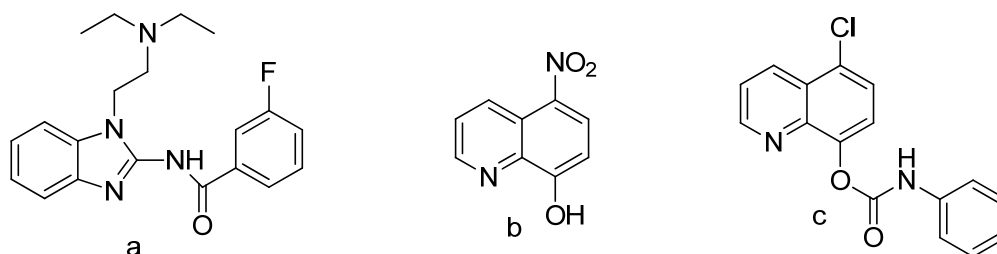


Figure 15: Lead structures that reactivate mutant p53 in human tumor cells: a benzimidazole (a), Nitroxoline (b), and quinoline (c)

Since activated p53 also inhibits angiogenesis (Teodoro et al. 2007), it was logical to investigate if compounds in the quinoline class also reactivate p53. Data from the lab indicated that compounds in this compound class do in fact reactivate mutant p53 in human tumor cells and may contribute to the anti-angiogenic and anti-tumor effects of this quinoline class of compounds. These result led to an investigation in the optimization of the p53 reactivating ability of these compound classes so as to develop a novel anticancer therapy.

Most of this work was focused on compounds in the quinoline class. Other group members prepared compounds in the benzimidazole class. However, compounds in both

classes were utilized to evaluate drug like properties that would be necessary in treating GBM. The initial goal was to synthesize compounds in the quinoline class of compounds, and develop an SAR (structure activity relationship) for p53 reactivation. Some of the proposed structural changes of the lead quinoline compound are summarized in Figure 16.

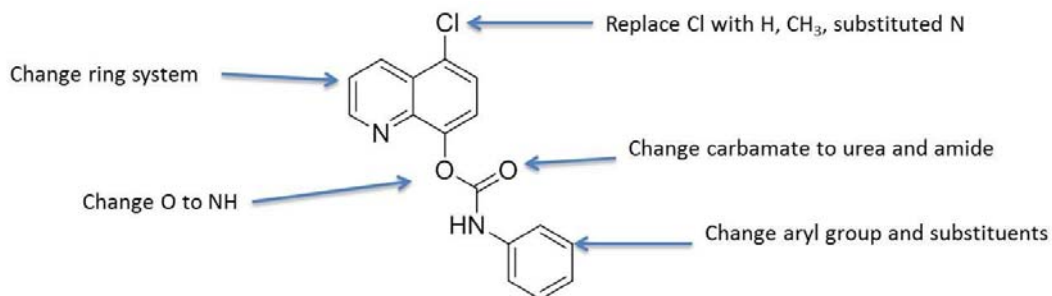


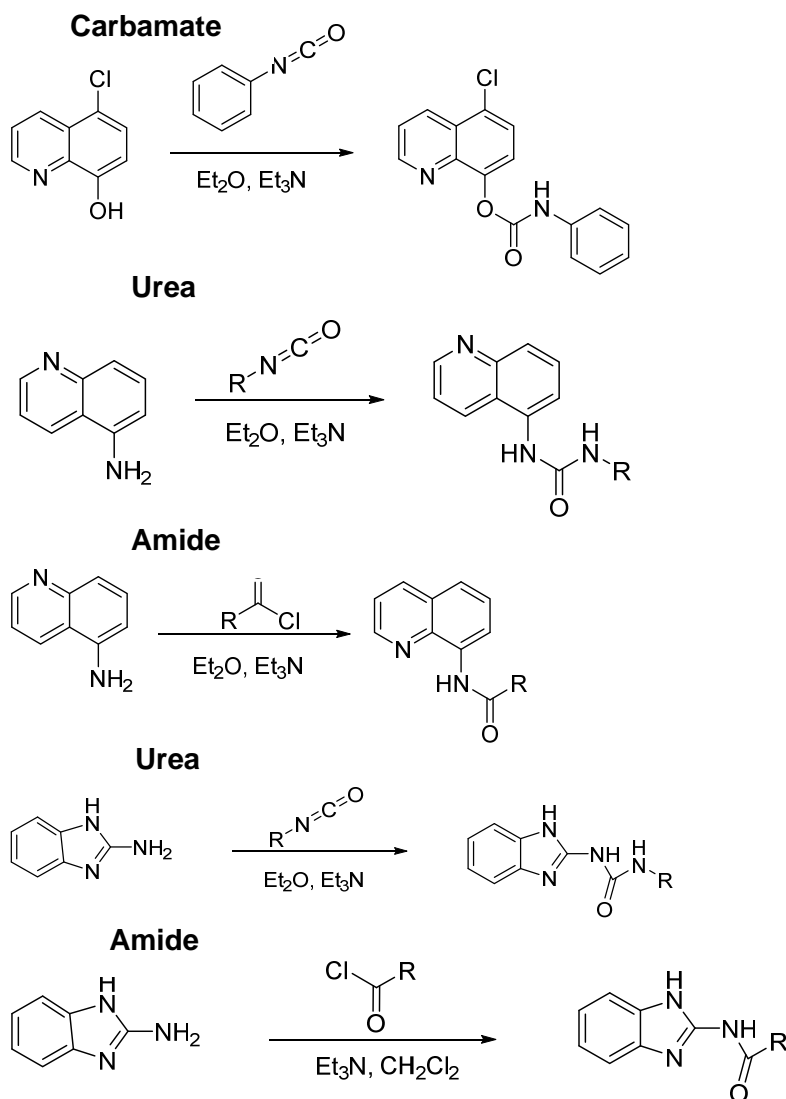
Figure 16: Potential structural changes to the quinoline class to develop an SAR.

Over the course of this research, several compounds were synthesized and characterized. For further analysis, only a sample of the quinoline compounds as well as compounds in the benzimidazole class were chosen. In both the benzimidazole and quinoline classes, amides and ureas were prepared. A selection of the four types of compounds were chosen for the analyses.

2. Synthesize analogous structures to optimize potency, selectivity, and drug-like properties

The first step in the process involves the successful synthesis and characterization of compounds. All reactions were performed in a similar manner using commercially purchased starting materials. Amino or hydroxyl quinolines and 2-aminobenzimidazole

were acylated with an isocyanate or acid chloride to yield carbamates, ureas or amides. Over 60 compounds have been synthesized and characterized to date. Only seven of these compounds were used for the purpose of this study. General synthetic routes to the compounds are shown in Figure 17.



Where R indicates any group

Figure 17: General synthetic routes for quinoline amides, quinoline ureas, benzimidazole amides and benzimidazole ureas

The LC/MS characterization spectra are depicted in two separate graphs. The first displays two chromatograms—one using UV detection of compounds and the other using total ion current (TIC) from the mass spectrometer. The UV analysis is most indicative of purity of compound, as only organic compounds will be reflected by peaks on the graph. Thus, a single strong peak suggests high purity. The mass spectrograph should show a strong peak at a time point analogous to that of the UV spectra, but may show other small peaks, as well. A closer look of the area under the strong peak results in the second graph is necessary for LC/MS characterization. This closer look reveals the exact mass that is most prevalent in the compound. An M+1 peak is usually seen, indicating the mass of the ionized compound. With the compounds containing chlorine, a P+2 peak can also be visualized, the parent peak with the ^{37}Cl isotope. The end of the mass spectrograph often reveals several peaks. This is normal, as at the end of the run, the column is self-cleaned with solvents to prepare for the following run. The MS is also significantly more sensitive than the UV. The highest peak is normalized to 100, making peaks indicating impurities disproportionate in their size. This issue can be resolved by running a more diluted sample of the compound, as the disproportionality of peak height and width is due to over saturation of the detector. Thus, the use of UV to accurately analyze purity is recommended by the American Chemical Society and is used in this study.

All compounds were characterized by NMR and LC/MS.

NMR characterization of compounds

RD1:

MS Electrospray-TOF, $m/z = 299$, M+H

NMR H (400 MHz, DMSO) 10.5 (H, s, NH), 10.2 (H, s, NH), 9.1 (1H, d, 2-quinoline aromatic), 8.6 (1H, d 4-quinoline aromatic), 7.9 (1H, d, 6-quinoline aromatic), 7.8 (1H, m, 3-quinoline aromatic), 7.6 (2H, d, ortho-phenyl), 7.6 (2H, t, meta-phenyl), 7.1 (1H, m, para-phenyl)

RD 4:

MS Electrospray-TOF, $m/z = 256$ (M+H)

H NMR (400 MHz, DMSO) 12.3(1H, s, NH), 8.3(2H, m, 4,7-benzimidazole aromatic), 7.5(2H, m, 5,6-benzimidazole aromatic), 7.4 (2H, m meta-phenyl), 7.1(2H, ortho-phenyl)

RD13:

MS Electrospray-TOF, $m/z = 252$ (M+H)

H NMR (400 MHz, DMSO) 12.4(2H, s, NH), 7.9(2H, m, ortho-phenyl), 7.4(4H, m, 4,5,6,7-benzimidazole aromatic), 7.1 (2H, m meta and para-phenyl), 3.4 (3H, s, methyl)

RD14:

MS Electrospray-TOF, $m/z = 264.09$ (M+H)

H NMR (400 MHz, DMSO) 9.1(1H, s, NH), 8.86(1H, d, 2-quinoline aromatic), 8.82 (1H, s, NH), 8.46(1H,d, 4-quinoline aromatic), 8.03 (1H,dd 6- quinoline aromatic), 7.67 (2H,

m, 7,8-quinoline aromatic), 7.61 (1H, dd, 3-quinoline aromatic), 7.43 (2H, d, ortho-phenyl), 7.23 (2H, t, meta-phenyl), 7.0 (1H, t, para-phenyl)

RD 27:

MS Electrospray-TOF, $m/z = 332$ (M+H)

H NMR (400 MHz, DMSO) 9.4(1H, s, NH), 9.1 (1H, s, NH), 9.2(1H, d, 2-quinoline), 8.0(1H, d, 4-quinoline), 7.8(2H, m, 3 and 6-quinoline), 7.65(1H, m, 7-quinoline), 7.60(2H, s, 2 and 6-phenyl), 7.2(1H, s, 4-phenyl)

RD29:

MS Electrospray-TOF, $m/z = 332$ (M+H)

H MNR (400 MHz, DMSO) 9.3(1H, s, NH), 9.0 (1H, s, NH), 8.9(1H, d, 2-quinoline), 8.5(1H, d, 4-quinoline), 8.0(2H, m, 6 and 8-quinoline), 7.8(2H, m, 3 and 7-quinoline), 7.7(1H, m, 5-phenyl), 7.6(1H, d, 2-phenyl), 7.4(1H, d, 5-phenyl).

RD39:

MS Electrospray-TOF, $m/z = 287$ (M+H)

H NMR (400 MHz, DMSO) 11.4(1H, s, NH), 9.6(1H, s, NH), 7.64(2H, d, 4,7-quinoline), 7.36 (3H, m, 5,6-benzimidazole, ortho-[phenyl), 7.10 (2H,m, meta-phenyl)

The LC/MS characterization of RD 1 follows. However, characterization spectra for compounds RD 4, 13, 14, 27, 29 and 39 are found in **APPENDIX A**.

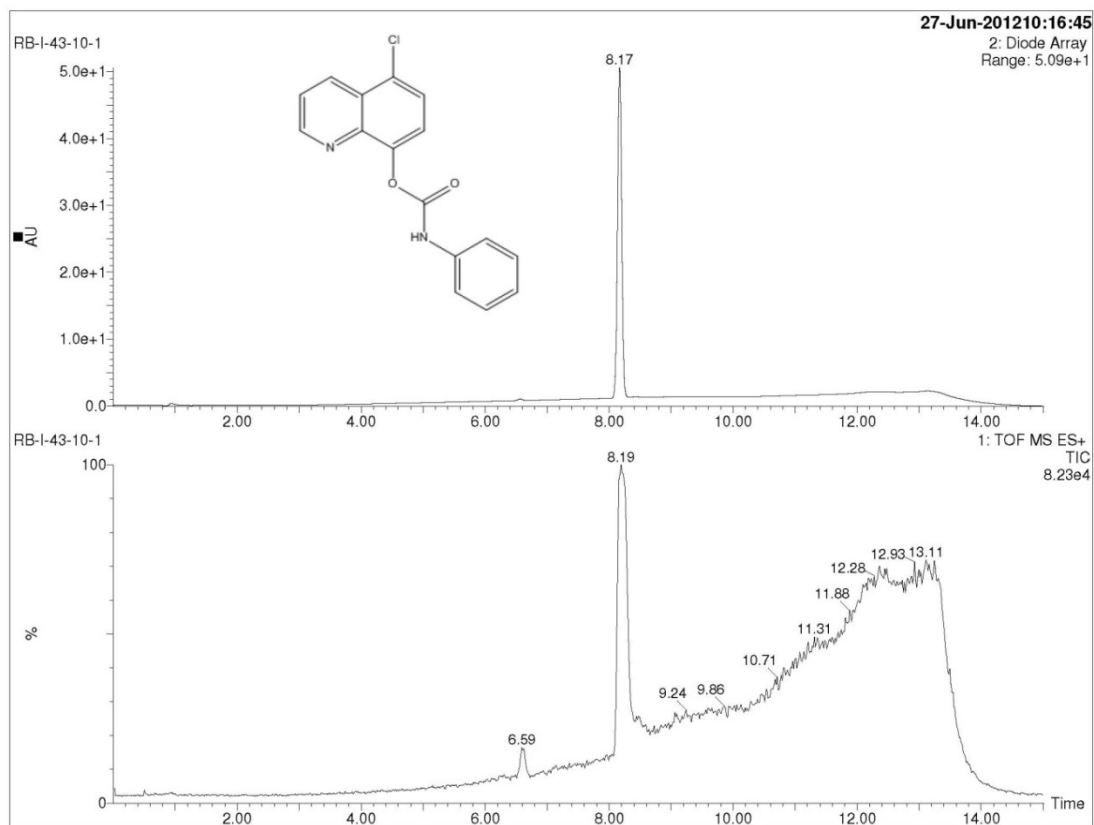


Figure 18: LC/MS chromatogram of RD1. Top graph depicts UV spectra with one sharp peak around 8 minutes, indicating the presence of a single organic compound. The bottom graph depicts the mass spectrograph with a single large peak corresponding to that of the UV spectra.

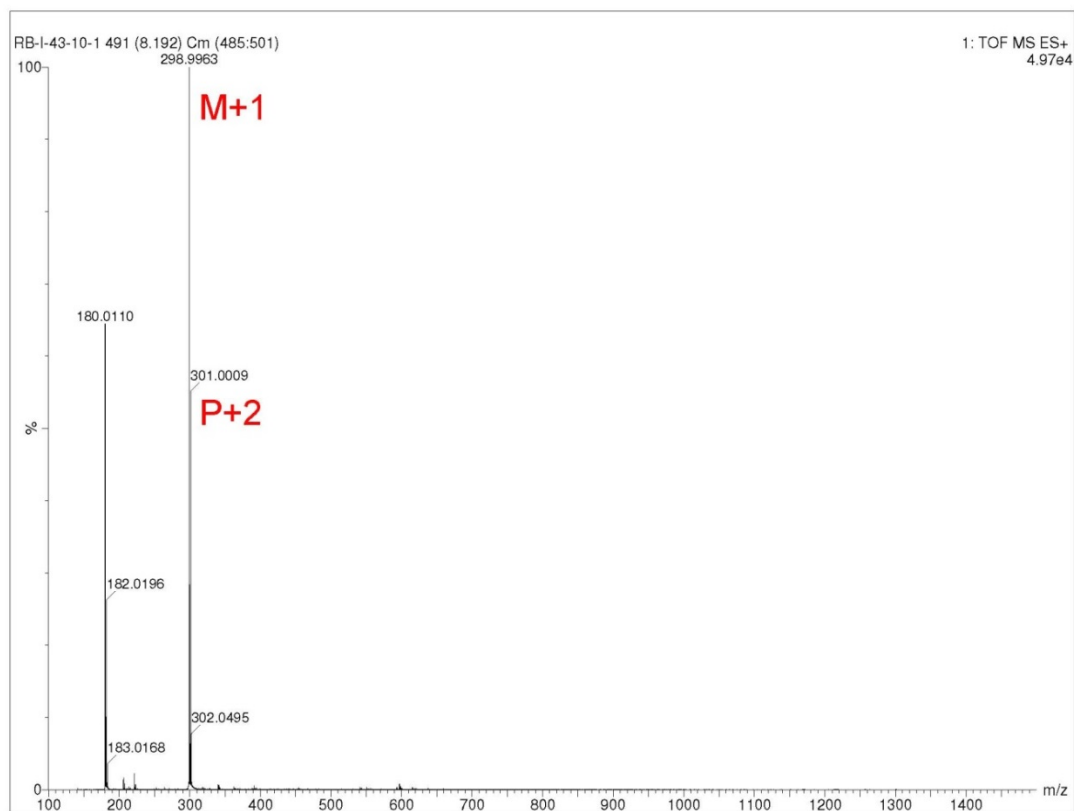


Figure 19: Area under large peak of RD 1 MS around 8 minutes. Major peak is M+1, consistent with compound MW=298. Shorter peak is P+2, consistent with compound containing ^{37}Cl isotope.

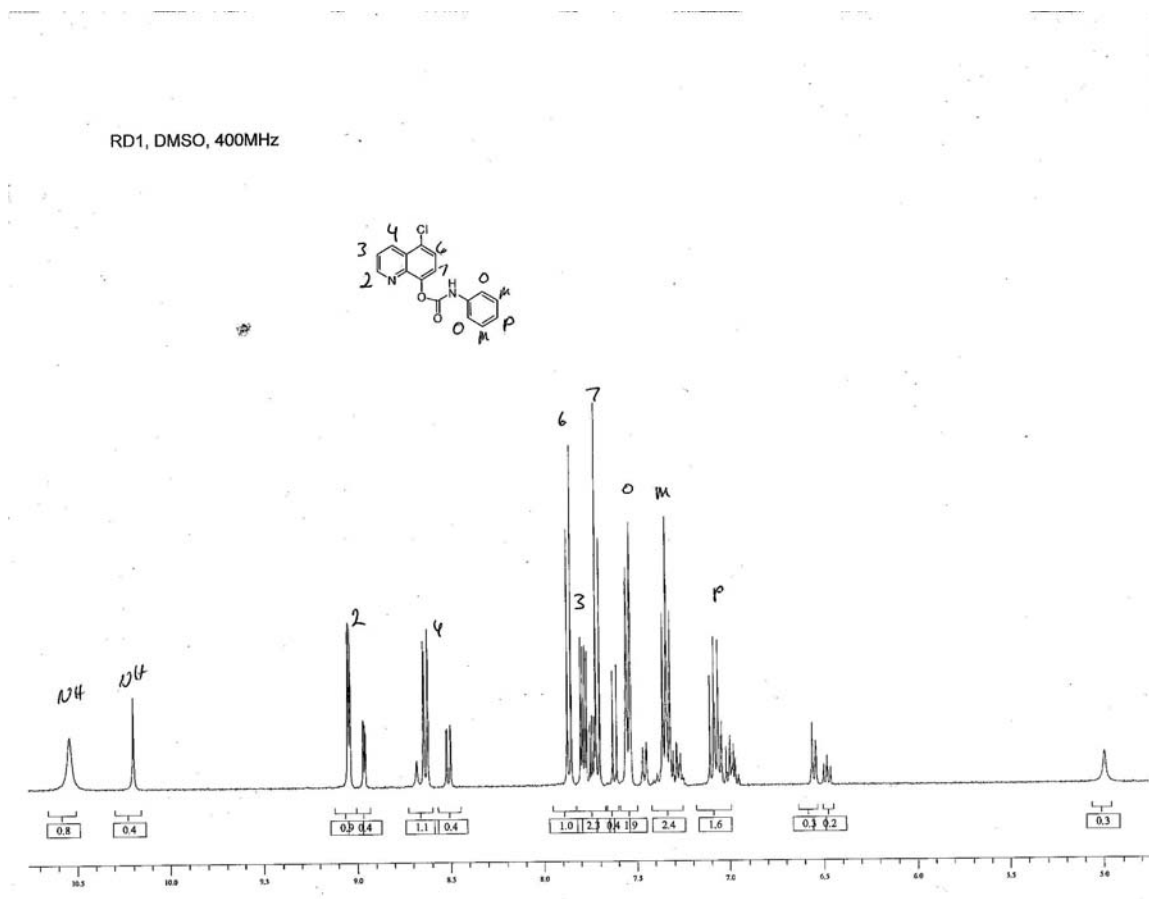


Figure 20: NMR spectra of RD 1: MS Electropray-TOF, $m/z = 299$, $M+H$; NMR H (400 MHz, DMSO) 10.5 (H, s, NH), 10.2 (H, s, NH), 9.1 (1H, d, 2-quinoline aromatic), 8.6 (1H, d 4-quinoline aromatic), 7.9 (1H, d, 6-quinoline aromatic), 7.8 (1H, m, 3-quinoline aromatic), 7.6 (2H, d, ortho-phenyl), 7.6 (2H, t, meta-phenyl), 7.1 (1H, m, para-phenyl)

3. Evaluate the potency and selectivity of compounds in human tumor cell assays

Glioblastoma SF295 human tumor cells were chosen for this study since they contain mutant p53 (Mitchell et al. 2010). Using western blot analysis, the production of p21, a protein produced by active p53, was followed after the tumor cells were treated with a solution of the compounds. Analysis of gel consisted of visualizing a band at 53 kilodaltons for p53 and a band at 21 kilodaltons for p21. The presence of a p21 band (in addition to the p53 band) indicated that the compound was successful in reactivating the mutant p53. A lack of p21 band indicated that the compound was not successful in

reactivating p53. This process does not quantify the potency of the compound. That is, while a compound may be observed to indeed reactivate p53, it has not been possible to know just how much of the mutant p53 is reactivated. A procedure to quantify activity is now in progress. This western blot analysis was conducted by members of the Dr. DasMahapatra lab, and an example is shown in Figure 21.

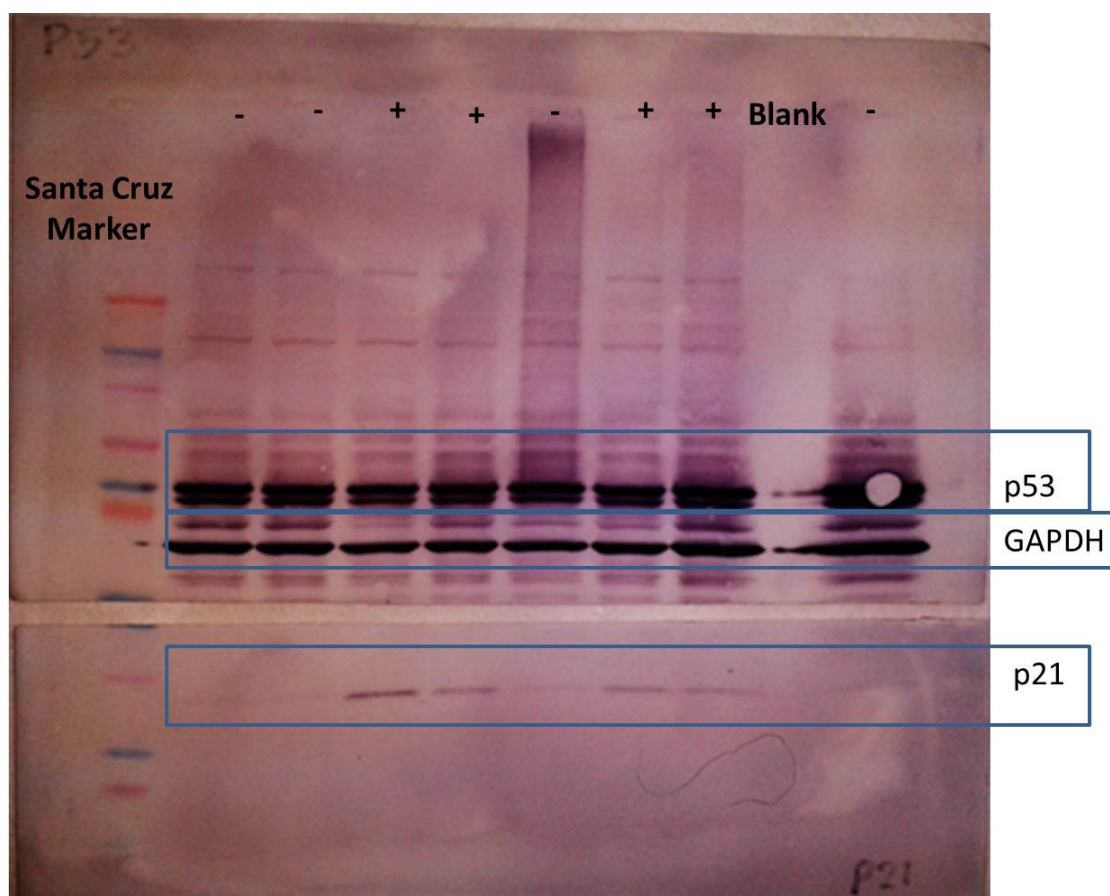


Figure 21: Sample western blot showing Santa Cruz marker, which is used to track position of bands on gel, positive and negative compounds (positive indicates the presence of a p21 band and thus the successful reactivation of mutant p53 using said compound; negative indicates no p21 production and thus no reactivation of p53. Western blot image was provided by members of the Dr. DasMahapatra lab.

A summary of the mutant p53 reactivation biological results is shown in Figure 36. The seven compounds for this study were selected because they had already shown mutant p53 reactivation in a human colon cancer cell line, DID1. The potency analysis conducted via western blot indicated that RD 1, 4, 14, 27, 29, and 39 do reactivate mutant p53 in SF295 glioblastoma cells (Figure 22). This can be determined through the visualization of a band at 21 kilodaltons (kDa). RD 13 did not reactivate mutant p53. However, interestingly, in a separate project, RD 13 was shown to reactivate mutant p53 in DID1 colon cancer cells. Reasons for this are still being investigated.

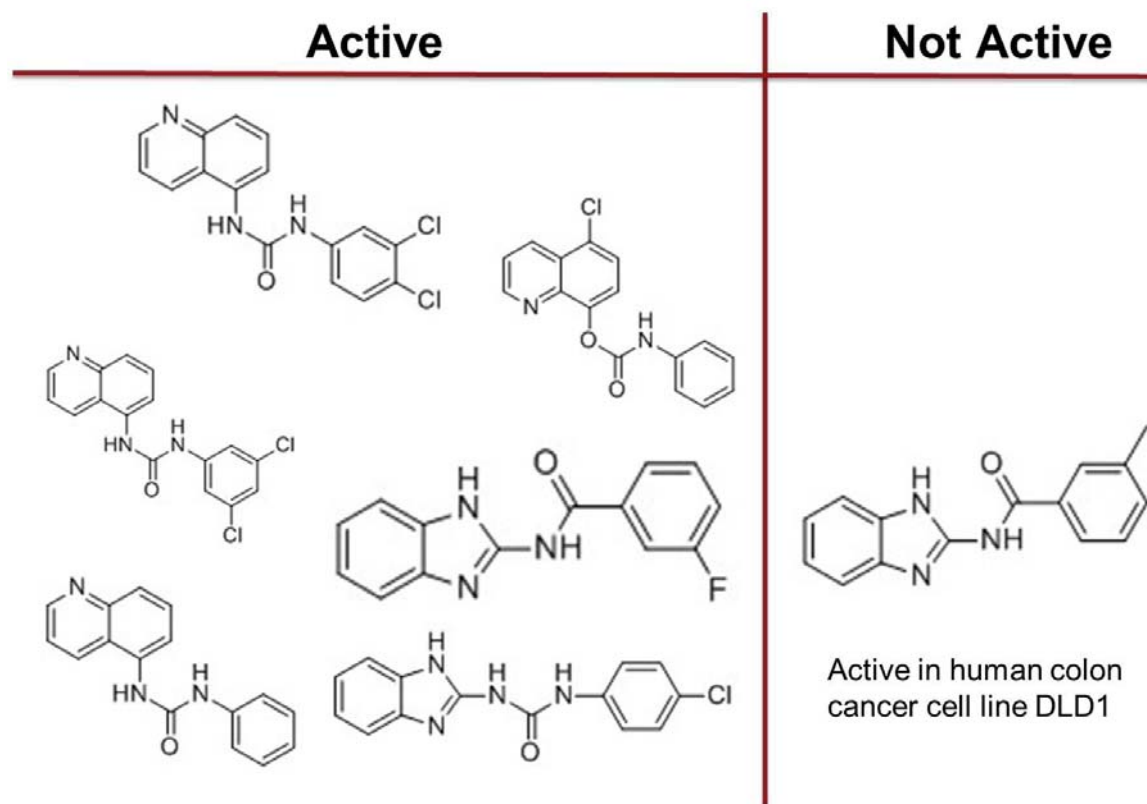


Figure 22: Structure of compounds that reactivated mutant p53 in SF295 glioblastoma cells and structure that did not reactivate mutant p53 in SF295, but did reactivate mutant p53 in colon cancer cell line, DID1.

Compounds that showed reactivation of mutant p53 in tumor cells were further analyzed in a cell replication assay. Compounds that reactivate mutant p53 should induce apoptosis (cell death) in tumor cells. These compounds should have no effect on normal cells or p53 null cells (cells without p53). To assess selectivity, off-target effects, and general toxicity of the compounds on the cells, the ratio of the compound EC₅₀ causing tumor cell death to the compound EC₅₀ causing p53 null cell death (H1299 cell line) was evaluated. The EC₅₀ is the concentration of drug administered at which 50% of cells die. This ratio is expressed as a therapeutic index (TI), such that:

$$TI = \frac{\text{Apoptosis EC}_{50} \text{ H1299 Cells}}{\text{Apoptosis EC}_{50} \text{ Tumor Cells}}$$

The goal is to achieve a TI of 10-100 fold. The TIs of some of the compounds have been determined and are shown in Figure 30. Off target cytotoxic effects of the compound are causing cell death in the H1299, p53 null cells.

4. *Develop an assay to determine transport across the BBB membrane*

Compounds that reactivated mutant p53 in the glioblastoma tumor cells were further assayed for potential CNS drug like properties. *In vivo* animal assays measuring BBB transport are available. However, *in vitro* assays have been reported to be predictive, and are used in the pharmaceutical industry. These *in vitro* assays employ an artificial membrane in a Boyden chamber as shown below in Figure 23.

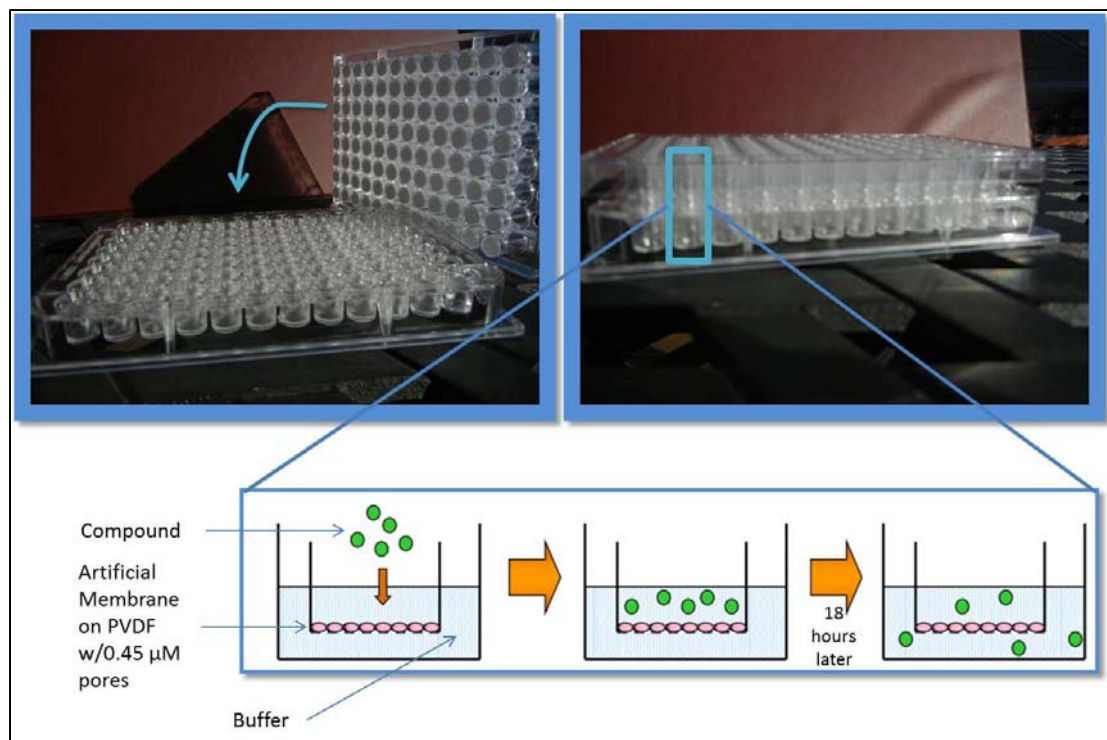


Figure 23: BBB permeability apparatus close-up of wells displaying two individual plates: top plate with PVDF membrane and bottom plate with wells. Close up reveals process by which compound will cross the membrane in the 18-hour period. Artificial membrane for BBB consisted of dodecane with bovine polar brain lipids.

96 well Stirwell PAMPA Sandwich plates (PN 110-243) from Pion were used as the Boyden chambers. The bottom plate served as the receiver. Each well received 200 μL of 0.05M TRIS buffer. The filters of the top well were coated with bovine polar brain lipid/dodecane solution, as described by Li Di, et al. 2003. The apparatus was left for 18 hours at room temperature. This is so the transfer does not reach equilibrium. Quantification of compound amounts in the donor and receiver wells was determined by LC/MS, integrating the compound peaks in the TIC (total ion current) chromatogram. The blood brain barrier transfer rate, BBBTR, was then determined using the following formula:

$$\text{BBBTR} = \frac{[\text{compound}]_{\text{receiver}}}{[\text{compound}]_{\text{donor}}}$$

For controls, progesterone (Figure 24a) was used as a compound that crosses the BBB, and hydrocortisone (Figure 24b) as a compound that does not cross the BBB (Di et al. 2003).

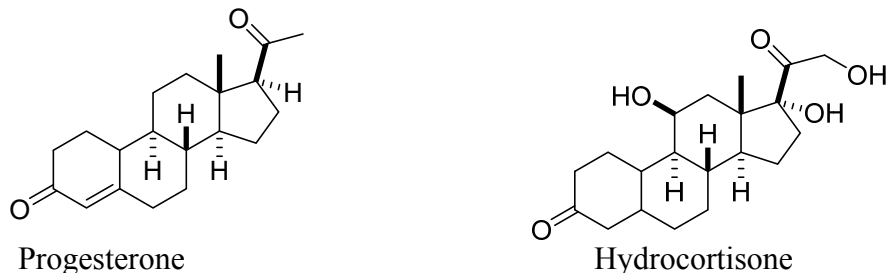


Figure 24: Structures of controls used for the BBBTR assay— (a) progesterone as the positive control and (b) hydrocortisone as the negative control.

The assay indicated successful transports of progesterone (Figure 26), RD 4 (Figure 49), RD 14 (Figure 50), and RD 39 (Figure 51); but, unsuccessful transports of hydrocortisone (Figure 27), RD 1 (Figure 52), RD 27 (Figure 53), and RD 29 (Figure 54). In comparison to the positive control, progesterone, RD 4 and 14 moved faster toward equilibrium, while RD 39 moved at about the same rate. It is important to note that this assay is strictly a model for the blood brain barrier and does not include the various significant channels and transporters typically found on the membrane *in vivo*. However, even if the transport is not exactly the same, this *in vitro* model provides a good prediction about the success of a drug in entering the CNS.

Each Figure presents two graphs. The first is an analyzed MS spectra obtained when the solution in the well of the top plate (donor well because it donates the compound) is run through the LC/MS. It is analyzed by running a search for the molecular weight of compound; thus, highlighting only the time at which this compound appears (as signified by a large peak) and eliminated background compounds and

impurities. The area under this peak is then integrated. The same analysis is run for the receiver well (the bottom plate well that receives from the donor well). The red circled numbers indicate the integrated area of each of the peaks pertaining to the compounds. The transport rate is thus obtained by dividing the receiver area by the donor area—giving a number less than 1.0 (at 1.0 compound is at equilibrium in both wells).

The data in Figure 25 shows BBBTR for the two controls and the three quinoline analogues that cross the BBB. The two controls that used are in agreement with the literature, that is, progesterone crosses the BBB and hydrocortisone does not.

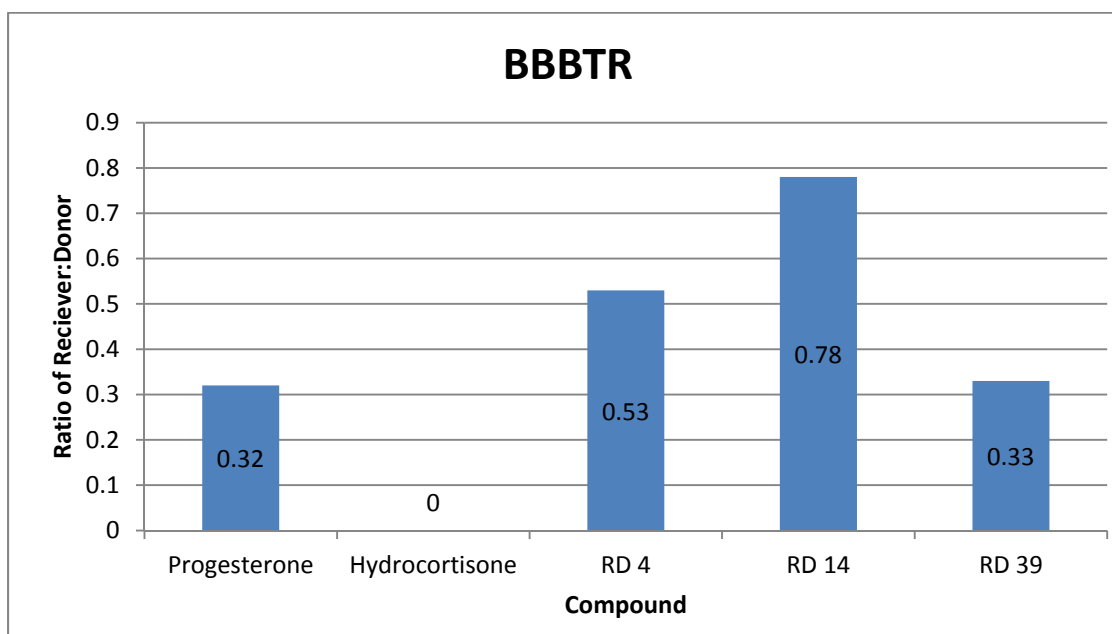


Figure 25: Graph displaying differences in BBBTR in compounds RD 4, RD 14, and RD 39, as compared to the positive control, Progesterone (other compounds, RD 1, RD 27, and RD 29 indicated a ratio of 0, similar to the negative control, Hydrocortisone).

The BBBTR spectra for the controls follow. The BBBTR spectra for the compounds used in this study are found in **APPENDIX B**.

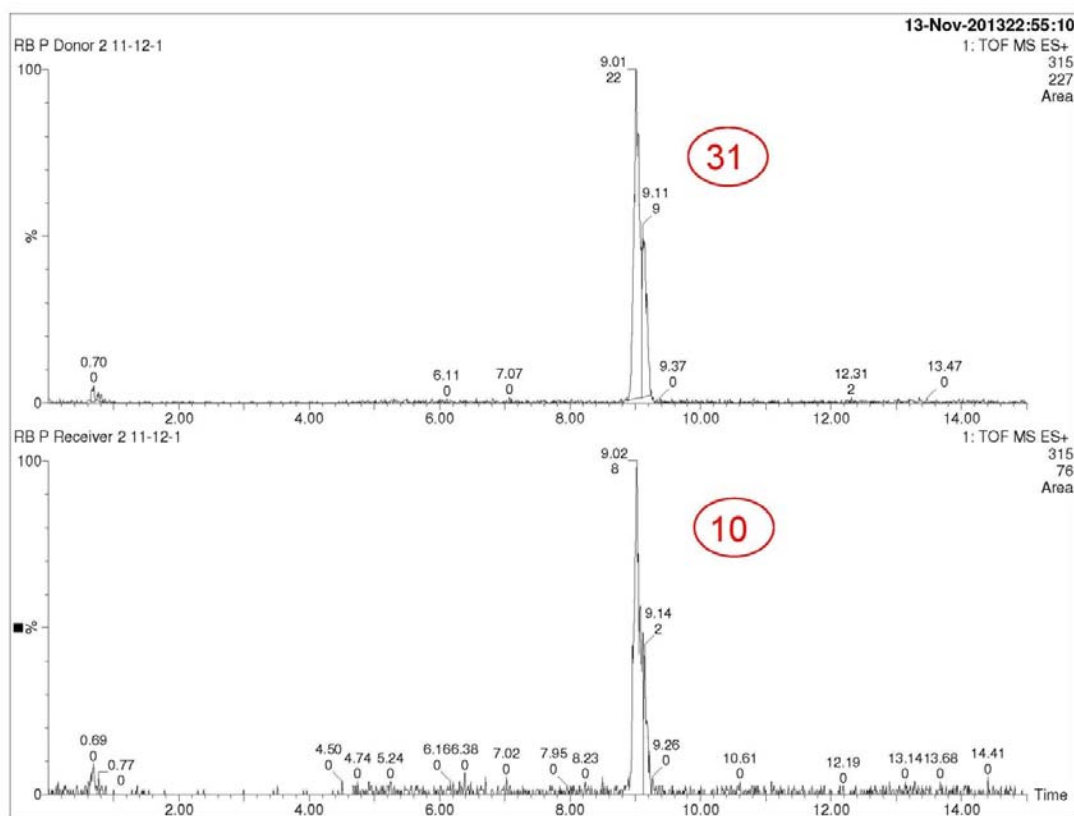


Figure 26: Progesterone (positive control) BBB Assay; the top spectra is the analyzed MS spectra for the top donor well, while the bottom spectra is the analyzed MS spectra of the receiver well; the area under the peaks (highlighted to show only the compound in question) is integrated; a ratio of the integrated areas of receiver: donor indicate that BBBTR= 0.32 (10/31)

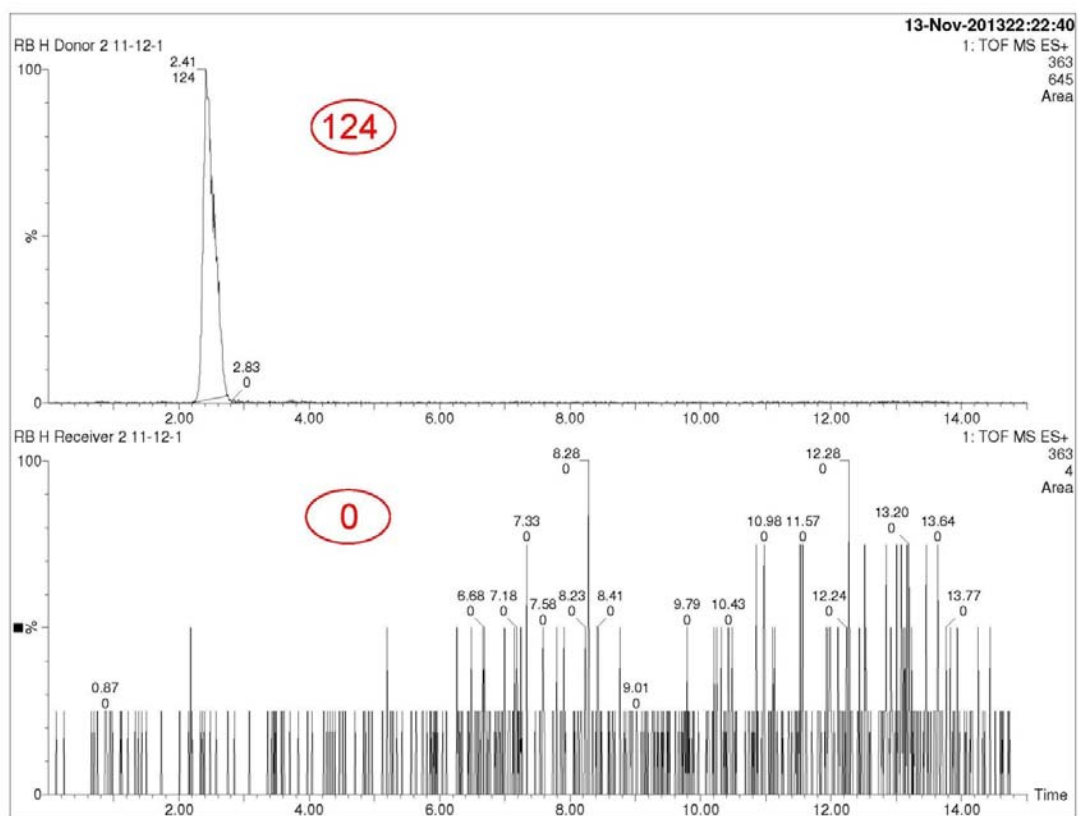


Figure 27: Hydrocortisone BBB Assay; the top spectra is the analyzed MS spectra for the top donor well, while the bottom spectra is the analyzed MS spectra of the receiver well; the area under the peaks (highlighted to show only the compound in question) is integrated; a ratio of the integrated areas of receiver: donor indicate that BBTR: 0.0

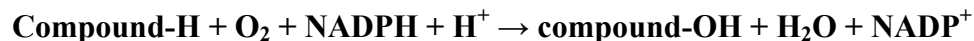
5. *Develop an assay that measures the relative human metabolic rate for compounds*

In drug discovery, pharmacokinetics, the study of metabolism rates and clearance of a drug, is critical for the advancement of a compound into clinical trials. Thus, the absorption, distribution, metabolism and excretion (ADME) rates must be analyzed (Balani et al. 2005). Failure to adhere to ADME standards can cause even a potent compound to not succeed as a drug (Singh, 2006). The first step in determining a human pharmacokinetic profile of a drug is accomplished by measuring the *in vitro* human metabolic rate, known as intrinsic clearance, using commercial human liver cells or human liver microsomes. This study can also identify potential human metabolites. The intrinsic clearance can be used to determine free drug concentrations in the plasma of a human or animal, in the *in vivo* pharmacokinetic profile studies. This *in vivo* pharmacokinetic profile study in animals is then used to predict the appropriate dose for treatment in humans.

For a compound to be a suitable drug, it must resist human metabolism such that drug concentrations in the blood are sufficient to produce the desired biological effect. If a drug is cleared too quickly, it may not have enough time to impart its effect on the tumor cells. However, if the drug remains in the body for too long, it may accumulate and have toxic effects on the body. The plan is to evaluate the *in vitro* human metabolic rate (intrinsic clearance) of all compounds that show biological activity in reactivating mutant p53 and also cross the BBB. The *in vitro* metabolic rate is determined by quantifying, using LC/MS, the amount of drug remaining at increasing times during the *in vitro* human metabolism assay. LC/MS analysis of the metabolism experiment may also give

insight into the structures of the metabolites.

Within the liver microsome are cytochrome p450 enzymes. Cytochrome p450 (CYP) is responsible for oxidizing organic compounds such as those that are used here (Korzekwa, 2014). This results in the free radical hydroxylation of the compound by the following equation:



Multiple -OH groups may be added to the compound, resulting in several metabolites. A human microsomal metabolism assay using excess NADPH in a pH7 TRIS buffer containing magnesium ion was developed.

The process was performed for RD 1, personally, while a colleague repeated the process on another compound, RD 39. RD 1 displayed very rapid metabolism to a di-OH metabolite. Within the first 15 minutes of incubation, all of RD 1 was consumed (Figure 28). This makes for a very poor drug as its administration would likely require several doses over the course of the day, in order to achieve the required exposure for biological activity. Various analogues of RD1 were prepared to improve the metabolic profile. The metabolic rate of these compounds has not yet been determined.

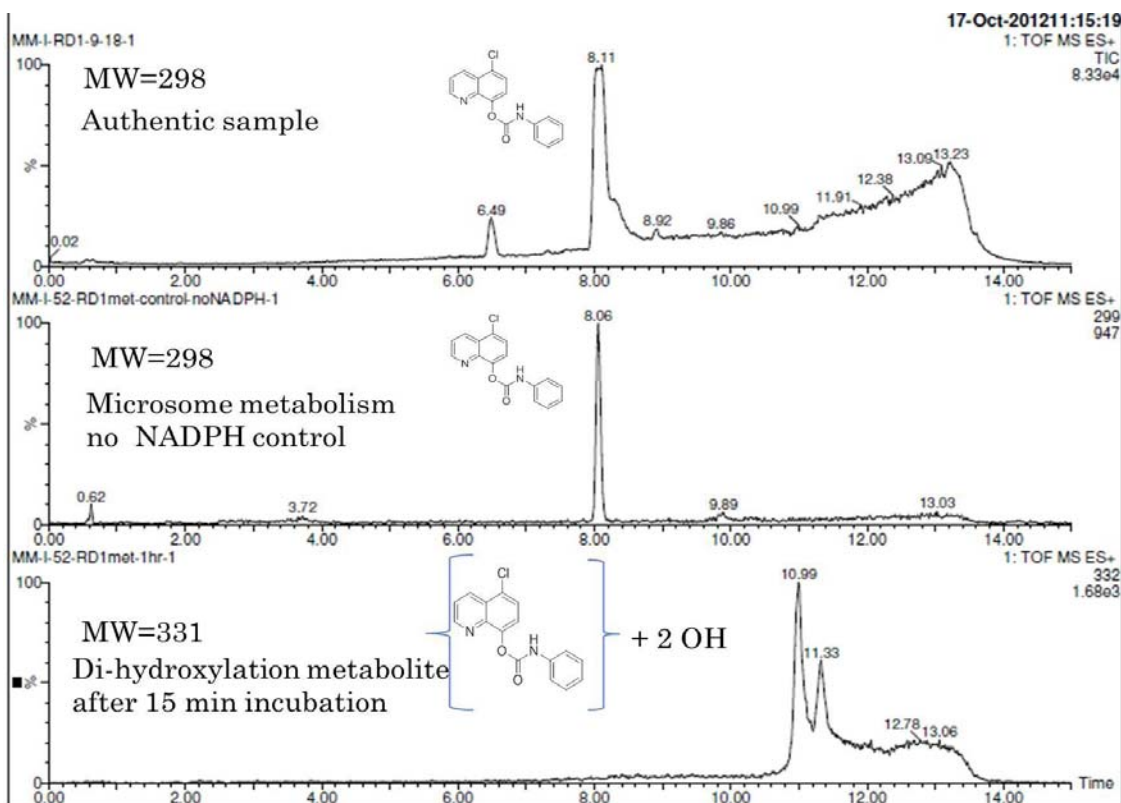


Figure 28: RD 1 Metabolism; Authentic Sample indicates compound in acetonitrile; control (no NADPH) depicts a lack of metabolism of the compound; sample containing NADPH metabolizes completely within 15 minutes

As opposed to RD 1, RD 39 resisted metabolism much better. In fact, after 2 hours of incubation, 90% of RD 39 remained, with 10% being a mono-OH metabolite (Figure 29). This compound, thus, could potentially be a drug with reasonable dosage rates.

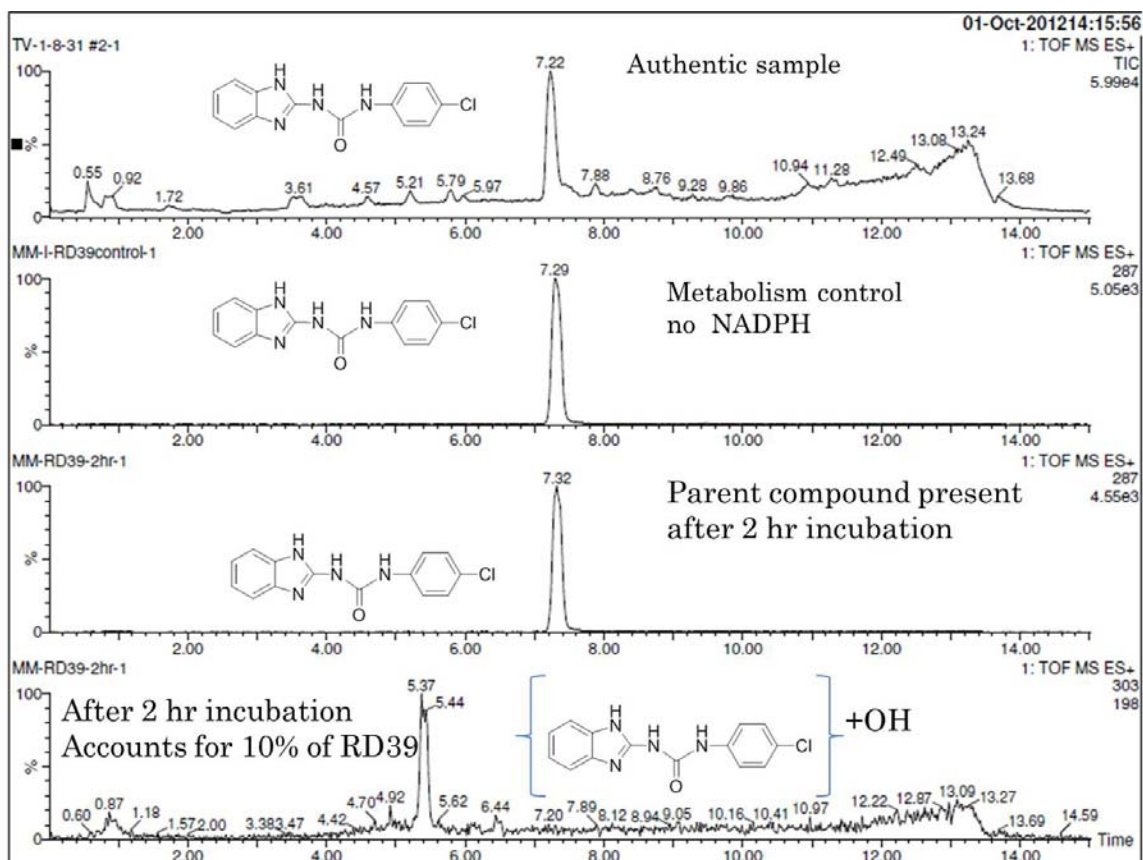
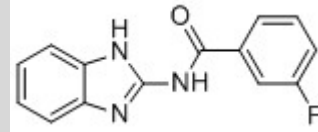
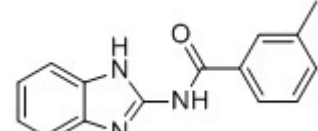
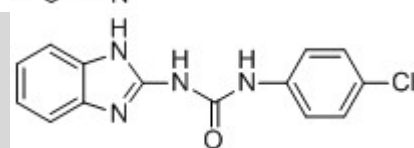
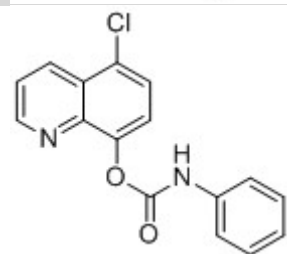
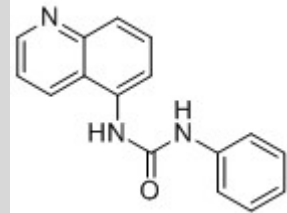
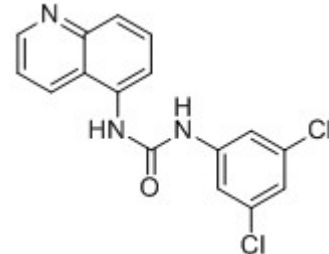


Figure 29: RD 39 metabolism (work and analysis credit to Megan McAleavy); Authentic Sample indicates compound in acetonitrile; control depicts a lack of metabolism of the compound; sample after 2 hours indicates presence of parent compound as well as mono-OH metabolite in a 90:10 ratio, respectively.

6. Optimize the lead structures to improve the total profile the compounds

New analogues were synthesized and evaluated for *in vitro* in-cell potency, selectivity and drug-like properties. This information is used to construct a structure activity relationship (SAR) that correlates compound structural features with biological activity and drug-like properties. This SAR can then be used to design new analogues that should have improved biological profiles. Complete data of the compounds discussed here, are shown in Figure 30.

RD #	Structure	Class	tPSA (Å)	CLogP	P53 reactivation in SF295	BBBTR	TI	EC ₅₀ μM
4		Benzimidazole Amide	53.49	3.11	Positive	0.53	N/D	N/D
13		Benzimidazole Amide	53.49	3.40	Negative*	N/D	N/D	N/D
39		Benzimidazole Urea	77.88	3.51	Positive	0.33	N/D	N/D
1		Quinoline Carbamate	50.69	4.29	Positive	0	4.68	1.4
14		Quinoline Urea	53.49	3.63	Positive	0.78	No Apoptosis	>10
27		Quinoline Urea	53.49	5.19	Positive	0	1.60	11.4

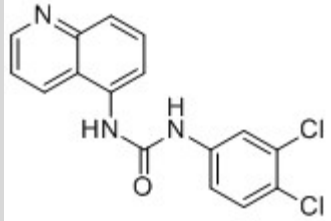
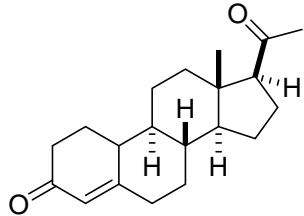
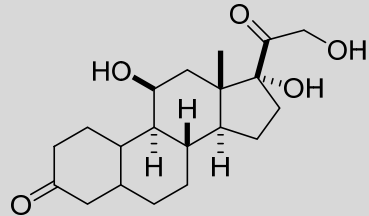
29		Quinoline Urea	53.49	5.07	Positive	0	>1	15
		Progesterone Control	34.14	3.26	N/D	0.32	N/D	N/D
		Hydrocortisone Control	94.80	-1.05	N/D	0	N/D	N/D

Figure 30: Data on selected compounds. Biological results in SF29 cells indicate reactivation of mutant p53. *RD 13 did not reactivate mutant p53 in the SF295 glioblastoma cell line, but was shown to reactivate mutant p53 in DID1, a colo-rectal tumor cell line. BBBTR for RD 13 was not obtained. tPSA=topological polar surface area; CLogP= calculated Partition coefficient of a compound between octanol and water (tPSA and CLogP calculated using ChemBio Draw®). BBBTR: blood brain barrier transport rate; TI: therapeutic index. EC₅₀ μM: concentration of compound at which 50% of tumor cells died. *N/D indicates no data

CONCLUSION

Even with a limited number of compounds in this study, certain conclusions can be drawn regarding the structure activity relationship (SAR). Firstly, the potency, selectivity, BBBTR, and metabolic rate each have separate SARs. One of the biggest conclusions seem to lie in the benzimidazole amide class, where the compound with a methyl group did not reactivate mutant p53 in SF295, but the compound with a fluorine, did. Therefore, halogens may play a critical role in the biological profile of this class of compounds. This finding is even more interesting because RD 13 failed to reactivate mutant p53 in SF295 glioblastoma cells, but was successful in reactivating mutant p53 in DID1, colon cancer cells. This finding will be replicated to validate. However, if proven true, this discovery will indicate that the compounds used here are perhaps not universal for all tumors with mutant p53, but can depend on the type of or ratio of mutations in the p53. The compounds may also not reactivate all mutant p53 equally. This will require analysis of various tumors with different mutations of p53.

The CLogP seemed to also have a dramatic effect on the BBBTR in all the classes. Compounds with a CLogP close to or greater than 5 did not cross the BBB, but those with a ClogP of less than 4, did. While literature had stated that a CLogP of less than 6.1 is ideal for drugs to cross the BBB, this study indicates that benzimidazole and quinoline classes may not cross the BBB with a CLogP of greater than 4. Additionally, changing the carbamate to a urea in the quinoline class seemed to significantly increase. The benzimidazole urea, with the greater tPSA crossed the BBB at a lower rate than the benzimidazole amide with the lower tPSA. There was not significant variety in tPSA across all of the compounds to make further conclusions regarding the implication of

tPSA on the compounds' drug-like properties. Even though only one compound in each of the classes was analyzed in the *in vitro* human metabolism assay, the big difference in metabolic rate may indicate that the benzimidazoles resist metabolism a lot better than the quinolines. However, the metabolic rate of other analogs in both classes must be evaluated.

Of the compounds analyzed in the therapeutic index (TI) assay, all have values greater than one, indicating that the reactivation of the p53, not just general toxicity, is contributing to the apoptosis of the tumor cells. The quinoline carbamates had the greatest TI, so far. However, the goal is to achieve a TI of 10-100 fold. Therefore, more studies into both classes' TIs are necessary. The apoptosis EC50s are in the μM range. Apoptosis EC50s in the nM range are desired. One of the most surprising findings of this study is seen in RD 14, where mutant p53 is reactivated (evident through presence of p21 on western blot); however, in the MTT assay, cells treated with the compound did not exhibit apoptosis. This means that while p53 is being reactivated the proteins responsible for apoptosis might not have been expressed. This is strange because it was predicated that reactivation of the mutated p53 will lead to apoptosis of the tumor cells, due to the multiple mutations found in tumor cells. This, however, reiterates the fact that not all downstream proteins of active p53 are expressed simultaneously, but vary depending on many factors such as signaling, DNA damage, etc. It is unclear as to whether or not the compounds are also acting on dissociating p53 from MDM2. If this is happening in normal cells, p53 might be activated, expressing downstream proteins, and potentially causing on-target toxicities in normal cells. However, because the concentration of p53/MDM2 in the normal cell is so low, this might be an issue of less concern.

Individually, each compound exhibits promising properties. However, so far, no compound has shown a complete profile suitable for development into a drug.

Future Directions

The drug discovery process was used to identify several compounds that displayed biological activity in reactivating mutant p53 in human glioblastoma cells and could cross the BBB. The data also indicate that the benzimidazole class may be metabolically more stable than the quinoline class. To further this research into establishing drugs to enter into clinical trials, other steps must also be completed. Firstly, further tests into metabolism are required for the other compounds. With the results, structures can be manipulated to increase or decrease metabolism rates, as needed. The same is also true for TI studies. Secondly, a favorable drug is one that is administered orally. Thus, a test similar to that mimicking the BBB can be utilized to mimic the gastrointestinal tract to provide an impression of oral absorption. Lastly, the compound concentrations used now are in the μM range, a very small concentration that already kills 50% of cells. Ideally, these compound concentrations that would kill 50% of cells should be around 100 nM. These values and modifications could lead into an *in vivo* study in rodents and perhaps humans later on. By studying the *in vivo* functions of these compounds, difference between the activity of the compounds in primary and secondary GBM can also be observed.

The data show that compounds in both the benzimidazole and quinoline classes are suitable lead structures for an anti-tumor drug discovery study. A SAR concerning biological activity, metabolic stability, selectivity, and the ability of compounds to cross the BBB is now developing. However, more compounds with complete profiles are

necessary for an accurate depiction of the direction to new compound design. This SAR will be used to optimize the overall profile of the compounds so as to identify a potential drug candidate to treat the brain cancer, glioblastoma multiforme.

APPENDIX A-Characterizations of compounds

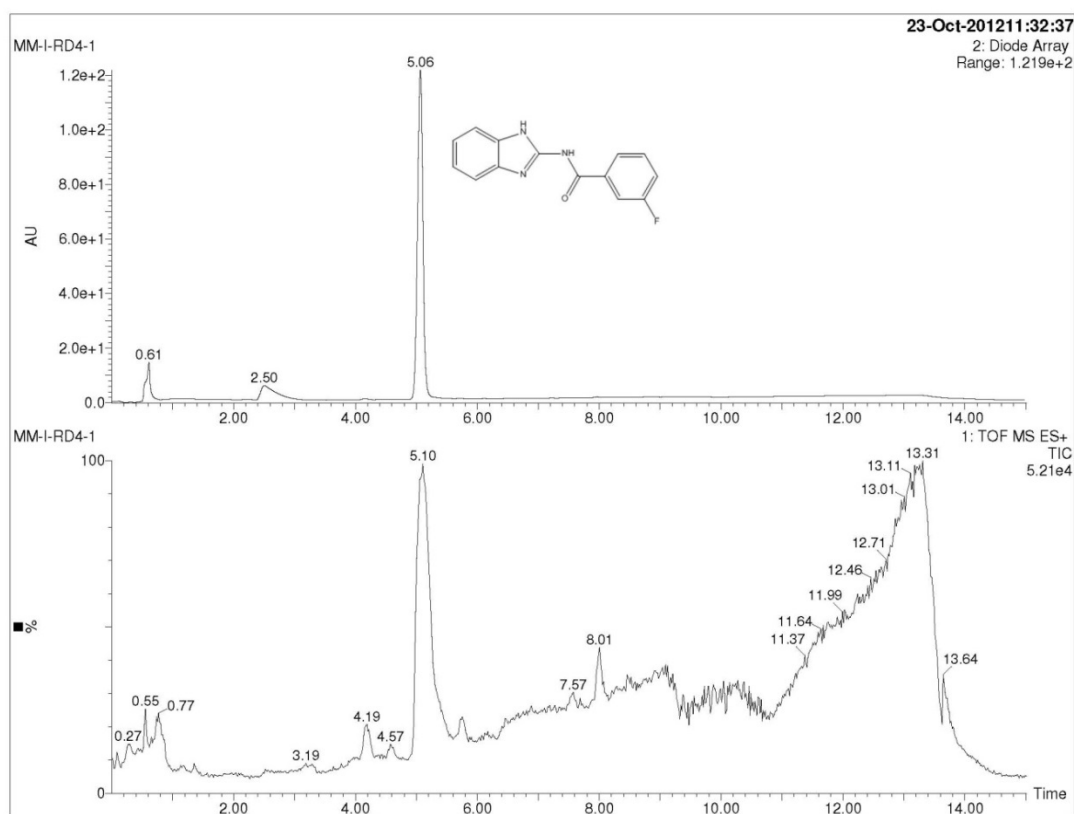


Figure 31: LC/MS chromatogram of RD4. Top graph depicts UV spectra with one sharp peak around 5 minutes, with 2 smaller peaks. This indicates the presence of a major compound with a few impurities. Analysis report indicated a purity greater than 95%, nonetheless. Bottom graph depicts mass spectrograph with a single large peak corresponding to that of the UV spectra.

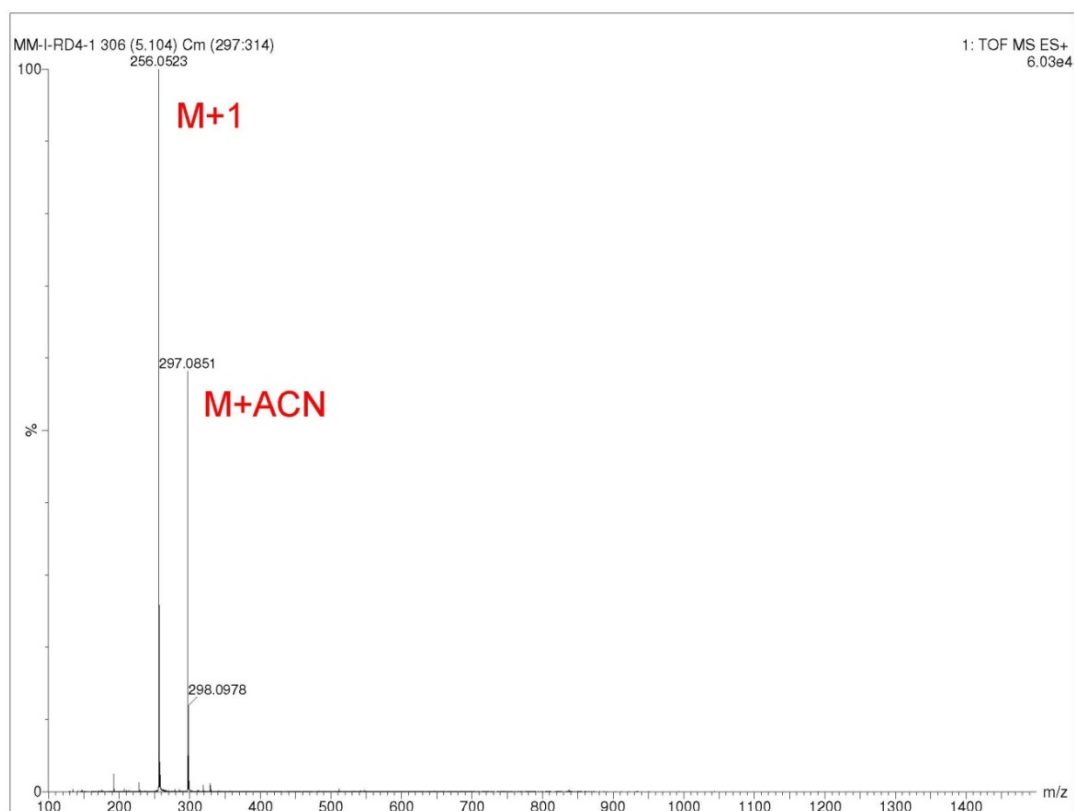


Figure 32: Area under large peak of RD 4 MS around 5 minutes. Major peak is M+1, consistent with compound MW=255. Shorter peak is P+ACN, consistent with compound coupling with acetonitrile, the most prevalent solvent in the system.

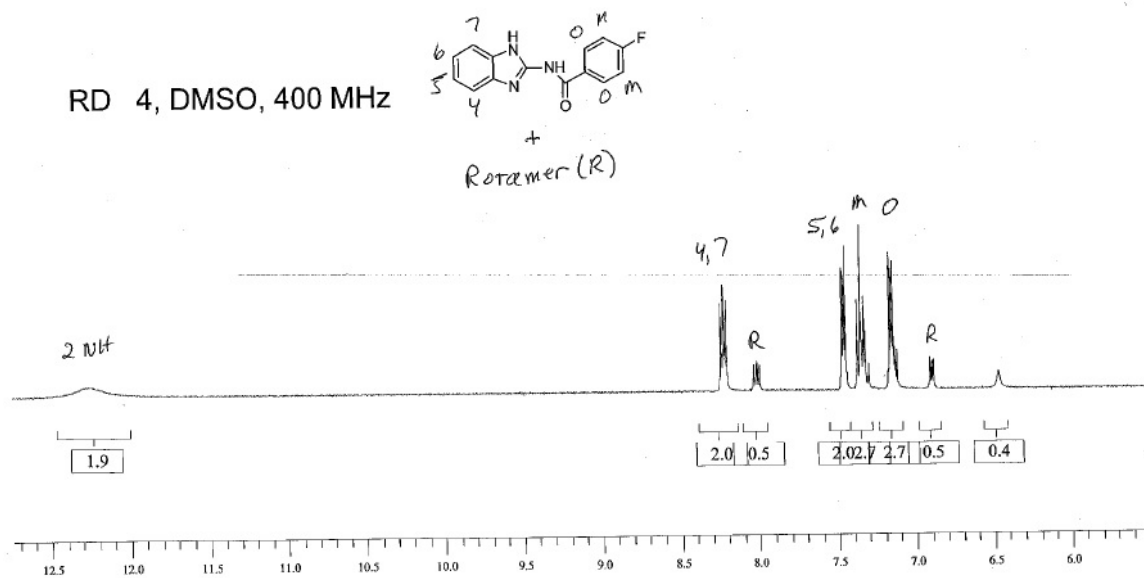


Figure 33: NMR spectra of RD 4: MS Electropray-TOF, $m/z = 256$ (M+H); ^1H NMR (400 MHz, DMSO) 12.3(1H, s, NH), 8.3(2H, m, 4,7-benzimidazole aromatic, 7.5(2H, m, 5,6-benzimidazole aromatic), 7.4 (2H, m meta-phenyl), 7.1(2H, ortho-phenyl)

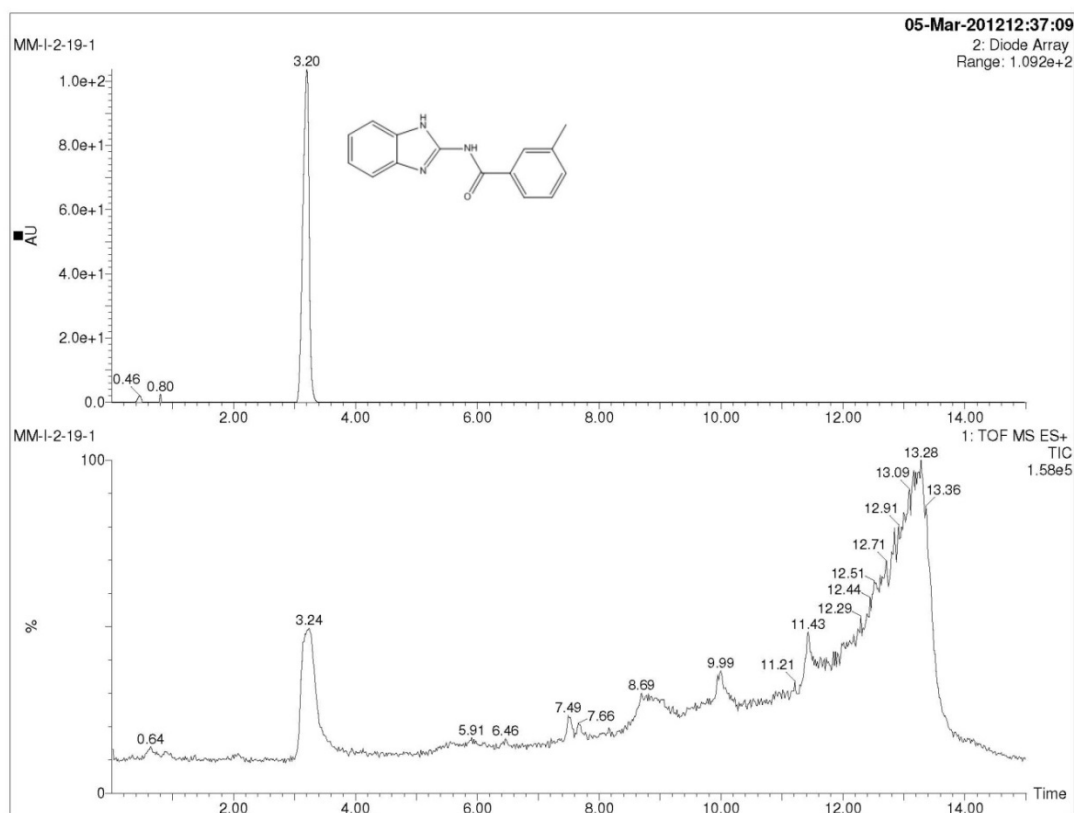


Figure 34: LC/MS chromatogram of RD13. Top graph depicts UV spectra with one sharp peak around 3 minutes, indicating the presence of a major compound. Bottom graph depicts mass spectrograph with a single large peak corresponding to that of the UV spectra.

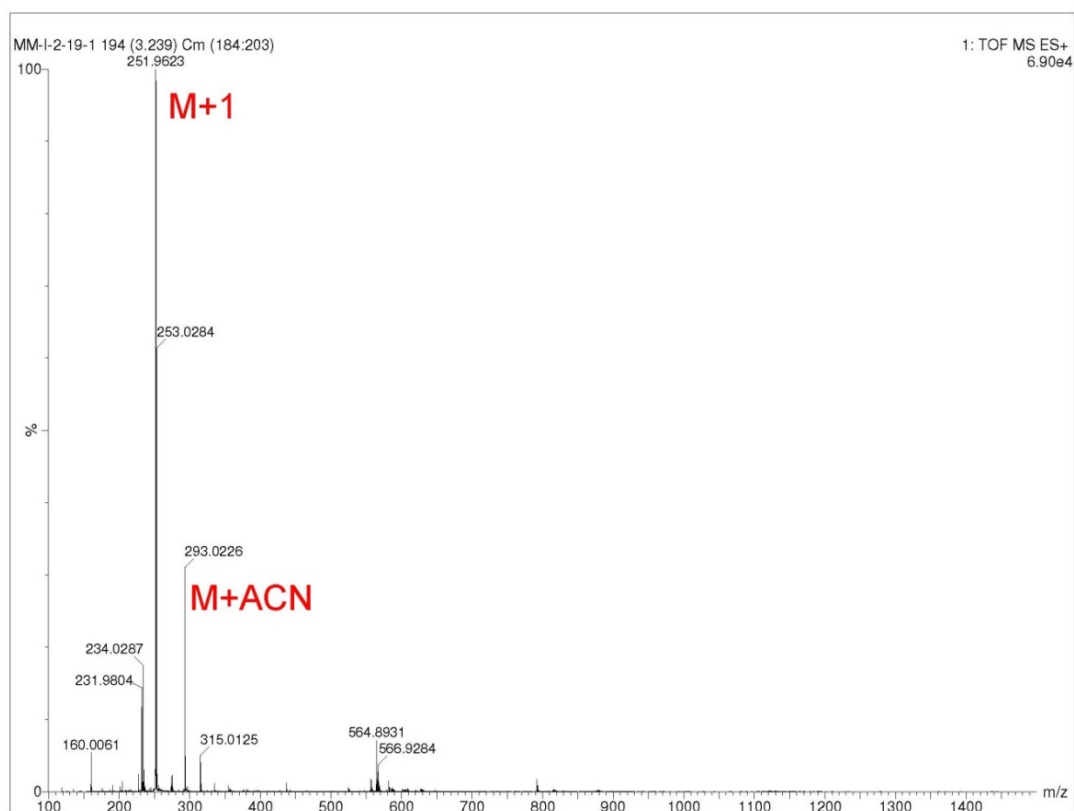


Figure 35: Area under large peak of RD 13 MS around 3 minutes. Major peak is M+1, consistent with compound MW=251. Shorter peak is P+ACN, consistent with compound coupling with acetonitrile, the most prevalent solvent in the system.

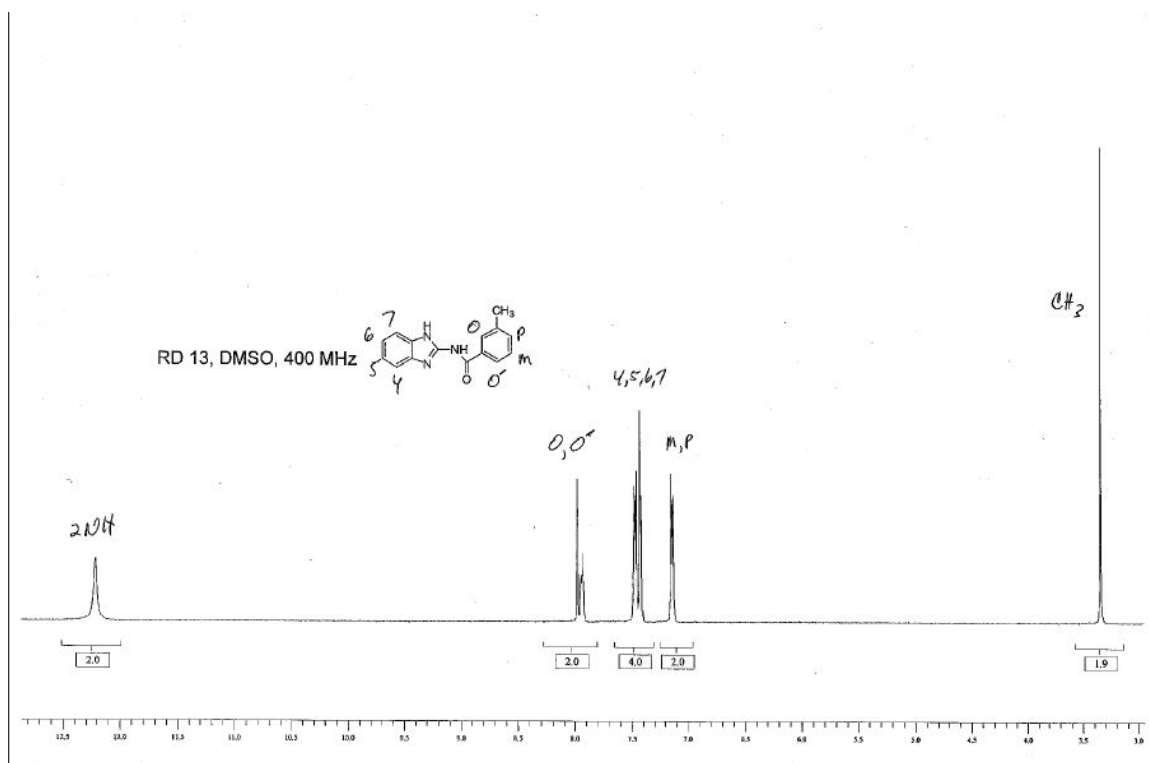


Figure 36: NMR spectra for RD 13. MS Electrospray-TOF, $m/z = 252$ (M+H); ^1H NMR (400 MHz, DMSO) 12.4(2H, s, NH), 7.9(2H, m, ortho-phenyl), 7.4(4H, m, 4,5,6,7-benzimidazole aromatic), 7.1 (2H, m meta and para-phenyl), 3.4 (3H, s, methyl)

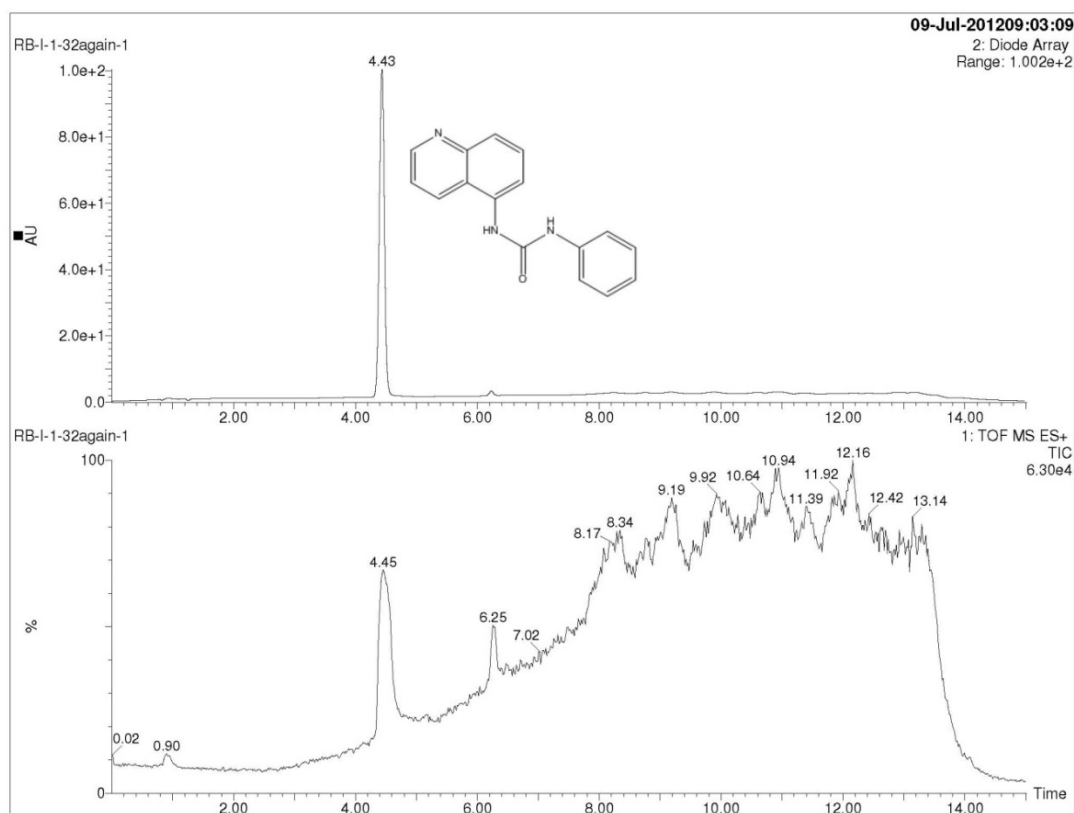


Figure 37: LC/MS chromatogram of RD14. Top graph depicts UV spectra with one sharp peak around 4 minutes, indicating the presence of a single organic compound. Bottom depicts mass spectrograph with a single large peak corresponding to that of the UV spectra.

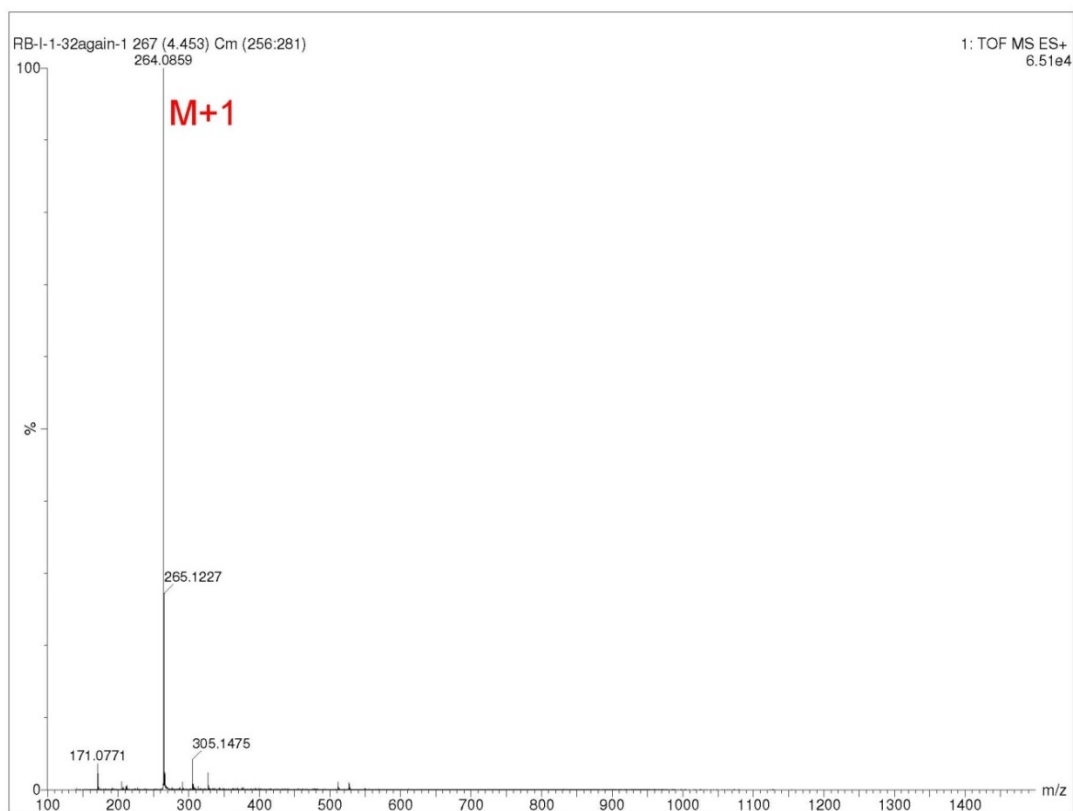


Figure 38: Area under large peak of RD 14 MS around 8 minutes. Major peak is M+1, consistent with compound MW=263.

RD 14, DMSO, 400MHz

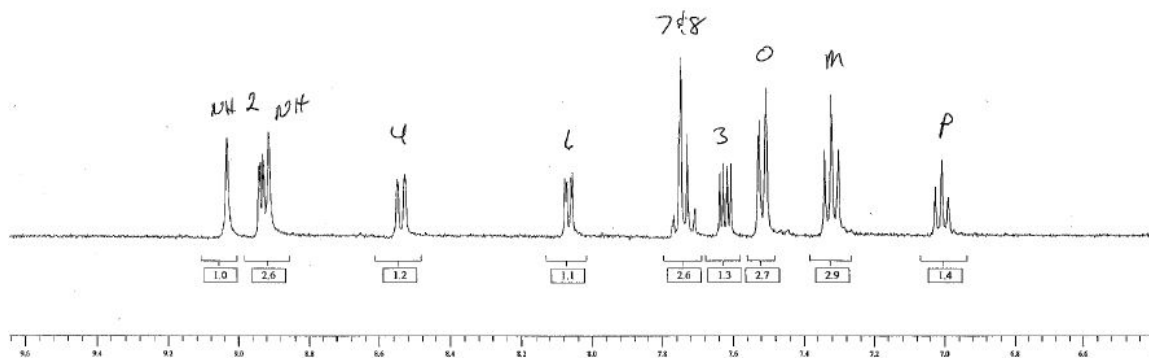
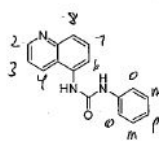


Figure 39: NMR spectra for RD 14. MS Electrospray-TOF, $m/z = 264.09$ (M+H); ¹H NMR (400 MHz, DMSO) 9.1(1H, s, NH), 8.86(1H, d, 2-quinoline aromatic), 8.82 (1H, s, NH), 8.46(1H,d, 4-quinoline aromatic), 8.03 (1H,dd 6- quinoline aromatic), 7.67 (2H, m, 7,8-quinoline aromatic), 7.61 (1H, dd, 3-quinoline aromatic), 7.43 (2H, d, ortho-phenyl), 7.23 (2H, t, meta-phenyl), 7.0 (1H, t, para-phenyl)

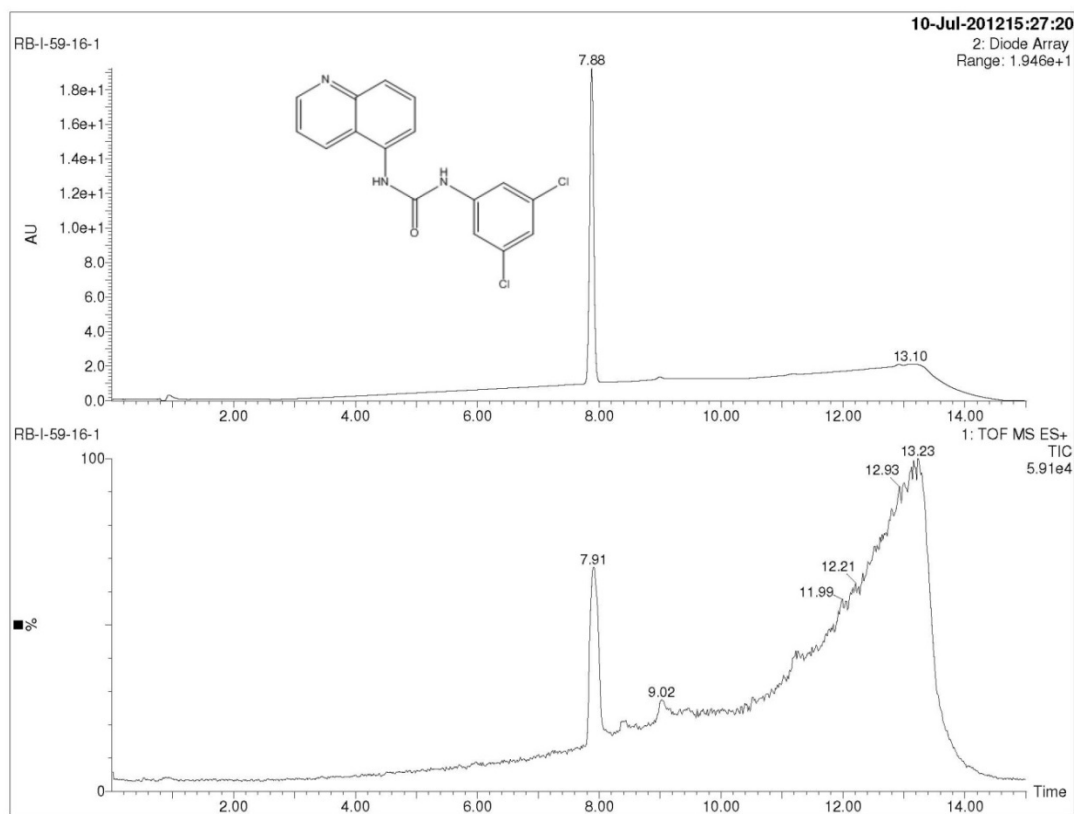


Figure 40: LC/MS chromatogram of RD27. Top graph depicts UV spectra with one sharp peak around 8 minutes, indicating the presence of a single organic compound. Bottom graph depicts mass spectrograph with a single large peak corresponding to that of the UV spectra.

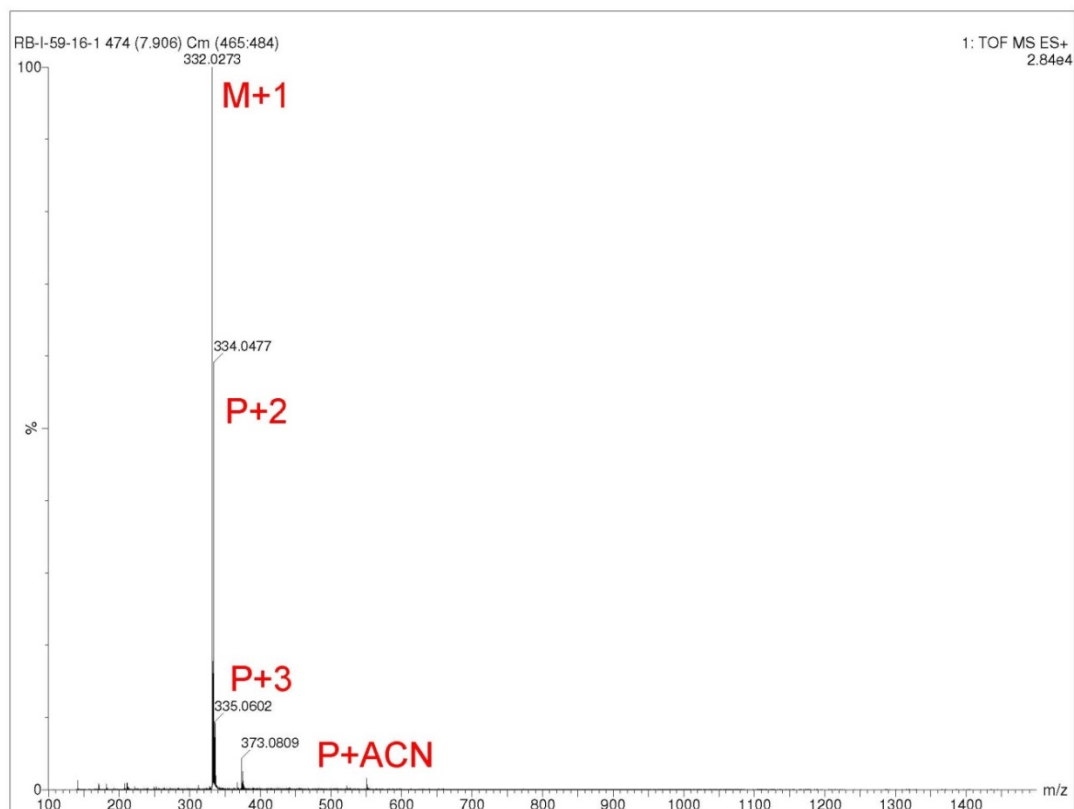


Figure 41: Area under large peak of RD 27 MS around 8 minutes. Major peak is M+1, consistent with compound MW=331. Smaller peaks include P+2, indicative of compound with ^{37}Cl ; P+ACN, indicative of compound coupled with acetonitrile.

RD 27, DMSO, 400 MHz

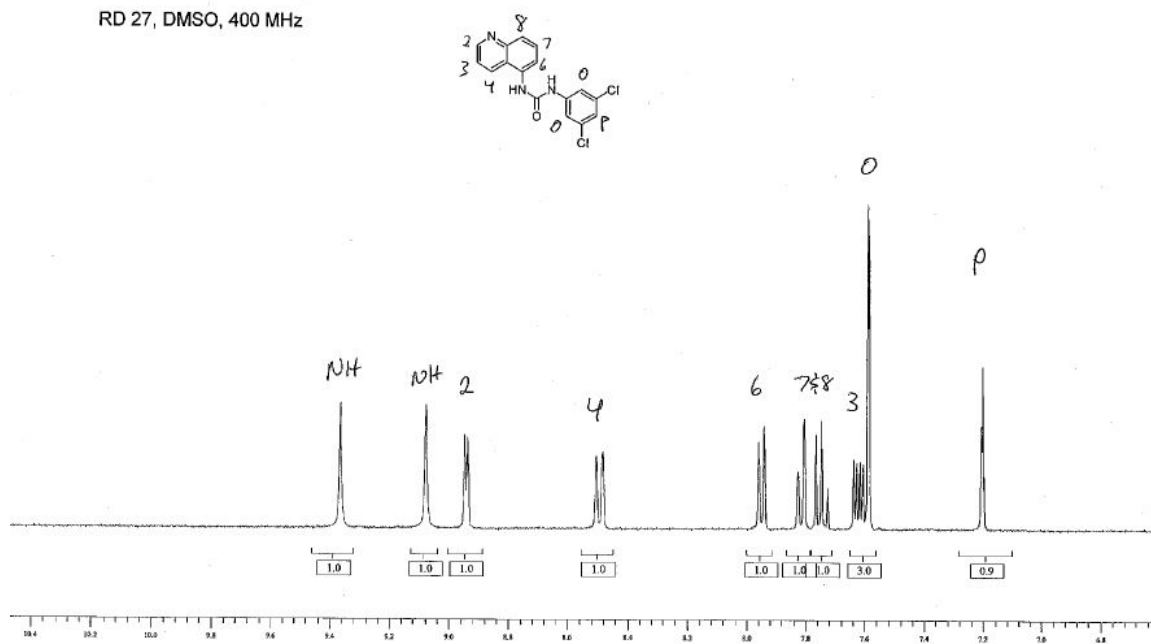


Figure 42: NMR Spectra for RD 27. MS Electrospray-TOF, $m/z = 332$ ($M+H$); ¹H NMR (400 MHz, DMSO) 9.4(1H, s, NH), 9.1 (1H, s, NH), 9.2(1H, d, 2-quinoline), 8.0(1H, d, 4-quinoline), 7.8(2H, m, 3 and 6-quinoline), 7.65(1H, m, 7-quinoline), 7.60(2H, s, 2 and 6-phenyl), 7.2(1H, s, 4-phenyl)

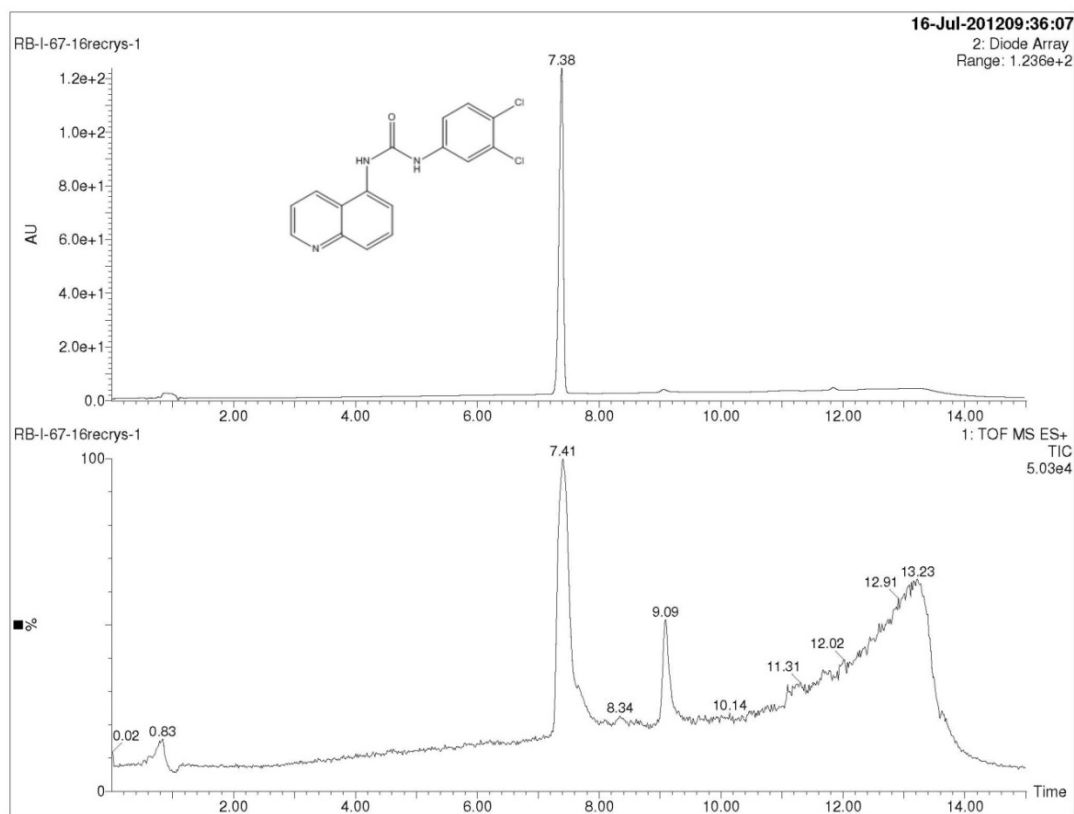


Figure 43: LC/MS chromatogram of RD29. Top graph depicts UV spectra with one sharp peak around 7 minutes, indicating the presence of a single organic compound. Bottom graph depicts mass spectrograph with a single large peak corresponding to that of the UV spectra.

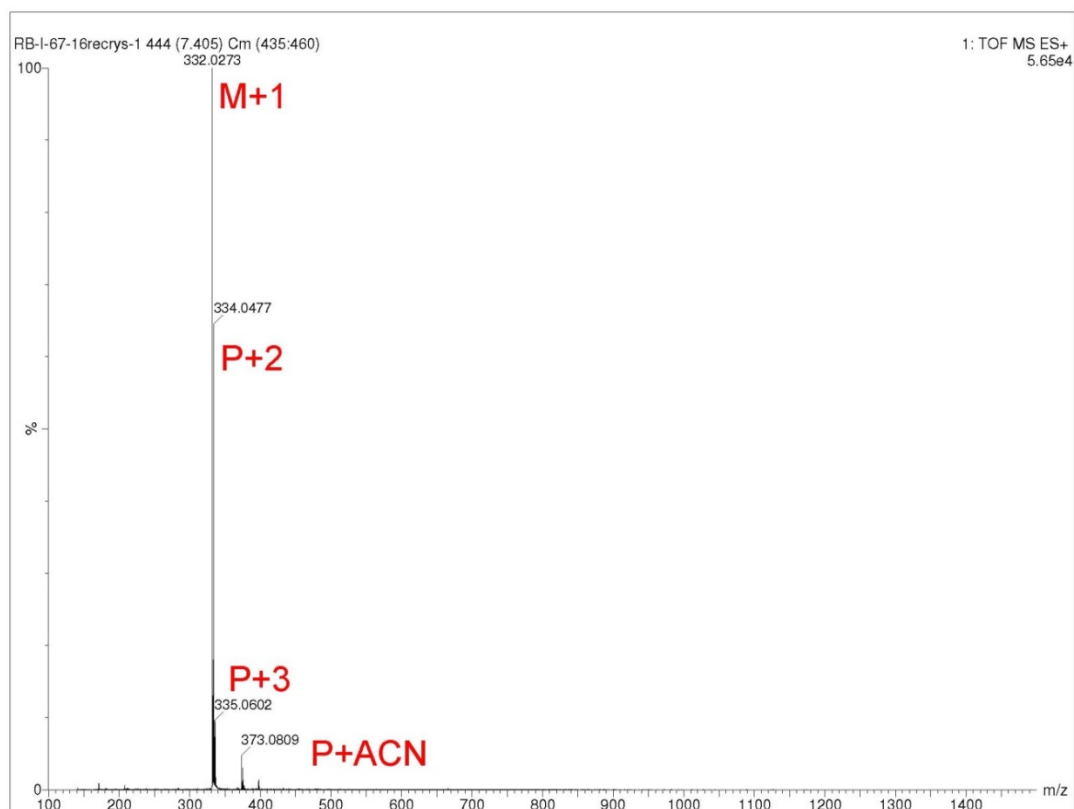


Figure 44: Area under large peak of RD 29 MS around 7 minutes. Major peak is M+1, consistent with compound MW=331. Smaller peaks include P+2, indicative of compound with ^{37}Cl isotope; P+ACN, indicative of compound coupled with acetonitrile

RD29, DMSO, 400 MHz

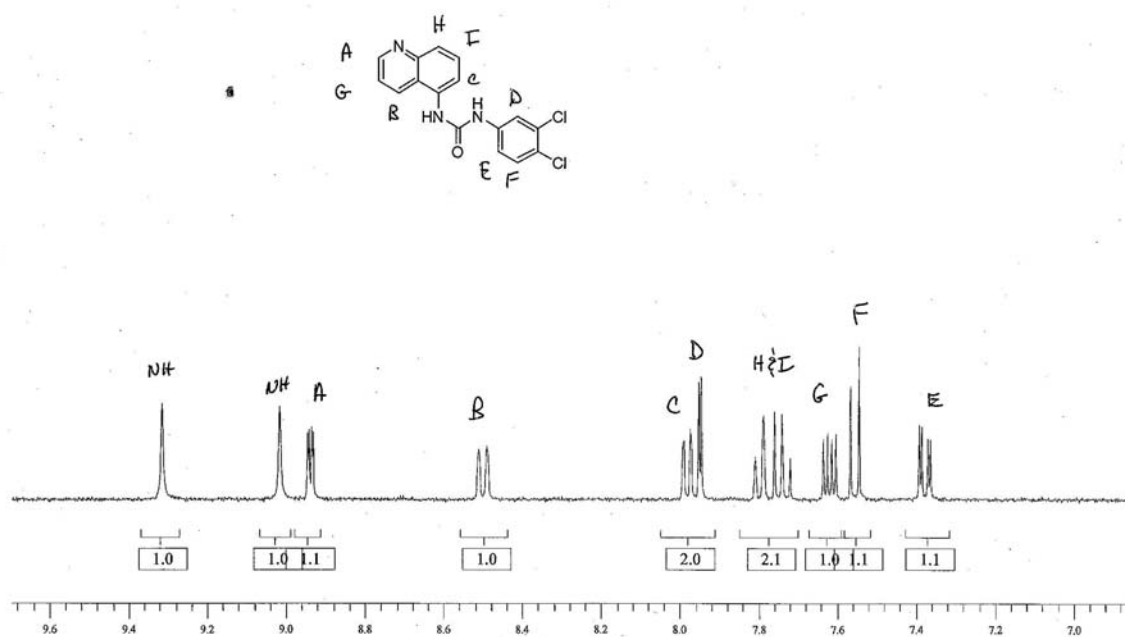


Figure 45: NMR Spectra for RD 29. MS Electrospray-TOF, $m/z = 332$ (M+H) H MNR (400 MHz, DMSO) 9.3(1H, s, NH), 9.0 (1H, s, NH), 8.9(1H, d, 2-quinoline), 8.5(1H, d, 4-quinoline), 8.0(2H, m, 6 and 8-quinoline), 7.8(2H, m, 3 and 7-quinoline), 7.7(1H, m, 5-phenyl), 7.6(1H, d, 2-phenyl), 7.4(1H, d, 5-phenyl).

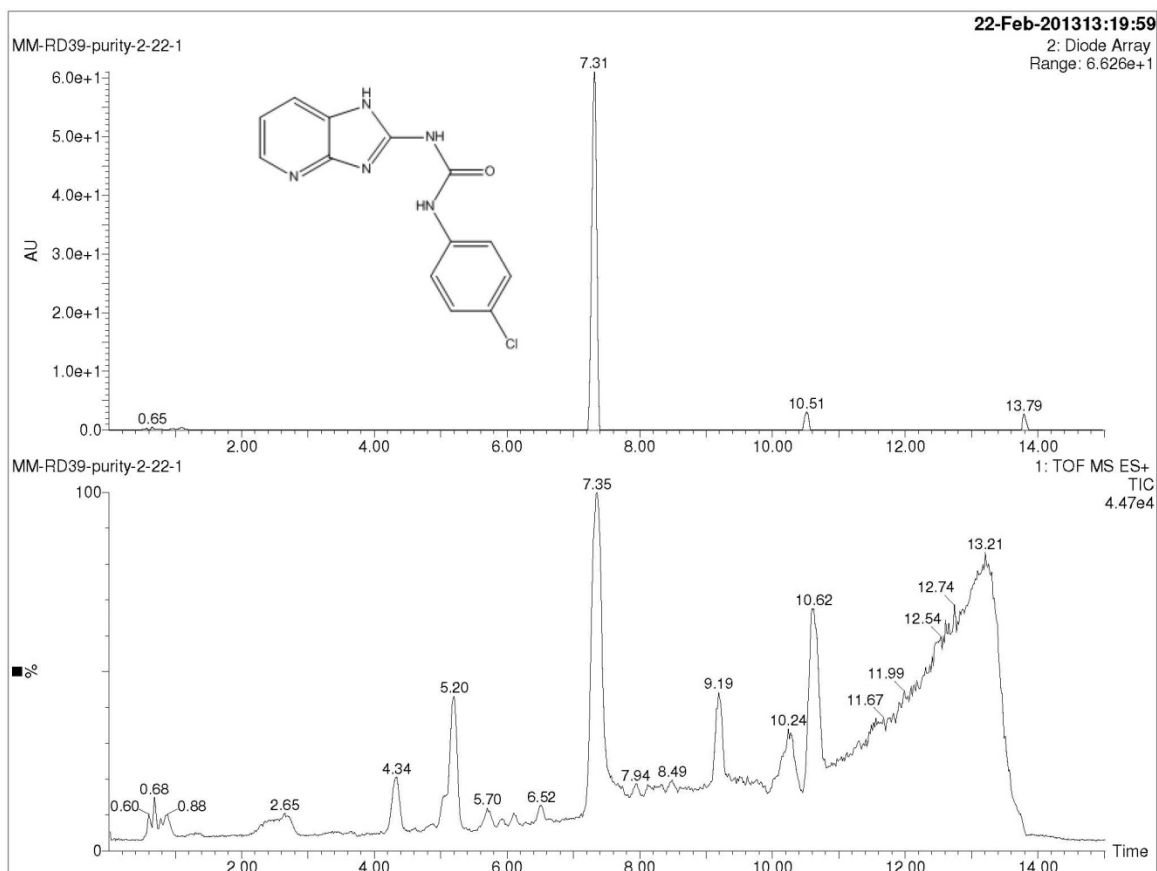


Figure 46: LC/MS chromatogram of RD39. Top graph depicts UV spectra with one sharp peak around 7.5 minutes, indicating the presence of a major compound. Bottom graph depicts mass spectrograph with a single large peak corresponding to that of the UV spectra.

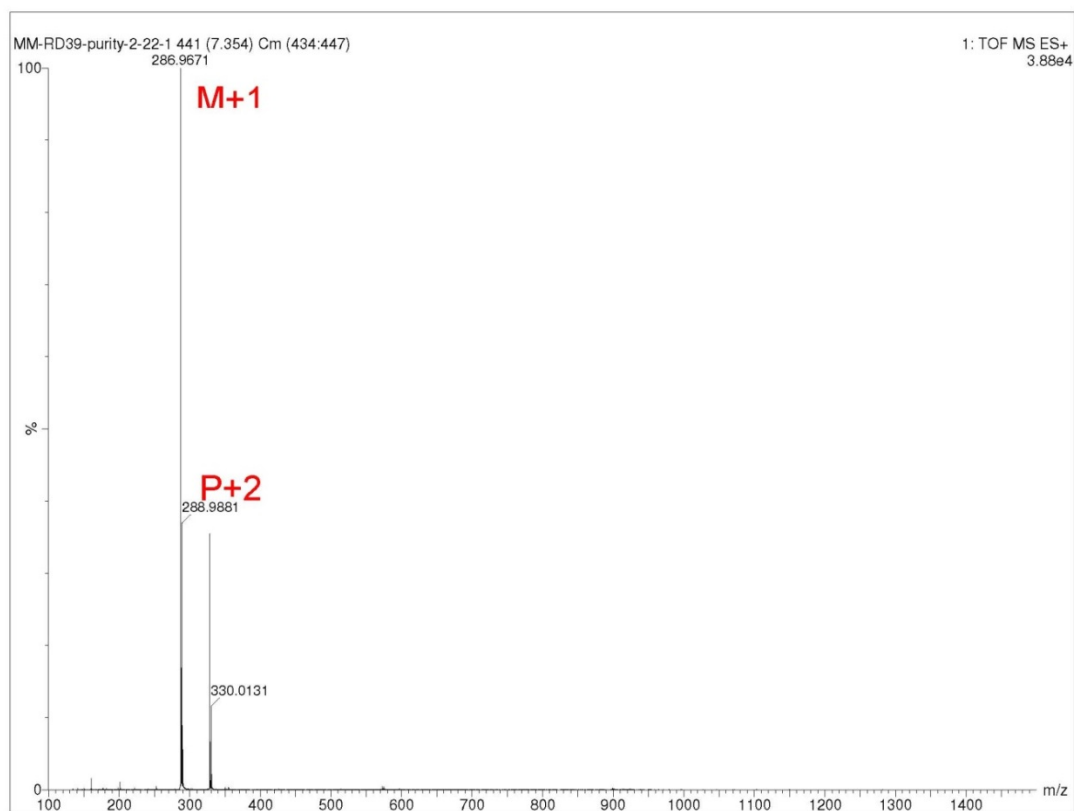


Figure 47: Area under large peak of RD 39 MS around 7.5 minutes. Major peak is M+1, consistent with compound MW=286. Shorter peak is P+2, indicative of compound with ^{37}Cl isotope.

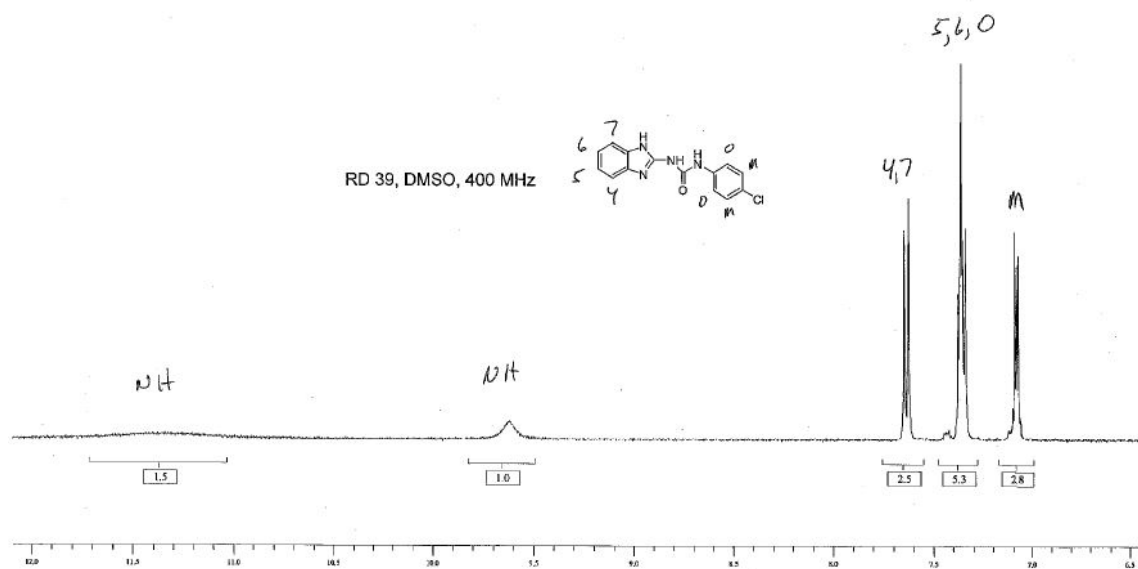


Figure 48: NMR spectra for RD 39. MS Electrospray-TOF, $m/z = 287$ (M+H); ^1H NMR (400 MHz, DMSO) 11.4(1H, s, NH), 9.6(1H, s, NH), 7.64(2H, d, 4,7-quinoline), 7.36 (3H, m, 5,6-benzimidazole, ortho-phenyl), 7.10 (2H,m, meta-phenyl)

APPENDIX B-BBBTR

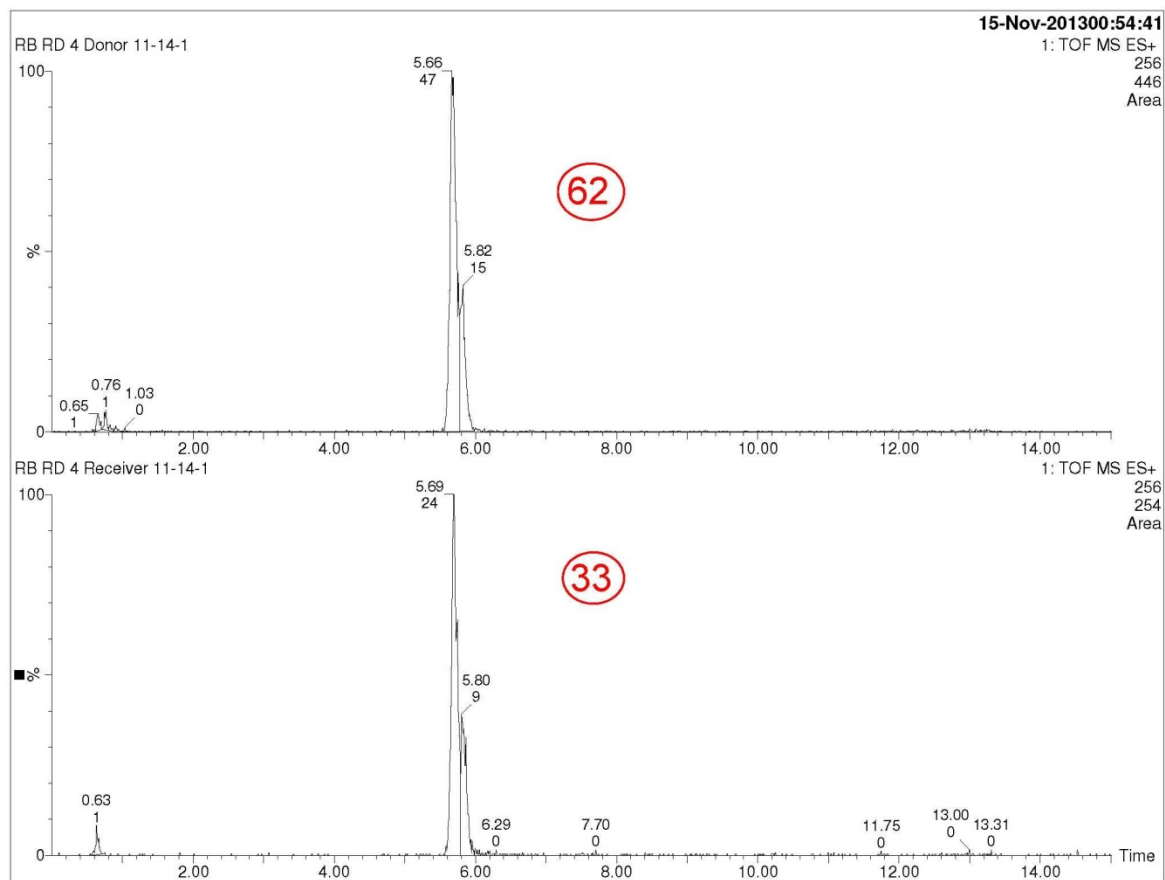


Figure 49: RD 4 BBB Assay; the top spectra is the analyzed MS spectra for the top donor well, while the bottom spectra is the analyzed MS spectra of the receiver well; the area under the peaks (highlighted to show only the compound in question) is integrated; a ratio of the integrated areas of receiver: donor indicate that BBBTR: 0.53 (33/62)

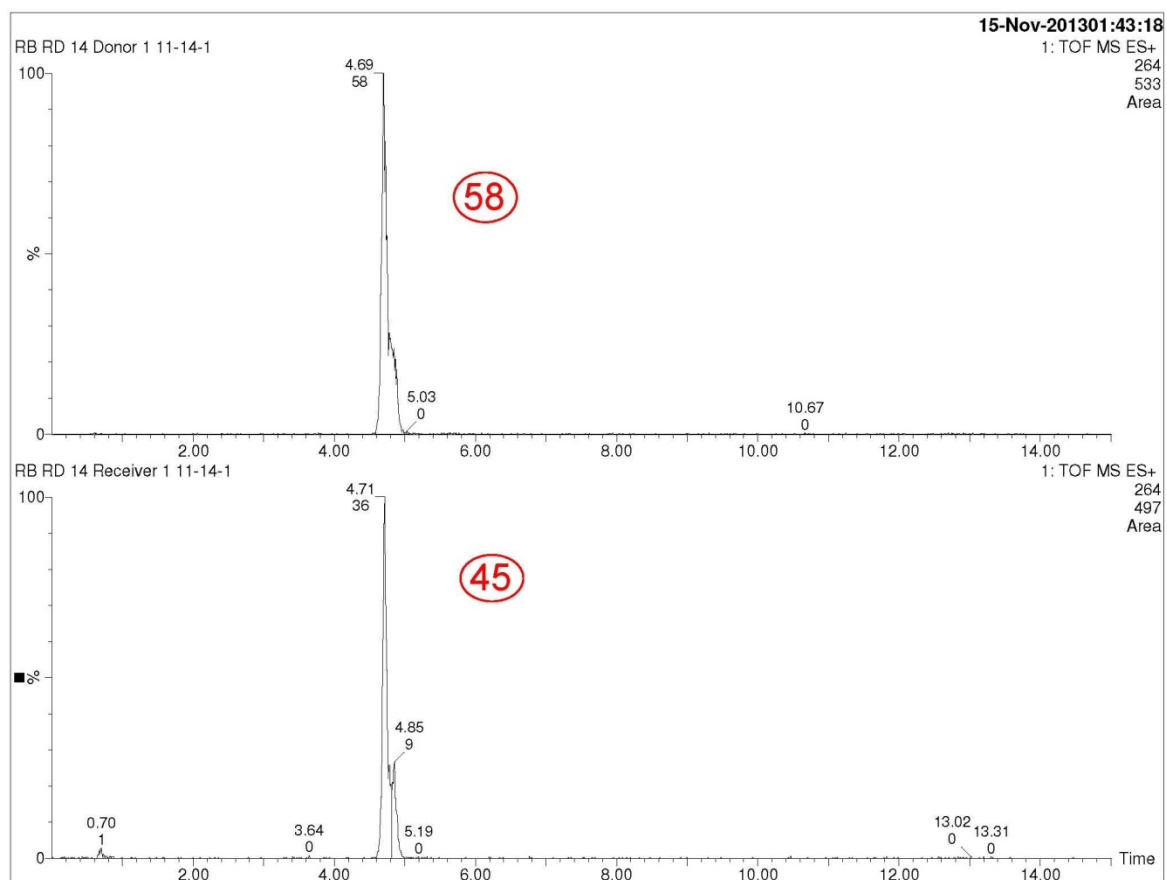


Figure 50: RD 14 BBB Assay; the top spectra is the analyzed MS spectra for the top donor well, while the bottom spectra is the analyzed MS spectra of the receiver well; the area under the peaks (highlighted to show only the compound in question) is integrated; a ratio of the integrated areas of receiver: donor indicate that BBBTR: 0.78 (45/58)

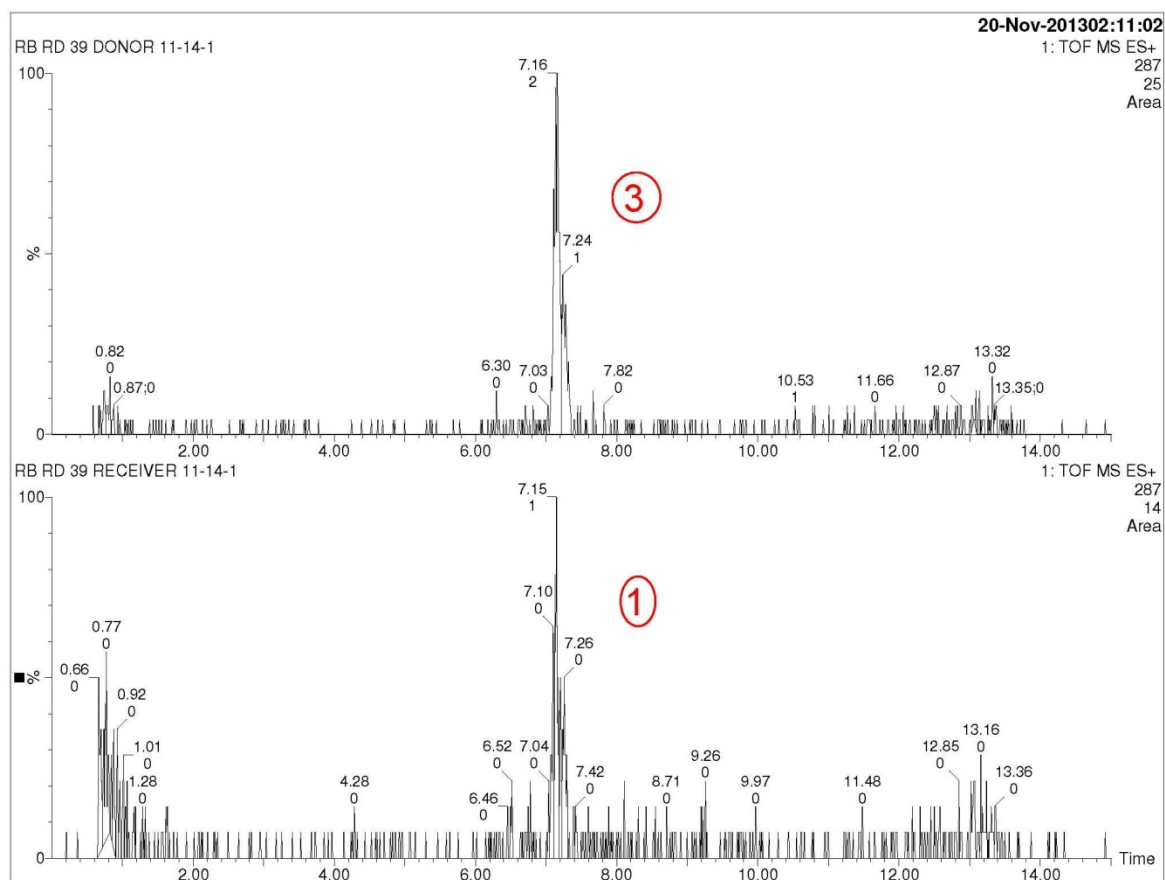


Figure 51: RD 39 BBB Assay; the top spectra is the analyzed MS spectra for the top donor well, while the bottom spectra is the analyzed MS spectra of the receiver well; the area under the peaks (highlighted to show only the compound in question) is integrated; a ratio of the integrated areas of receiver: donor indicate that BBBTR: 0.33

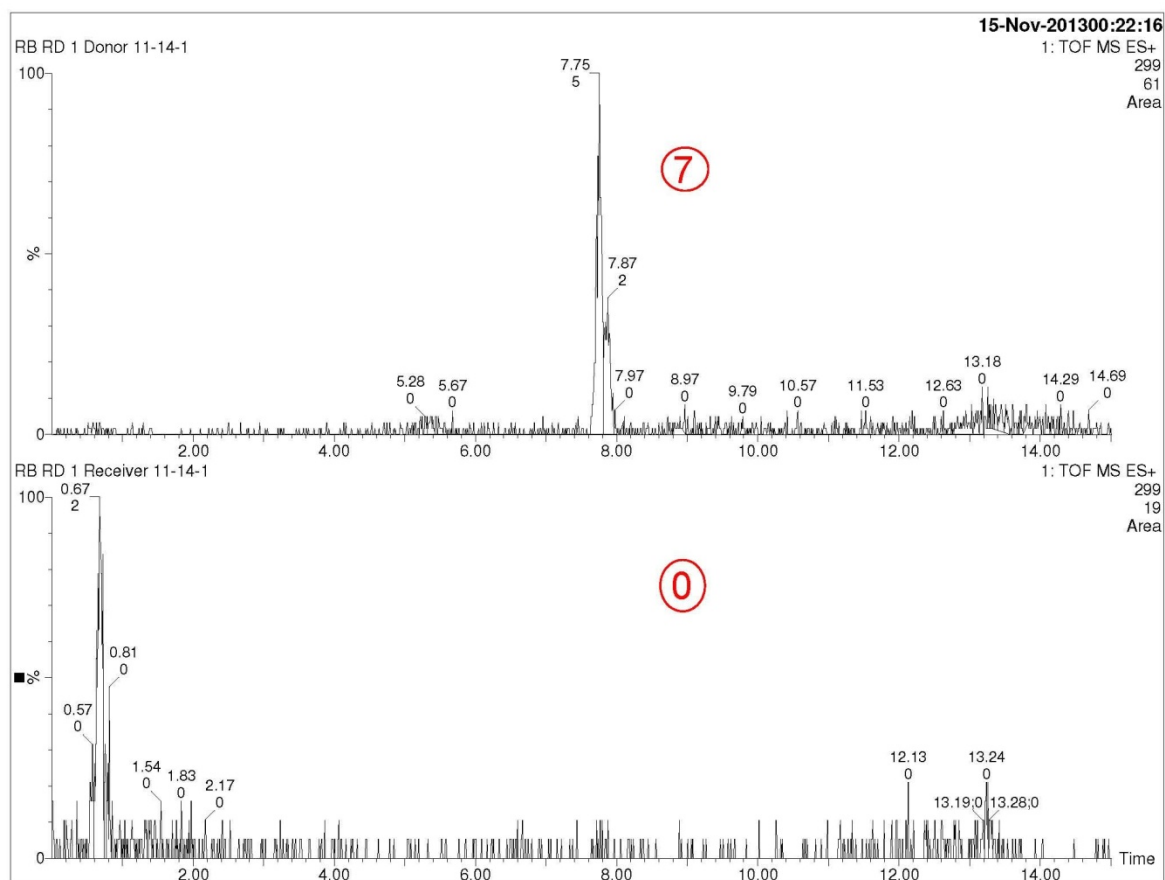


Figure 52: RD 1 BBB Assay; the top spectra is the analyzed MS spectra for the top donor well, while the bottom spectra is the analyzed MS spectra of the receiver well; the area under the peaks (highlighted to show only the compound in question) is integrated; a ratio of the integrated areas of receiver: donor indicate that BBBTR: 0.0

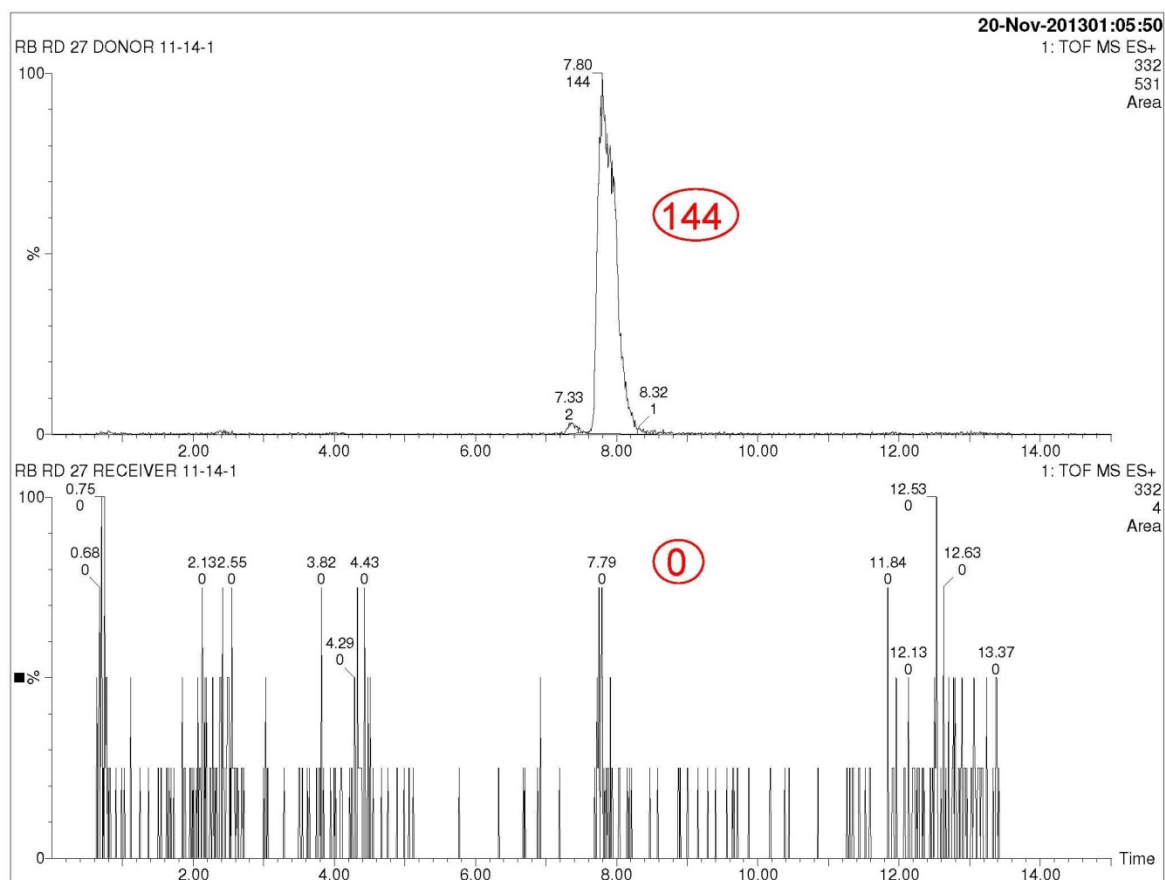


Figure 53: RD 27 BBB Assay; the top spectra is the analyzed MS spectra for the top donor well, while the bottom spectra is the analyzed MS spectra of the receiver well; the area under the peaks (highlighted to show only the compound in question) is integrated; a ratio of the integrated areas of receiver: donor indicate that BBBTR: 0.0

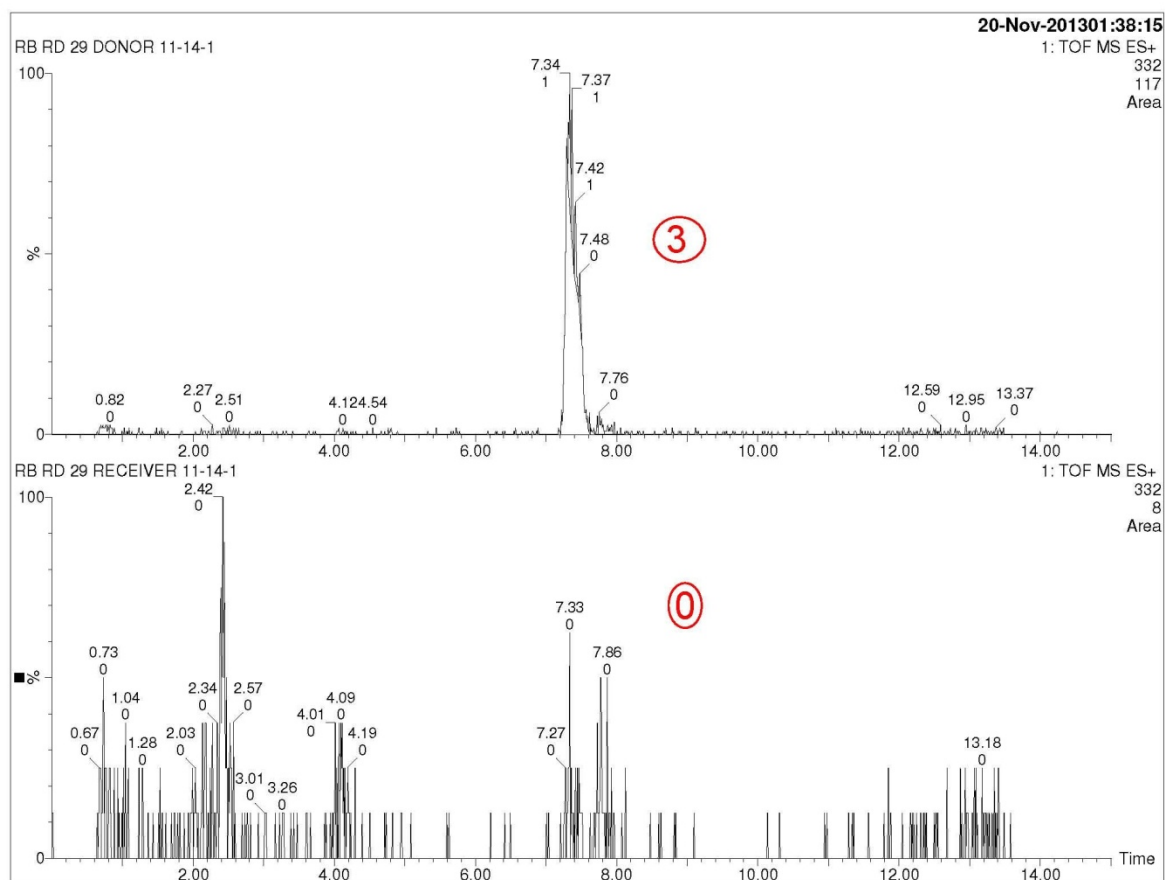


Figure 54: RD 29 BBB Assay; the top spectra is the analyzed MS spectra for the top donor well, while the bottom spectra is the analyzed MS spectra of the receiver well; the area under the peaks (highlighted to show only the compound in question) is integrated; a ratio of the integrated areas of receiver: donor indicate that BBBTR: 0.0

BIBLIOGRAPHY

- Abraham, R. (2001) "Cell cycle checkpoint signaling through the ATM and ATR kinases" *Genes and Development* 15: 2177-2196.
- American Cancer Society. (2003) *Cancer Facts & Figures 2013*. Atlanta, GA: American Cancer Society.
- Anand, P., Kunnumakara, B., Sundaram, C., Harikumar, B., Tharakan, T., Lai, S., Sung, B. and Aggarwal, B. (2008) "Cancer Is a Preventable Disease That Requires Major Lifestyle Changes." *Pharmaceutical Research* 25(9): 2097-2116.
- Armulik, A. (2010) "Pericytes Regulate The Blood–Brain Barrier" *Nature* 468: 557-561.
- Attardi, L., Reczek, E., Cosmas, C., Demicco, E., McCurrach, M., Lowe, S., Jacks, T. (2000) "PERP, an Apoptosis-associated Target of p53, is a Novel Member of the PMP-22/gas3 Family" *Genes and Development* 14(6): 704-718.
- Balani, S., Miwa, G., Gan, L., Wu, J., and Lee, F. (2005) "Strategy of Utilizing In Vitro and In Vivo ADME Tools for Lead Optimization and Drug Candidate Selection." *Current Topics in Medicinal Chemistry* 5(11): 1033-1038.
- Bennett, M., Macdonald, K., Chan, S., Luzio, J., Simari, R., Weissberg, P. (1998) "Cell Surface Trafficking of Fas: A Rapid Mechanism of p53-Mediated Apoptosis" *Science* 282:290-293.
- Berube, C., et al. (2005) "Apoptosis Caused by P53-Induced Protein with Death Domain (PIDD) Depends on the Death Adapter Protein RAIDD" *Proceedings of the National Academy of Sciences* 102(40):14314-14319.
- Bourdon, J., Renzing J., Robertson, P., Fernandes, K., Lane, D. (2002) "Scotin, a Novel p53-inducible Proapoptotic Protein Located in the ER and the Nuclear Membrane" *The Journal of Cell Biology* 158(2): 235-246.
- Bykov, V., Selivanova, G., Wiman, K. (2003) "Small Molecules That Reactivate Mutant p53" *European Journal of Cancer* 39(13): 1828-1834.
- Clarke, J., Penas, C., Pastori, C., Komotar, RJ., Bregy, A., Shah, AH., Wahlestedt, C., and Ayad, NG. (2013) "Epigenetic Pathways and Glioblastoma Treatment." *Epigenetics* 8: 785-95.
- Chen, P., Chen, Y., Bookstein, R., and Lee, W. (1990) "Genetic Mechanisms of Tumor Suppression by the Human P53 Gene." *Science* 250(4987): 1576-580.
- Christiani, D. (2011) "Combating Environmental Causes of Cancer." *New England Journal of Medicine* 364(9): 791-93.
- Coates, A, Abraham, S., Kaye, S., Sowerbutts, T., Frewin, C., Fox, R., and Tattersall, M. (1983) "On the Receiving End—Patient Perception of the Side-effects of Cancer Chemotherapy." *European Journal of Cancer and Clinical Oncology* 19(2): 203-08.
- Corrie, P. (2008) "Cytotoxic Chemotherapy: Clinical Aspects" *Medicine* 36:24-28.
- Cui B, Yang Q, Guan H, Shi B, Hou P, Ji M. (2014) "PRIMA-1, a Mutant p53 Reactivator, Restores the Sensitivity of TP53 Mutant-type Thyroid Cancer Cells to the Histone Methylation Inhibitor 3-Deazaneplanocin A (DZNep)" *The Journal of Clinical Endocrinology and Metabolism*
- Di, L., Kerns, E., Fan, K., McConnell, O., and Carter, G. (2003) "High Throughput Artificial Membrane Permeability Assay for Blood–brain Barrier." *European Journal of Medicinal Chemistry* 38(3): 223-232.
- Dingli, D., and Nowak, M. (2006) "Cancer Biology: Infectious Tumour Cells." *Nature* 443(7107): 35-36.

- Edwards, B., Brown, M., Wingo, P., Howe, H., Ward, E., Ries, L., Schrag, D., Jamison, P., Jemal, A., Wu, X., Friedman, C., Harlan, L., Warren, J., Anderson, R., and Pickle, L. (2005) "Annual Report to the Nation on the Status of Cancer, 1975-2002, Featuring Population-Based Trends in Cancer Treatment." *Journal of the National Cancer Institute* 97(19):1407-427.
- Elledge, S. (1996) "Cell Cycle Checkpoints: Preventing an Identity Crisis." *Science* 274: 1664-1672.
- Foster, B. (1999) "Pharmacological Rescue of Mutant P53 Conformation and Function." *Science* 286(5449): 2507-510.
- Gabathuler, R. (2010) "Approaches to Transport Therapeutic Drugs Across the Blood-brain Barrier to Treat Brain Diseases" *Neurobiology of Disease* 37: 48-57.
- Goodsell, D. (1999) "The Molecular Perspective: The Ras Oncogene" *The Oncologist* 4(3): 263-264.
- Gordon, D., Resio, B., and Pellman, D. (2012) "Causes and Consequences of Aneuploidy in Cancer." *Nature Reviews Genetics* 13: 189-203.
- Greenblatt M., Bennett, W., Hollstein, M., Harris, C. (1994) "Mutations in the p53 Tumor Suppressor Gene: Clues to Cancer Etiology and Molecular Pathogenesis" *Perspectives in Cancer Research* 54: 4855-4878.
- Hanahan, D., and Weinberg, A. (2011) "Hallmarks of Cancer: The Next Generation." *Cell* 144(5): 646-74
- Jakate, S., Saclarides, T. (1993) "Immunohistochemical Detection Of Mutant P53 Protein And Human Papillomavirus-Related E6 Protein In Anal Cancers" *Diseases of the Colon and Rectum* 36(11): 1026-1029.
- Jeffrey, P., and Summerfield, S. (2010) "Assessment of the Blood-brain Barrier in CNS Drug Discovery." *Neurobiology of Disease* 37(1): 33-37.
- Jemal, A., Bray, F., Center, M., Ferlay, J., Ward, E. and Forman, D. (2011) "Global Cancer Statistics." *CA: A Cancer Journal for Clinicians* 61(2): 69-90.
- Joerger A., Ang H., Fersht A. (2006) "Structural Basis for Understanding Oncogenic p53 Mutations and Designing Rescue Drugs." *Proceedings of the National Academy of Sciences* 103(41): 15056-15061
- Johnson, D., and O'Neill, B. (2012) "Glioblastoma Survival in the United States Before and During the Temozolomide era" *Journal of Neuro-oncology* 107(2): 359-364.
- Joshi, A., Parsons, D., Velculescu, V., Riggins, G. (2011) "Sodium Ion Channel Mutations In Glioblastoma Patients Correlate With Shorter Survival" *Molecular Cancer* 10:17
- Korzekwa, K (2014) "Enzyme Kinetics of Oxidative Metabolism: Cytochromes P450" *Methods in Molecular Biology* 1113: 149-166.
- Lambert, J. et al. (2009) "PRIMA-1 Reactivates Mutant p53 by Covalent Binding to the Core Domain" *Cancer Cell* 15(5):376-388.
- Levine, A., Momand, J., Finlay, C. (1991) "The P53 Tumour Suppressor Gene." *Nature* 351(6326): 453-56.
- Li, L., and Zou, L. (2004) "Sensing, Signaling, And Responding To DNA Damage: Organization Of The Checkpoint Pathways In Mammalian Cells" *Journal of Cellular Biochemistry* 94(2): 298-306.
- Liekens, S., Bronckaers, A., Balzarini, J. (2009) "Improvement Of Purine And

- Pyrimidine Antimetabolite-Based Anticancer Treatment By Selective Suppression Of Mycoplasma-Encoded Catabolic Enzymes" *The Lancet Oncology* 10(6): 628-635.
- Liu, X. (2004) "Development of a Computational Approach To Predict Blood-Brain Barrier Permeability." *Drug Metabolism and Disposition* 32(1): 132-139.
- Liu, X., Wilcken, R., Joerger, A., Chuckowree, I., Amin, J., Spencer, J. and Fersht, A. (2013) "Small Molecule Induced Reactivation of Mutant P53 in Cancer Cells." *Nucleic Acids Research* 41(12): 6034-044.
- Liu, J. Quinoline Compounds as Inhibitors of Angiogenesis, Human Methionine Aminopeptidase, and Sirt1, and Methods of Treating Disorders. Johns Hopkins University, Patent PCT/US2009/005475. 6 Oct. 2009 WO 2010/042163 A2.
- Lipinski, C., Lombardo, F., Dominy, B., and Feeney, B. (2012) "Experimental and Computational Approaches to Estimate Solubility and Permeability in Drug Discovery and Development Settings" *Advanced Drug Delivery Reviews* 64: 4-17.
- Ma, C., Janetka, J., Piwnick-Worms, H. (2011) "Death by releasing the breaks: CHK1 inhibitors as cancer therapeutics" *Trends in Molecular Medicine* 17(2):88-96.
- McCormick, F. (1999) "Signalling Networks That Cause Cancer" *Trends in Biochemical Sciences* 24(12): M53-M56.
- Meerlo, J., Kaspers, G., Cloos, J. (2011) "Cell Sensitivity Assays: The MTT Assay" *Cancer Cell Culture: Methods in Molecular Biology* 731:237-245.
- Mesri, E., Feitelson, M., Munger, K. (2014) "Human Viral Oncogenesis: A Cancer Hallmarks Analysis" *Cell Host and Microbe* 15(3): 266-282.
- Minotti, G., Menna, P., Salvatorelli, E., Cairo, G., Gianni, L. (2004) "Anthracyclines: Molecular Advances and Pharmacologic Developments in Antitumor Activity and Cardiotoxicity" *Pharmacological Reviews* 56(2): 185-229.
- Mischel, P. et al. (2003) "Identification of Molecular Subtypes of Glioblastoma by Gene Expression Profiling" *Oncogene* 22:2361-2373.
- Mitchell, J., Choudhuri R., Fabre, K. (2010) "In vitro and in vivo Radiation Sensitization of Human Tumor Cells by a Novel Checkpoint Kinase Inhibitor, AZD7762" *Clinical Cancer Research* 16(7): 2076-2084.
- Morris, E., et al. (2001) "Cyclin-Dependent Kinases and P53 Pathways Are Activated Independently and Mediate Bax Activation in Neurons after DNA Damage" *The Journal of Neuroscience* 21(14): 5017-5026.
- Muehlbacher, M., Spitzer, G., Liedl, K., and Kornhuber, J. (2011) "Qualitative Prediction of Blood-brain Barrier Permeability on a Large and Refined Dataset." *Journal of Computer-Aided Molecular Design* 25(12): 1095-1106.
- Nagpal, J., Jamoona, A., Gulati, N, Mohan, A., Braun, A., Mural, R., and Jhanwar-Uniyal, M. (2006) "Revisiting the Role of p53 in Primary and Secondary Glioblastomas" *Anticancer Research* 26: 4633-4640.
- Nigg, E. (1995) "Cyclin-dependent Protein Kinases: Key Regulators of the Eukaryotic Cell Cycle." *BioEssays* 17(6): 471-80.
- Oda, E., Ohki, R., Murasawa, H., Nemoto, J., Shibue, T., Yamashita, T., Tokino, T., Taniguchi, T., Tanaka, N. (2000) "Noxa, A BH3-Only Member Of The Bcl-2 Family And Candidate Mediator Of P53-Induced Apoptosis" *Science* 12: 1053-1058.
- Oda, K., et al. (2000) "p53AIP1, a Potential Mediator Of P53-Dependent Apoptosis, and

- its Regulation by Ser-46-Phosphorylated p53" *Science* 102(6): 849-862
- Ohgaki, H., and Kleihues, P. (2005) "Epidemiology and Etiology of Gliomas." *Acta Neuropathologica* 109 (1): 93-108.
- Ohgaki, H., and Kleihues, P. (2007) "Genetic Pathways to Primary and Secondary Glioblastoma." *The American Journal of Pathology* 170(5): 1445-453.
- Pietenpol, J., and Steward, Z. (2002) "Cell Cycle Checkpoint signaling: Cell Cycle Arrest Versus Apoptosis" *Toxicology* 181: 475-481.
- Rajasekhar, V., Viale, A., Socci, N., Wiedmann, M., Hu, X., Holland, E. (2003) "Oncogenic Ras and Akt Signaling Contribute To Glioblastoma Formation By Differential Recruitment Of Existing Mrnas To Polysomes" *Molecular Cell* 12(4):889-901.
- Roofian, R., Noori-Daloi, M., Saeed-Rad, S., Modarresi, M., GHaffari, S., Mojarrad, M., Abolhasani, F., Heidari, M. (2013) "Differential Expression of Human Homeodomain TGIFLX in Brain Tumor Cell Lines." *Acta medica Iranica* 51(12): 834-41.
- Rubin, L. (1999) "The Cell Biology Of The Blood-Brain Barrier" *Annual Review of Neuroscience* 22: 11-28.
- Shaheen M, Allen C, Nickoloff J, Hromas R. (2011) Synthetic Lethality: Exploiting the Addiction of Cancer to DNA Repair. *Blood* 117(23): 6074-6082
- Shim, J., Matsui, Y., Bhat, S., Nacev, BA., Xu, J., Bhang, H., Dhara, S., Han, K., Chong, C., Pomper, M., So, A., and Liu, J. (2010) "Effect of Nitroxoline on Angiogenesis and Growth of Human Bladder Cancer." *Journal of the National Cancer Institute* 102(24): 1855-873.
- Siegel, R., Naishadham, D., and Jemal, A. (2013) "Cancer Statistics, 2013." *CA: A Cancer Journal for Clinicians* 63(1): 11-30.
- Singh, S. (2006) "Preclinical Pharmacokinetics: An Approach Towards Safer and Efficacious Drugs." *Current Drug Metabolism* 7(2): 165-82.
- Siti, Y. (2010) "Structure and Function of the Blood-brain Barrier." *Frontiers in Pharmacology* 37: 13-25.
- Slee, E., O'Connor, D., Lu, X. (2004) "To Die or Not to Die: How Does p53 decide?" *Oncogene* 23:2809-2818
- Smith, J., Tho, L., Xu, N., Gillespie, D. (2010) "The ATM-Chk2 And ATR-Chk1 Pathways in DNA Damage Signaling And Cancer" *Advancement in Cancer Research* 108:73-112.
- Sorensen, C., and Syljuasen, R. (2012) "Safeguarding Genome Integrity: The Checkpoint Kinases ATR, CHK1 And WEE1 Restrain CDK Activity During Normal DNA Replication." *Nucleic Acids Research* 40(2): 477-86.
- Stupp, R., et al (2009) "Effects of radiotherapy with concomitant and adjuvant temozolomide versus radiotherapy alone on survival in glioblastoma in a randomised phase III study: 5-year analysis of the EORTC-NCIC trial" *The Lancet Oncology* 10(5): 459-466.
- Tager, F. et al. (2010) "The Cognitive Effects Of Chemotherapy In Post-Menopausal Breast Cancer Patients: A Controlled Longitudinal Study" *Breast Cancer Research and Treatment* 123:25-34.
- Takimoto, R., Wang, W., Dicker, D., Rastinejad, F., Lyssikatos, J., El-Deiry, W. (2002) "The Mutant p53-conformation Modifying drug, CP-31398, Can Induce Apoptosis of Human Cancer Cells and Can Stabilize Wild-type p53 Protein"

Cancer Biology and Therapy 1: 47-55

- Teodoro, J., Evans, S., Green, M. (2007) "Inhibition of Tumor Angiogenesis by P53: A New Role for the Guardian of the Genome." *Journal of Molecular Medicine* 85(11): 1175-186.
- Truman, A., et al. (2012) "CDK-Dependent Hsp70 Phosphorylation Controls G1 Cyclin Abundance and Cell-Cycle Progression" *Cell* 151(6): 1308-1318.
- Vogelstein, B., Lane, D., Levine, A. (2000) "Surfing the p53 Network" *Nature* 408: 307-310.
- Vogelstein, B. (2010) "p53: The Most Frequently Altered Gene in Human Cancers" *Nature Education* 3(9):6.
- Vousden, K., Lu, X. (2002) "Live or Let Die: The Cell's Response to p53" *Nature* 2:594-604.
- Wang, W., Takimoto, R., Rastinejad, F., El-Deiry W. (2003) "Stabilization of p53 by CP-31398 Inhibits Ubiquitination Without Altering Phosphorylation at Serine 15 or 20 or MDM2 Binding" *Molecular and Cellular Biology* 23: 2171-2181.
- Wang, W., Haiping, C., Siglinde, W., Camacho-Horvitz, M., Holak, T., and Domling, A. (2013) "Benzimidazole-2-one: A Novel Anchoring Principle for Antagonizing p53-Mdm2" *Bioorganic and Medicinal Chemistry* 21(14): 3982-3995.
- Wiman, K. (2010) "Pharmacological Reactivation of Mutant p53: From Protein Structure to the Cancer Patient" *Oncogene* 29: 4245-4252.
- Wu, G., Kim, K., El-Deiry W. (2002) "KILLER/DR5, A Novel DNA-Damage Inducible Death Receptor Gene, Links The P53-Tumor Suppressor To Caspase Activation And Apoptotic Death" *Advances in Experimental Medicine and Biology* 465:143-151.
- Yue, Q., Liu, X., Guo, D. (2010) "Microtubule-Binding Natural Products for Cancer Therapy" *Planta Medica* 76(11): 1037-1043.
- Yurchenko, V., Xue, Z., and Sadofsky, M. (2006) "SUMO Modification of Human XRCC4 Regulates Its Localization and Function in DNA Double-Strand Break Repair" *Molecular and Cellular Biology* 26(5):1786-1794.
- Zhao, H., Rybak, P., Dobrucki, J., Traganos, F., Darzynkiewicz, Z. (2012) "Relationship Of DNA Damage Signaling To DNA Replication Following Treatment With DNA Topoisomerase Inhibitors Camptothecin/Topotecan, Mitoxantrone, Or Etoposide" *Cytometry* 8A: 45-51.